

TECHNOLOGICAL ATTRACTION POLES

FINAL REPORT

TRACING TRACEABILITY RULES AGAINST COUNTERFEITING FOR INTERNATIONAL NORMALIZATION GROUPS

PA-11

C. Bernardin

CENTEXBEL – ICT and engineering department

E. Emmerecht

CRIF - Department of Materials Engineering

J-F Delaigle

MULTITEL- Image Department & CRIPTO Research Group

J. De Coninck

UMH – Molecular Modeling

J. Cornelis

VUB - Department of Electronics and Informatics (ETRO)

February 2006



BELGIAN SCIENCE POLICY



Rue de la Science 8
Wetenschapsstraat 8
B-1000 Brussels
Belgium
Tel: +32 (0)2 238 34 11 – Fax: +32 (0)2 230 59 12
<http://www.belspo.be>

Contact person:
Dimitri Harmegnies
Secretariat: +32 (0)2 238 37 61

Neither the Belgian Science Policy nor any person acting on behalf of the Belgian Science Policy is responsible for the use which might be made of the following information. The authors are responsible for the content.

No part of this publication may be reproduced, stored in a retrieval system, or transmitted in any form or by any means, electronic, mechanical, photocopying, recording, or otherwise, without indicating the reference.

Table of Contents

1. Project Presentation.....	4
1.1. Project description and Goals.....	4
1.2. Work distribution	5
2. Scientific and Technical Report.....	6
2.1. State of the Art	6
2.1.1. State of the art of anti-counterfeiting techniques for manufactured goods	6
2.1.2. State of the art of patents concerning coding, encryption and physical engraving of information.....	16
2.1.3. State of the art of photolithography	17
2.1.4. State-of-the-art of nanoreplication techniques	18
2.1.5. State-of-the-art of the “Watermarking 3D graphical objects represented as a MeshGrid model”.....	20
2.2. Research description and results	24
2.2.1. Physical encoding	24
2.2.2. Production of the master with MAPs	29
2.2.3. MAPs replication	36
2.2.4. Optical reading device	46
2.2.5. Design of the new MAP.....	50
2.2.6. Photolithography of the new MAP	51
2.2.7. Polymer tests for replication	53
2.2.8. Vision system and software decoder.....	58
2.2.9. Textiles and fibers studies.....	59
2.2.10. Watermarking 3D graphical objects.....	60
2.2.11. Texture and morphology analysis	76
2.2.12. Products authentication protocol.....	83
2.3. Standardization activities	83
2.4. References	85
2.4.1. References related to “Watermarking 3D graphical objects represented as a MeshGrid model”.....	85
2.4.2. References related to “Texture and morphology analysis”	86
2.5. Appendices	87
2.5.1. Nickel electroforming, Processes and applications	87
3. Achieved goals and industrial considerations.....	93
3.1. The Users Committee.....	93
3.2. Publications	93
3.3. Patents activities	94
3.4. Industrial exploitation possibilities	95

1. Project Presentation

1.1. Project description and Goals

TRACING

Traceability Rules and Actions against Counterfeiting for International Normalization Groups

Funded by the Belgian Science Policy

<http://www.belspo.be>

Project Goals

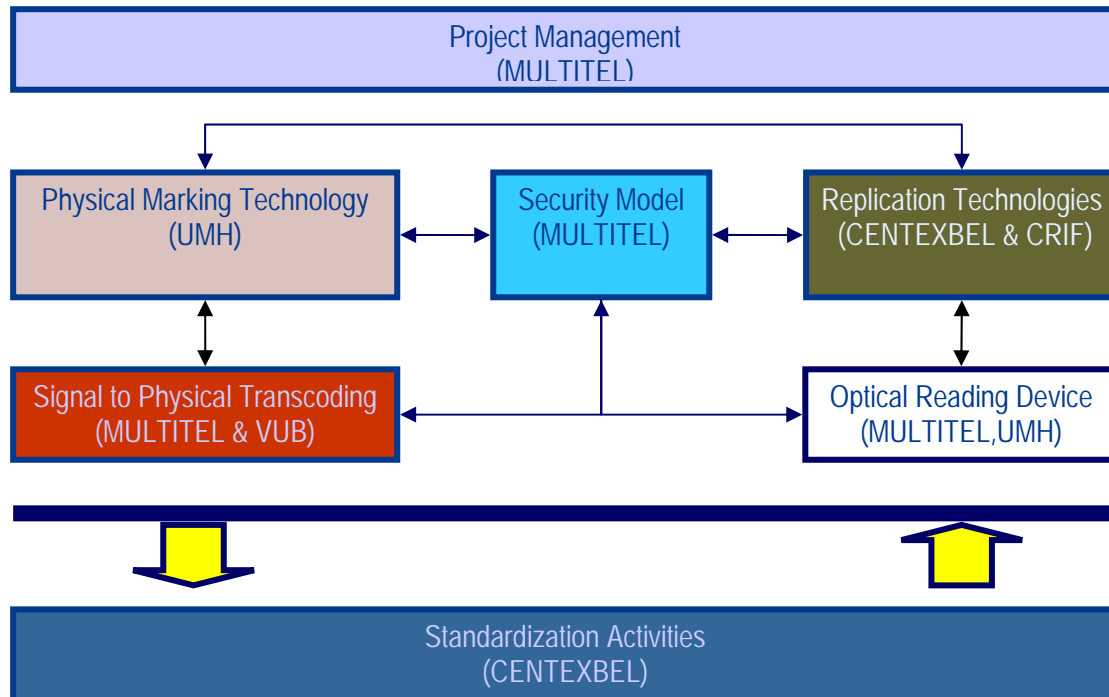
This project aims at studying innovative techniques for protecting two kind of commercial products against counterfeiting: textile fibers and fabrics on one hand, and manufactured goods containing a thermoplastic substrate on the other hand. The idea is to try to embed identification information directly on material surfaces, using micro and nanotechnologies (coating). In the textile case, one dimensional information could be encoded during the coating process, by controlling the thickness coated layer on the fiber. In the case of plastic-based products, we could use coating techniques to hide tracing information, but on a plane surface instead. The information would be encoded by means of special patterns. In both cases, the protection against copy would be based on cryptographic techniques and on the complexity and cost of the coating equipment. Finally, this project will address the standardization issue at different levels, with possible actions at the European level in active groups such as CEN, EAN or ETSI. The Standard definition of the identifiers is needed for interoperability reasons. The delivery of the identifiers must make use of trusted delivery protocols as well as certification centers that will bring trust in the IDs deliverance.

Partners in the project

	CENTEXBEL: The Belgian Textile Research Centre (http://www.centexbel.be)
	CRIF/WTCM: The Belgian Research Centre for the Technological Industry (http://www.crif.be)
	MULTITEL: The Research Centre in Information, Signal and Image Processing (http://www.multitel.be)
	Université de Mons Hainaut (http://www.umh.ac.be)
	VUB: Vrije Universiteit Brussel - Department of Electronics & Information Processing (ETRO) (http://www.etro.vub.ac.be)

1.2. Work distribution

The research in this project has been split in different parts according to each partner's' expertise:



2. Scientific and Technical Report

2.1. State of the Art

2.1.1. State of the art of anti-counterfeiting techniques for manufactured goods

Introduction

Counterfeiting is today a major problem in the world of industry. It is impossible to start talking about anti-counterfeiting techniques before having a clear vision of the magnitude of the problem. And for that, we present some facts to catch the economic impact of counterfeiting:

(source: *The International Anti-Counterfeiting Coalition (IACC)* <http://www.iacc.org>)

1. The Business Software Alliance estimates the cost of software piracy alone to be about \$12 billion a year.
2. The International Chamber of Commerce estimates that seven percent of the world trade is in counterfeit goods and that the counterfeit market is worth \$ 350 billion. George W. Abbott, Jr. and Lee S. Sporn, *Trademark Counterfeiting* § 1.03[A][2] (2001).
3. In 1982 the International Trade Commission estimated counterfeiting and piracy losses at 5.5 billion. In 1996, that number stood at \$200 billion. (Bank robberies, by contrast, involve less than \$50 million per year, but seem to garner more public attention and more law enforcement resources). -- *S. Rep. No. 104-177, 104th Cong., 1st Sess. 1-2 (1995)*; George W. Abbott, Jr. and Lee S. Sporn, *Trademark Counterfeiting* § 1.03[A][2] (2001).
4. Counterfeit automobile parts, like brake pads, cost the auto industry alone over \$12 billion dollars in lost sales. If these losses were eliminated the auto industry could hire 200,000 additional workers. George W. Abbott, Jr. and Lee S. Sporn, *Trademark Counterfeiting* § 1.03[A][2] (2001); Richard C. Noble, *From Brakes to Plugs to Engines, Counterfeiters Produce, Push Parts*, Flint J., September 3, 1995; H.R. Rep. No. 104-556 (1996), *reprinted in* 1996 U.S.C.C.A.N. 1074, 1075.

In Europe,

1. Europe's software, music and audiovisual sectors are estimated to lose some **4.5 billion euros** annually from counterfeiting and piracy.
2. The Anti-Counterfeiting Group (ACG) who organized the survey on behalf of the Global Anti-Counterfeiting Group (GACG) now reckon that the survey shows the total loss to the EU economy from counterfeiting and piracy could be as high as 250 billion per year.

Industries affected by counterfeiting:

Sector	Share of counterfeit goods as a percentage of turnover
Watches ¹	5
Medicine ¹	6
Perfumes ²	5
Aircraft spare parts (SUP) ²	10
Toys ¹	12
Music ²	33
Video ²	50
Software ²	43

1. Not related to any year, estimation without any account for analysis.

2. Figures for 1996, ostensibly with some analysis.

Source: Various trade associations and press.

Figure 1: Share of counterfeit products in total sales of the sector (source OCDE)

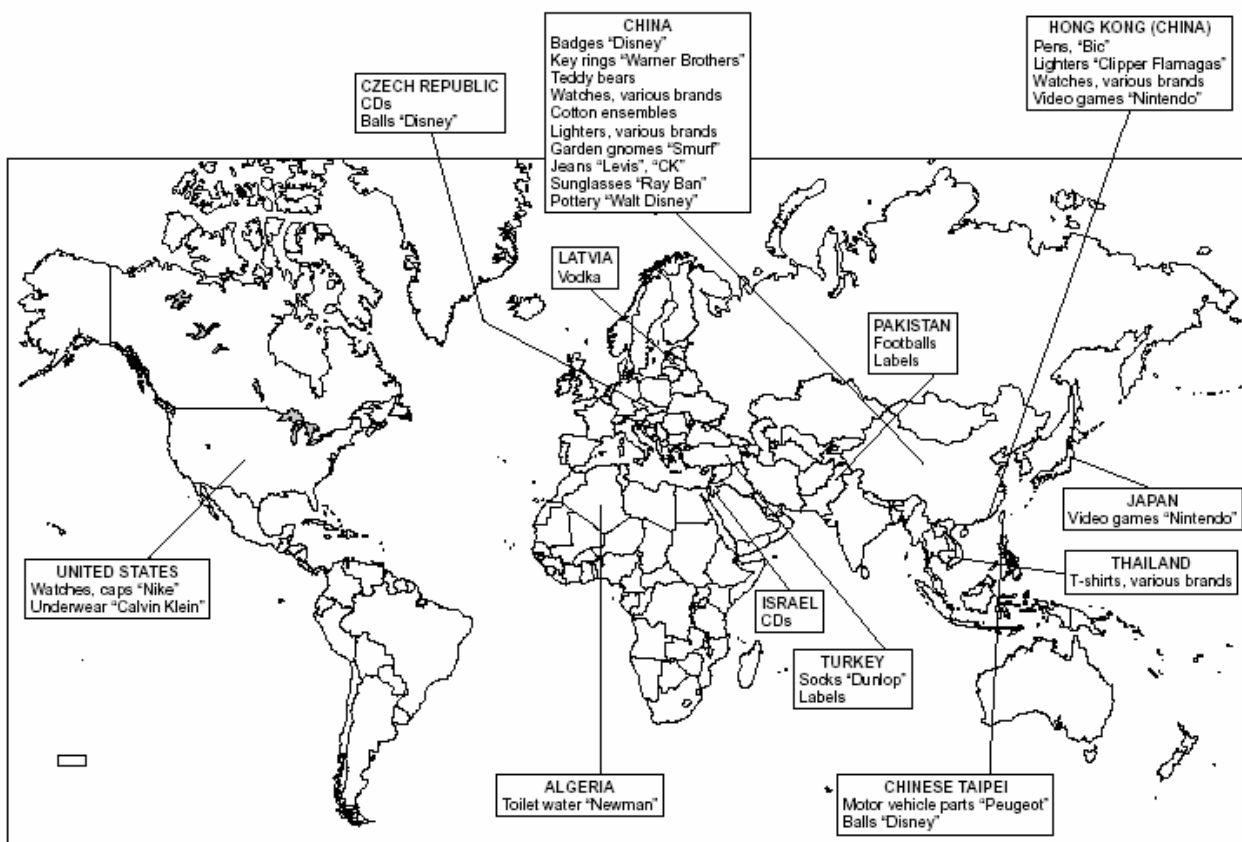
The European Commission surveyed seizures by European Union Customs Authorities between July 1995 and June 1997. Of 4 133 cases reported, the vast majority of products arrived from Poland (740) and Thailand (724). Turkey and the United States were also very common sources, with 497 and 438

seizures. Most cases reported from Spain involved products arriving from the United States. In Germany, most cases involved, not surprisingly, products arriving from Poland, Turkey and the Czech Republic (EC, 1998).

Country	Percentage share
Poland	17.9
Thailand	17.5
Turkey	12.0
United States	10.5
Hong Kong (China)	5.8
China	4.7
Czech Republic	3.6
Korea	2.3
Indonesia	1.2
Chinese Taipei	1.1
Total	100.0

Figure 2: Origins of counterfeits seized by EU customs services (July 1995 to June 1997) (Source: OCDE) Report from the European Commission, Document 98/0018 (ACG), 28 January 1998.)

The impact of counterfeiting on the world economy is clear, and a lot energy and money has been dedicated to fight against this problem. The purpose of this document is to present the main anti-counterfeiting technologies developed till today. The next section is dedicated to the presentation to some theoretical aspects about the anti-counterfeiting approaches. A very general and theoretical scheme is used to classify the different technologies existing today. In the following two sections, the technologies are explored classified and presented according to the theoretical scheme. Finally, some final considerations and remarks will be exposed in the last section.



Source: European Commission, 28 January 1998.

Figure 3: Geographical origin of some IPR-infringing goods seized by EU customs, 1995-1997

Approaching anti-counterfeiting

Almost every commercial good is concerned by Counterfeiting and Piracy, and specially those which are associated with well known international brands. Counterfeiting and Piracy affect intellectual property, pharmaceutical, luxury goods, etc. The need for counterfeiting is clear:

A brand proprietary manufactures a good for which it has a patent and for which he has invested some resources (research, money, time...). This good satisfies standards of quality and the manufacturer expects a high value-added.

The counterfeiter duplicates the good and proceeds to mass production.

His idea: use the brand and original good notoriety, and the manufacturer know-how to sell the copied products.

But he must: invest a small amount of money to make good duplications in order to convince (mislead) the buyer.

In all cases, the following inequality must be satisfied:

$$C < OM$$

C = counterfeiter investment per manufactured unit;

OM = original manufacturer investment per manufactured unit

The counterfeiter must spend much less money to produce each unit than the proprietary manufacturer, and should look for the highest sell value, both in order to guaranty the most elevated benefit.

Original Manufactured Good

- Original physical characteristics and specifications;
- Satisfies quality standards;
- Comes with warranties from the manufacturer.

Counterfeited Good

- Poor physical characteristics, but enough for a convincing visual quality;
- No quality standards are guarantied;
- No warranties

The good counterfeiter is the one which is able to produce the most similar (visual characteristics and quality, physical and functional properties) copied object at the least cost per unit.

It is important to keep in mind the following principle:

*Every manufactured good can be duplicated to a certain level of perfection.
It is just a matter of effort (time and money).*

The counterfeiter must maximize the benefits when duplicating manufactured goods, and for that he should:

1. choose to copy goods with high added-values;
2. minimize the effort (time and money) to produce the fakes.

Since the counterfeited good success is based on its ability to delude the customers, the approach to anti-counterfeiting must be centered on different techniques to raise the amount of effort to produce good quality copies, and by *good quality* we mean enough quality to mislead the customer.

Almost everything that is visible today can be duplicated with small effort, and all the investigations in anti-counterfeiting world have been done in the following directions:

1. To insert visible/invisible tags with certain (special) physical properties that need more and more effort to reproduce without some knowledge and experience. This is what we shall call the *tagging techniques* ;
2. To insert invisible information in the object such that it could be only retrieved by some certified *authenticators*. This is what we shall cal the *watermarking techniques*, where the

information lies in the object, but it is invisible (do not modify substantially neither the visual nor the functional properties of the object), and it cannot be retrieved unless some secret information is known.

The first approach is used extensively nowadays. A lot of research has been done in order to develop more and more difficult-to-duplicate tags. We shall classify the tagging techniques in two groups: *classical tagging techniques* based on the insertion of visible or less visible tags in the object to protect. The authentication is based on the presence of the tag, and *modern tagging techniques* using covert tags (non-readable directly by the human unless a reading device is used), and sometimes more *intelligent tags*. And here by *intelligent tags* we mean tags capable of delivering individualized (for each object) information and even capable of interchanging information with external devices (or persons) (real communicating tags).

The second approach has been essentially used for the protection of digital and multimedia content (digital images, movies, software, etc.). But it is a challenge today trying to use those techniques on physical manufactured objects.

In the next sections we shall try to make an overview of some techniques used nowadays in both approaches. The presentation is by far non-exhaustive.

Anti-counterfeiting tagging techniques

Tagging and object by inserting a physical mark is the oldest idea for fight counterfeiting.

Classical tagging technologies

This mark can be visible and the authentication process is validated by the presence of this mark. But since it is visible, it can sometimes, with little effort, be duplicated and then the anti-copy effort is broken. Therefore the idea is that the tag carries a very particular physical property in order to make the duplication process difficult. Among those visible classical tagging techniques (also called *overt tagging techniques*):

- **Embossed Hologram Stickers**

Description: A sticker containing a hologram is affixed on the surface. According the angle of incidence of visible light, some special patterns and colors are reflected from the holographic surface. The embossed holograms is made of microstructures on the aluminum surface, by a combination of reflection and diffraction of visible light, produces reflected patterns and colors.

Security: duplicating a holographic sticker from simple scanning or photocopy is not possible, since the complete range of patterns and colors emitted by the sticker after light reflection needs various angles of incidence. Reproducing a holographic sticker is possible but requires effort (and money).

Weakness: copying a holographic sticker is quite straight forward. The process only requires money and time, but is no longer a technological (or technical) challenge. Many copying techniques are available.

Usage: The use of embossed holographic tags is quite widespread nowadays in many goods requiring basic security and anti-counterfeiting measures such as:

- Banknotes (here the aluminum support for the hologram is hardly embedded on the paper),
- Credit Cards,
- Secure and confidential documents, etc.

Every object having a surface where a sticker could be affixed can use holographic sticker as an anti-counterfeiting measure.

References:

Stephen McGrew, *Countermeasures against hologram counterfeiting:*

<http://www.nli-ltd.com/publications/countermeasures.htm>

- **Hi Resolution Micro Printing**

Description: It is widely used in the manufacturing of banknotes. It consists in using hi resolution techniques to produce, with certain inks, extremely hi resolution lines and patterns on some papers (like banknotes cotton papers).

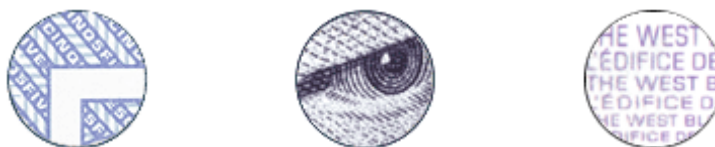


Figure 4: Hi Resolution Micrometric patterns, characters and lines on Canadian Banknotes

The lines are usually 10 to 50 microns in width, and are difficult to produce with wide public printing devices.

Security: it is based on the difficulty to produce such hi resolution. The key is the right combination of ink, paper and printing device, which remains confidential. A 10 micron width line needs a printing device with a least a 2000 DPI resolution. The authenticator uses magnifying lenses and devices to detect the presence of the patterns. Their sharpness is the key to the authentication.

Weakness: The limits are clear. The technique is based on the resolution of scanning and printing devices. It is just a matter of time to achieve the technological performances in order to scan and print equally sharp and precise line and dot patterns on papers.

Usage: Mainly on banknotes and Secure/Confidential paper documents.

References:

Counterfeit Detection on Banknotes of Canada

<http://www.bankofcanada.ca/en/banknotes/counterfeit/index.html>

- *Raised Ink (With an Intaglio Process)*

Description: It is possible to produce raised ink printings with a process called *Intaglio*. In intaglio printing, an image is incised with a pointed tool or "bitten" with acid into a metal plate, usually copper or zinc. The plate is covered with ink, and then cleaned so that only the incised grooves contain ink. The plate and dampened paper are run through a press to create the print. Usually, the plate is smaller than the paper, so that the impression of the plate, or the platemark, remains on the paper. When a limited edition of impressions has been printed, the plate is usually defaced with gouges or holes to ensure that it cannot be used again.

Security: this technique requires a certain amount of effort and artistic work. Raised inks are mainly used to differentiate original secure documents from duplicated/copied/scanned fake documents using cheaper printing processes.

Weakness: duplicating and producing documents with raised ink is just a matter of money, and there are no technical (or technological) difficulties with the process.

Usage: Banknotes and secure/confidential paper documents. It can also be used for producing hi quality paper labels.

References:

Counterfeit Detection on Banknotes of Canada

<http://www.bankofcanada.ca/en/banknotes/counterfeit/index.html>

Recognizing Original Banknotes

<http://www.cauley.co.th/f1/Recognize.htm>

- *Laser Surface Embossing*

Description: in addition to holographic patterns on aluminum labels, it is possible to emboss numbers or characters inside labels without *hurting* the surface. This embossing process is performed with laser engraving technology.



Figure 5: Laser embossed numbers and characters on holographic labels from JINDA

Security: the technique relies on the embossing effect produced on aluminized surfaces with laser engraving. Any other engraving or embossing technique would harm the surface by producing physical grooves. This technique must be seen as an extra security feature added to holographic stickers

Weakness: it is just an extra security feature for embossed holographic labels/stickers.

Usage: on aluminized foils and stickers such as holographic label.

References:

The JINDA Company

<http://www.jindaco.com/speciality/numbering/index.htm>

The techniques mentioned above and in general all overt tagging techniques have the disadvantage of offering now little technological challenges to counterfeiters. In many times, the security resides on the combination of several of these classical and cost-effective tagging techniques, which represent at the production level of original material little extra costs, but represent for the counterfeiter an important effort in both time and money.

Covert tags

A way of adding extra security is to use the so called *covert tagging techniques*. A covert (invisible) tag is not detectable by direct human inspection, but need the use of a machine, a reading device. A lot of research has been done in that direction, and we mention here some examples:

- *Ultraviolet and Infrared Inks*

Description: the use of ultraviolet fluorescent inks is one of the oldest anti-counterfeiting used for paper and document authentication. The principle is simple: the ink is invisible when exposed to visible light. When it is exposed to UV radiation the ink emits an electromagnetic radiation as a violet/blue visible light. Detecting the presence of such ink needs an UV emitting lamp. The same technique can also be used but with infrared emitting inks. The IR approach is newer, with some extra technological challenges.

Security: UV and IR inks are invisible to classical optical scanning/duplicating processes. Counterfeits of banknotes and secure documents will not contain these special inks and therefore should be detectable.

Weakness: the price of UV inks has dropped considerably during the last 5 years. It is even possible to buy for very competitive prices UV inks in the market. For IR inks, the situation is different since the technology is newer, and more difficult to find and to buy. Infrared inks may replace UV security inks for securing documents and labels.

Usage: UV fluorescent inks have been widely used for document protection. The list is somehow long (Banknotes, Secure ID documents: passports, Visas, ID cards).

The UV ink can be used:

- Directly on the paper to be secured by direct printing.
- On foils and transparent films to be placed directly on documents to be protected. Here the advantage is that the use of a transparent easy destructible film containing UV fluorescent ink protects against secure documents forgery.



Figure 6: Protective transparent film containing UV fluorescent patterns for protecting ID data on passports.

Reference:

Counterfeit Detection on Banknotes of Canada

<http://www.bankofcanada.ca/en/banknotes/counterfeit/index.html>

FASVER documents security

<http://www.fasver.com>

The JINDA Company (IR Luminescent Ink Print)

<http://www.jindaco.com/speciality/irp/index.htm>

Magnetic Inks

Description: this ink contains ferrous oxides and has a dark brown color. The oxides give the ink magnetic properties. Characters and patterns can be printed on some papers and labels with this magnetic ink. Its presence is detected by means of a magnetic reading device. If almost all the printed surface contains magnetic ink, it is even possible to produce a *magnetic image* of the surface:



Figure 7: Optical and Magnetic images of an old 10 DM banknote

Security: the authentication of the object is just based on the presence of the magnetic ink. This anti-counterfeiting method is generally combined with other tagging techniques such as UV/IR inks, etc.

Weakness: as for UV inks, it is possible to find for little cost magnetic inks in the market almost with the same quality as those ones used on banknotes and secure documents manufacturing. It should not be used as an anti-counterfeiting alone, but combined with other techniques.

Usage: banknotes, IDs security documents, etc.

References:

San Diego Magnetics (Magnetic Inks for Document Protection)

<http://www.sdmagnetics.com/>

Optical Variable Inks (OVI) and Optical Variable Patterns (OVP)

Description: these inks have special optical emitting properties according the angle of incidence of visible light and/or the frequency for some monochromatic lights. In some cases, OVI will change in color according to the angle of incidence of visible light.



Figure 8: Changing color from gold to green according to the angle of incidence of visible light

The Heriot-Watt University in Scotland has developed a special labels where a surface-relief diffractive optical element is capable of producing two distinct output patterns under different illumination wavelengths, different from either of the design wavelengths, produces a mixture of the two output patterns with a strong dc component. Here the physical property of this OVP label requires special single wavelength illumination and acquisition device.

Security: the optical properties of the OVI cannot be duplicated by simple optical scanning/copying. The effect can only be produced by the use of another OVI. Many of these inks are user proprietary.

Weakness: OVI can be manufactured by other firms and could become widely available. The OVP proposed by the Heriot-Watt University seems to offer a more important technological challenge, and therefore guaranties fewer possibilities for being manufactured, with the same optical properties, by another firm. But it is just a matter of time.

Usage: for security documents protection, such as passports, banknotes, IDs, Credit Cards, and any tangible surface on which a label can be affixed.

References:

Heriot-Watt University: Anti-Counterfeiting Optical Watermark

<http://www.tr.s.hw.ac.uk/servetoinid/licenses/Licenses/watermark.htm>

- **SECUTAG[®]**

Description: SECUTAG[®] is a proprietary technology (<http://www.security-codes.com>) consisting in the insertion of multilayer colored micro-particles in any surface by means of the ink or coating chemical used on the manufactured object. Each particle contains uniquely generated color code for the product, where a color code is a combination of 4 to 10 layers, each one uniquely colored.

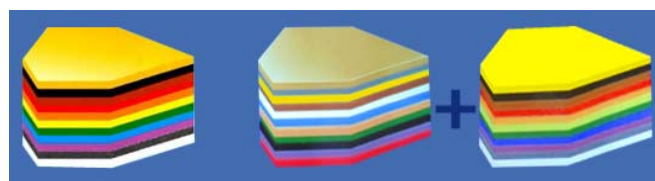


Figure 9: Basic particle geometry and layering

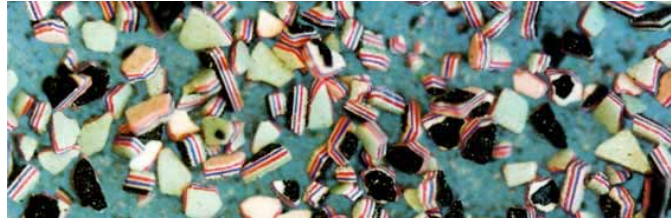


Figure 10: Particles to be embedded on the product surface

Each layer is around $1\mu\text{m}$ thick, and the particle size varies from $0,005\text{mm}$ to $0,045\text{mm}$. The material used for each particle is a Melamine Alkyd-Polymer resistant to organic solvents, chemicals, and to temperatures up to 350°C . The manufacturer estimates that the number of coded possibilities can be as high as 4.358.480.500, offering the possibility of assigning to each product unique color codes.

The detection of the particles and authentication is made by means of a proprietary SECUTAG[®] Micro-Reader based on a CCD camera together with a magnifying optic.

Security: it is based on a proprietary technology non-available to others. The generation of the color codes contains a random process which makes almost impossible to have to set of particles, generated at different moments, with the same color code.

Weakness: the approach is quite secure for the moment unless someone is able to reproduce the manufacturing of such multilayer colored particles. A good security level is maintained whenever is impossible to control the random process in the color coding process.

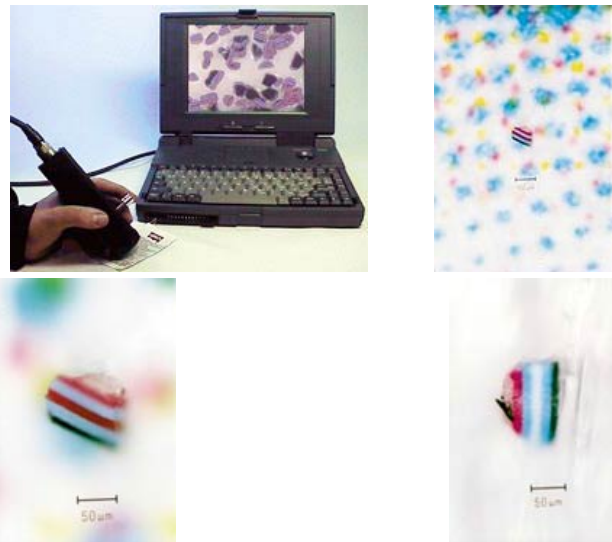


Figure 11: SECUTAG[®] Micro-Reader and snapshots of detected micro-particles

Usage: those particles can be embedded in any film, coating and ink, and therefore on any tangible surface. The density of the particles and their size make them more useful for protecting solid objects instead of papers and security documents such as passport, banknotes, etc.

References:

SECUTAG[®] (Security Codes)

<http://www.security-codes.com>

- *DNA Matrix[™] (DNA Technologies)*

Description: DNA Matrix[™] is a registered trademark from DNA technologies (<http://dnatechnologies.com>) bringing a new and highly advanced technology for protecting manufactured goods using DNA molecules for coding information. The DNA Matrix[™] combines identifiable DNA gene segments - the genetic material that defines the uniqueness of humans and every living organism - and unique optical labels into an ink that may then be applied as either a visible (overt) or invisible (covert) security marker on any tangible surface. These markers contain sufficient information to uniquely identify a product. The DNA Encoded Genetic Markers are a virtually impenetrable line of defense. Oligomers are assembled and encrypted. By arranging the As, Gs, Cs and Ts (the markers that make up the DNA alphabet) the number of variants possible in a DNA authentication mark is mind-boggling.

The components of the DNA Matrix™ can be selectively shifted and recombined in an infinite variety of ways to meet your specific tracking and authentication requirements.

Plus, the DNA Matrix™ is highly resistant to reverse engineering and can be used in conjunction with existing labels, serial numbers, holograms, and other marking systems for an even more cost-effective solution.

The patented DNA Matrix™ **SmartMark** process uses invisible markers that contain sufficient information to uniquely identify a product. It employs specific formulations of rare light-emitting chemicals that produce a complex spectral signature when excited by light of a specific color and intensity. The light emitting chemicals are stable, non toxic and may be readily incorporated into printing inks, dies, plastics, threads and other items as part of the normal printing or manufacturing process.

Security: manipulation of DNA molecules to produce certain arrangements in the bases sequence requires a highly advanced know-how in molecular biology. DNA technology is quite expensive and cannot be reproduced at large scales without effort. Its strength is based on its high technical level, but makes it also an expensive approach to anti-counterfeiting.

Weakness: its price and its technical level make DNA Technology sometimes not a first choice. But this is also part of its strength!

Usage: can be incorporated into printing inks, dies, plastics, threads and other items as part of the normal printing or manufacturing process. The *Thomas Kinkade Art Gallery* is implementing DNA Technology in the ink/paint used by the artists when they sign their creations.

References:

DNA Technologies

<http://dnatechnologies.com>

The Thomas Kinkade Art Gallery

<http://www.kinkadeartgallery.com/dna.html>

- **ISOTAG® Molecular Markers**

Description: the ISOTAG® proposes authentication techniques based on molecular markers. The patented process consists in developing a “mass-enhanced twin” molecule of an existing molecule in a product. Most often this is done by exchanging hydrogen with deuterium. For each hydrogen that is replaced by a deuterium, the molecule becomes one mass heavier. ISOTAG® integration specialists then work with clients to determine the most effective place to insert the markers within the existing manufacturing process and they are typically applied at the parts per billion or parts per trillion level. Once applied, the product has a permanent “fingerprint” only detectable by ISOTAG® technology to allow for authentication throughout the supply chain. They also propose the *ClirCode® Near-Infrared Fluorescent Markers*: they are comprised from an organic dye which is only visible in the infrared spectrum of light.

These molecular markers are detected by means of proprietary reading devices, incredibly accurate, portable and easy to use in the field. They use high-intensity laser light sources that respond to the presence of the near-infrared components formulated into our ClirCode® markers. And they can be used without interference from naturally occurring UV materials in many products, and work in hard-to-reach areas as well as environments with high temperatures or excessive vibration.

Security: the security is obviously based on the presence of these markers in the manufactured product. The strength relies, in the high technical complexity of the process, and its enormous amount of effort needed by the counterfeiter to duplicate the approach.

Weakness: maybe at a financial counterpart. But from the security point of view, the approach seems unbeatable...

Usage: can be incorporated into printing inks, plastics, threads and other items as part of the normal printing or manufacturing process.

References:

The ISOTAG® Company

<http://www.isotag.com>

- **Embedded RFID transponders**

Description: the idea is to embed RFID transponders inside the manufactured object to protect. RFID devices require a certain amount of space, and cannot be inserted in very tiny (or thin) objects such as paper sheets. The RFID transponders are used as passive devices needed to be placed in a variable magnetic field.

This field induces currents through an antenna in the RFID transponder, which are used to power the RFID. Once powered, the RFID send information via RF, and can even be interrogated. The

information interchanged can be performed under some cryptographic protocol, making this approach extremely secure for product authentication.

Security: the authentication is based on the presence of the RFID transponder, or by the information interchange established with the transponder. It is with any doubts the most sophisticated tagging technique available today.

Weakness: RFID transponders that only emit information when they are placed in the electromagnetic field (one-way transponders) present some weakness, since the counterfeiter could also place the same type of transponders in fake products. But if the communication is bi-directional combined with a cryptographic protocol, the technique is extremely powerful and secure.

Usage: RFID transponders can be embedded inside any manufactured object from clothes, molded plastic pieces to even some paper documents. Recently the FASVER firm proposes securing passports against counterfeiting using RFID technology:



Figure 12: Embedded RFID transponder in a passport

References:

The RFID journal

<http://www.rfidjournal.com>

FASVER documents security

<http://www.fasver.com>

Modern watermarking techniques

The watermarking approach to anti-counterfeiting is conceptually different from the classical tagging techniques: a watermark could be defined as piece of information which is embedded in an object, text, image, video, etc. such that it is below the minimal perceptual levels. A watermark is non-detectable by the unaided human senses.

The watermarking protection techniques have been successfully developed for digital and multimedia content, especially for digital images. Here the idea is to insert a specific pattern of bits into the file in such a way that they are invisible to the user. This invisibility must also be statistically invisible. The bits that compose the watermark must appear as noise, normal random data in digital files, and thus unidentifiable to insure that the watermarks are not manipulated. The digital watermark must be robust enough to remain constant when a file is compressed, or otherwise changed. Lossy compression, often used in video compression, shrinks a file by removing redundant or seemingly useless data and this can distort the hidden watermark. A program specifically created to extract watermark data is the only way to know that a file has such a mark. Every watermarking system has two main parts: watermark embedding and watermark extraction/detection.

Final considerations

They are so many anti-counterfeiting techniques available today that it was impossible to report all of them in this document. Our work consisted essentially in spotting out the main ideas and technologies available up to date. The efforts in developing anti-counterfeiting technologies just reflect the importance of counterfeiting problem in today's economical activities.

The different anti-counterfeiting activities explored here all have in common the fact that the object (real manufactured or with digital content) to be protected must be in some sort *tagged*: an extra mark of high technological characteristics must be inserted/affixed into/to the object. The tag can be physical, and in the case of modern watermarking techniques, this *tag* consists in extra information perceptually undetectable. But what could be the future in anti-counterfeiting technologies? The ideal approach is the one which maximizes the simple ratio:

Copy and Duplication Effort Production Costs

New research is being made in trying to use the watermarking approach to the non-digital world, i.e. using watermarking techniques directly on physical manufactured objects. But the task is not easy. Its advantage: we believe that the future lies in the correct combination of digital information insertion (watermarking) with up-to-date strong cryptographic protocols.

2.1.2. State of the art of patents concerning coding, encryption and physical engraving of information

At the beginning of the project, Centexbel made a first “Prior Art” search concerning coding, encryption and physical engraving of information; several patents were found and analysed (for example):

- **US Patent 6069955:** System for protection of Goods Against Counterfeiting; *Coppersmith et al.*
- **US Patent App. 2002/0167161:** Surface Labelled Object and Method Thereof; *Charles L. Butland*
- **US Patent 5592561:** Anti-counterfeiting System *Lewis J. Moore*
- **World Patent 0225599:** Method for Preventing Counterfeiting or Alteration of a Printed or Engraved Surface; *Martin Kutter et al.*
- **World Patent 0159745:** Label that can be Inscribed Using a Laser Beam and Corresponding Method and Device for the Production Thereof. *Alfred Frank*

Later, a more complete examination on prior art within patents was completed but still based of our intention of reading the encoded data with a laser beam. 49 “Anti-forgery” patents and 100 “Optical laser readers” patents were found; a complete list was given in the two-year report.

When the data extraction was changed from laser-based to camera-based, Centexbel made a further examination on prior art within patents concerning the new method and concept used.

The following regions were taken into account:

- WIPO
- EPO
- US, GB
- JP (no free translation of claims)
- FR, DE (problem using keywords)

After some queries with the Micropatent commercial data base, we ended with 193 patent families dealing with tracing and anti-counterfeiting by engraving coded information in goods, information that shall be read with a camera for genuineness validation. Here is an excerpt:

36	US6830188B2→	G06K	20041214	{n/a}	Method and apparatus for accessing electronic data via a familiar printed medium
37	WO2004006163A1→	G06K	20040115	SICPA HOLDING S.A.	METHOD AND DEVICE FOR CODING ARTICLES
38	US6415983B1→	G06K	20020709	Canada Post Corporation	Unique identifier bar code on stamps and apparatus and method for monitoring stamp usage with identifier bar codes
39	JP05197848A→	G06K	19930806	TOKYO JIKI INSATSU KK	INFORMATION RECORDING MEDIUM
40	US4929821A→	G06K	19900529	Skidata Computer G.m.b.H.	Method of forgery-protecting a data carrier, a forgery-protected data carrier and apparatuses for handling, processing and monitoring the data carrier
41	US20050087606A1→	G06K	20050428	DataCard Corporation	Card edge marking
42	GB2273595A→	G06K	19940622	Robert Bosch GmbH(DE)	Housing with readable structures
43	US20050036651A1→	G06K	20050217	{n/a}	Digital anti- forging method
44	WO9930269A1→	G06K	19990617	ROUSTAEL, Alexander, R.	SINGLE CHIP SYMBOLOGY READER WITH SMART SENSOR
45	US5996892A→	G06K	19991207	The Goodyear Tire & Rubber Company	Means and method of identifying objects using a zero contrast sensor
46	JP10055423A→	G06K	19980224	GOCHO SHOICHIRO	METHOD FOR RECORDING USAGE DEGREE OF PREPAID CARD
47	US20040129788A1→	G06K	20040708	Konica Minolta Holdings, Inc.	IC card, IC card manufacturing method, IC card manufacturing apparatus and IC card judgement system
48	US20040079803A1→	G06K	20040429	{n/a}	Hardware integration system
49	US5340973A→	G06K	19940823	Metrologic Instruments, Inc.	Automatic laser scanning system and method of reading bar code symbols using same
50	WO9419770A1→	G06K	19940901	HER MAJESTY IN RIGHT OF CANADA, as represented by THE MINISTER OF	SECURE PERSONAL IDENTIFICATION INSTRUMENT AND METHOD FOR CREATING SAME

Figure 13: List of patents dealing with tracing and anti-counterfeiting

2.1.3. State of the art of photolithography

In order to create on a microscopic or nanoscopic scale identifiable patterns several methods are nowadays used. The simple printing made by ink-jet allows printing on non planar surfaces and on many kinds of materials. But it is generally limited to droplets bigger of $30\mu\text{m}$ diameter. Only very recent advances on water droplet (ie without dye) can reach droplet size below $10\mu\text{m}$ (He *et al.*, "Electro-generation of single femtoliter- and picoliter-volume aqueous droplets in microfluidic systems", Appl. Phys. Let., 87, 31916, 2005 or Yogi *et al.* "On-demand droplet spotter for preparing pico- to femtoliter droplets on surfaces", Analyt. Chem., 73, 1896, 2001). When the drops are projected on the solid surface, depending on the wettability of the system and so the final equilibrium diameter of the drop (Rioboo *et al.*, Exp. Fluids, 33, 112, 2002) the dot given by the drop can reach several time the initial diameter of the drop. Thus final dot will be of several tens of microns.

Many anti-counterfeiting systems use an ink as their basic tool but mainly for document (thus only for paper material) such as UV, IR or magnetic inks.

The laser ablation is, by concentrating light to a target, producing localized evaporation of materials or chemical dissolution. This old technique can produce very precise features on a solid surface (down to 70 nm see for example "Laser ablation in analytical chemistry- a review", Talanta, 57, 425, 2002).

The figure 14 gives a summary of the non-photolithographic existing methods in 1998 with their resolution (nowadays some are improved in terms of resolution). Some of these methods are used for replication and some for creating a first mask or mould.

For practical reason and because the method is widely used and offers plenty of advantages the photolithography technique has been implemented in the UMH laboratory. Let's give here a short review of it. Invented at the end of the 50's this technique is used in microelectronics since then. The formidable growth of this domain is mainly due to the development of this technique as essentially all integrated circuit are made with this technique. The process consists to transfer a shape or a pattern from a mask to a polymer photoresist coated on a silicium wafer. The process can be depicted like on Figure 11. If the illumination is processed through a reduction stepper then only a small amount of the mask is illuminated. A system of scanning, stepping and control permit a patterning of large surfaces. This steppers or mask aligner are the main basis of a photolithography laboratory and cost often several hundreds of thousands Euros if not millions.

Method	Resolution
injection molding	10nm
embossing (imprinting)	25nm
cast molding	50nm
laser ablation	70nm
micromachining with a sharp stylus	100nm
laser-induced deposition	1 μ m
electrochemical micromachining	1 μ m
silver halide photography	5 μ m
pad printing	20 μ m
screen printing	20 μ m
ink-jet printing	50 μ m
electrophotography (xerography)	50 μ m
stereolithography	100 μ m
soft lithography	
microcontact printing (mCP)	35nm
replica molding (REM)	30nm
microtransfer molding (mTM)	1 μ m
micromolding in capillaries (MIMIC)	1 μ m
solvent-assisted micromolding (SAMIM)	60nm

Figure 14: Non-photolithographic methods for micro- and nano-fabrication [from Xia & Whitesides, *Soft Lithography*, *Angew. Chem. Int. Ed.*, 37, 550, 1998].

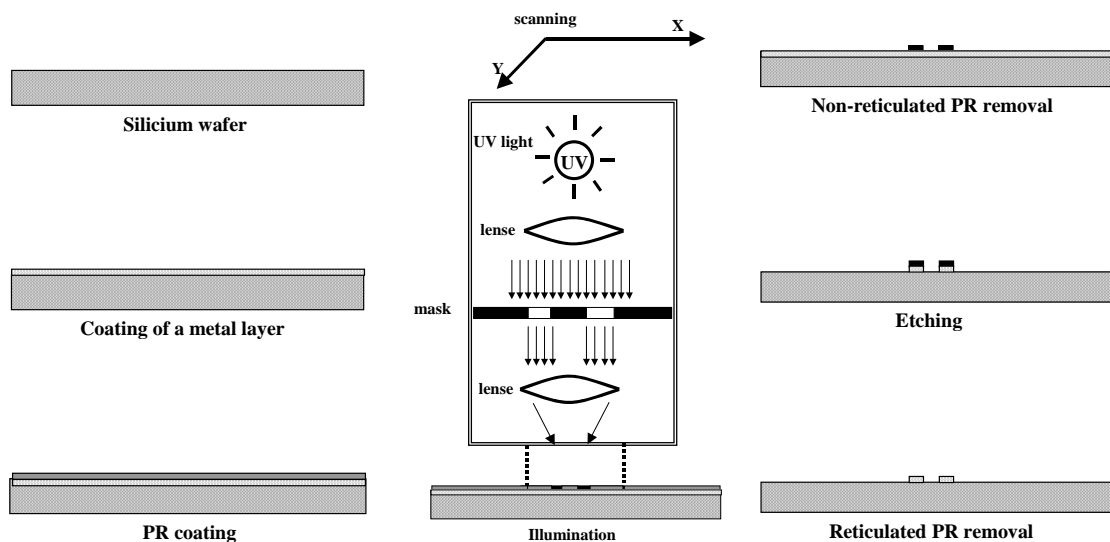


Figure 15: Different steps of the photolithography process. Left: On a silicium wafer (top) we coat or project metal (or semi-conductor) on the silicium wafer (left-middle) then a liquid photoresist polymer (left-bottom). Then with a stepper illumination through

Removal of the liquid (right-top) and etching remove the metal everywhere except on the photoresist places (right-middle). Then the hard photoresist is removed (right-bottom).

Depending on the particular application the method can be slightly adapted. For example the coating of a metal layer or the etching steps are not compulsory. Submicron features (with a clean environment) are nowadays possible on this basis with different light source (from UV to deep-UV and Extreme UV).

2.1.4. State-of-the-art of nanoreplication techniques

Over the past few years, research and industrial applications have been carried out in the field of nanoreplication by the different institutes or companies. Resolutions of clearly below 50 nm were achieved with replication through hot embossing and injection moulding. Use was generally made of silicon mould inserts. Although these inserts are very hard in mechanical terms, they are prone to

damage and will break in the same way as glass under notched stressing. For this reason, electroplated copies are frequently produced in nickel.

When a relief structure is replicated by electroplating, a negative is first made, as with plastic moulding. In other words, a silicon wafer with pits (the original) gives rise to a nickel disc with elevations (1st generation). If this is placed directly in a replication tool, pits will form in the polymer again. These negative structures are difficult to access for a profilometric measurement. It is only through further replication, by electroplating, of the first electroplated copy that a nickel disc is obtained with a structure profile identical to that of the original (2nd generation). When this is used for replication, "mountains" result, and these elevations are easier to measure on account of their positive shape.

Polymer Replication Methods:

The replication processes essentially differ on the basis of whether the replication material is a low-viscosity melt or fluid and whether it is cast onto or in a mould, or is formed locally through pressure in the form of a flowable substrate. Depending on the application involved, the range of replicated specimens extends from plastic discs with surface relief (CD) through to a 100nm - thin polymer layer on a silicon chip or an embossed foil.

In the case of **hot embossing** a flat, structured stamp is pressed into a layer or a sheet of thermoplastic material that has been heated to above its glass transition temperature of T_g . While the outer appearance of the layer scarcely undergoes any change during embossing, the relief on the embossing stamp is transferred to the surface of the material being embossed in the form of a negative. Hot embossing is a relatively slow process. It is thus frequently only used for small-series production, prototype production (low tool costs) and special-purpose applications. One example is nanoimprint-lithography for the lithographic manufacture of nanocomponents, where hot embossing is used to structure a spin-coated polymer film on the surface of a silicon chip.

In injection moulding, the temperature of the material being formed is generally considerably higher than with hot embossing. Since the hot melt is usually injected into a mould at a temperature of below T_g , it is possible to achieve very short process times. Compact discs, for example, can be injection moulded with an overall process cycle of only 3s or so.

There are whole ranges of **casting processes** which are frequently only employed for experimental applications, prototype production or special-purpose applications. In its basic state, a precursor material suitable for casting is a viscous material that is cast in a mould. The material can then be hardened through evaporation of the solvent or through a crosslinking reaction initiated by heat or light chemistry. Sol-gel materials can be used to produce hard, glass-type replicas of nanostructures.

In roll embossing, in the same way as with hot embossing, a structured stamp, also known as a "shim" is pressed into the surface of a thermoplastic material. The shim is mounted on a cylinder like a sleeve, and the cylinder is pressed on to a film in a rolling movement. The process runs continuously, since the cylinder runs over the film, and the relief on the curved stamp is transferred to the film which is supplied continuously by the roll embossing is a bulk process that is used for simple decoration material as well as for security features on passports or bank notes

Measuring Methods for Quality Control

Different profilometric measuring methods are available for measuring the surface relief. Atomic force microscopy (AFM) has become established in the scientific field, while mechanical profile measurement is standard in the semiconductor industry. While profilometers of this type are suitable for routine measurements, AFM allows structural details to be resolved. Extreme care is called for with plastics in both cases, since the specimen can be readily damaged during a measurement with a profilometer and, with AFM, there is a high susceptibility to error in the measurement of nonconducting specimens on account of electrostatic charges.

Scanning electron microscopy (SEM) is particularly suitable for a qualitative assessment of the surface, while precise measurement of the structure height of CD data pits, for example, is very difficult, since the structures can only be viewed from above. It is thus virtually impossible to reveal undercuts or deviations from the ideal profile. This can, however, be done if the fracture edges of specimens can be viewed. The CSEM developed two methods to get round this problem. Both are based on the production of a further replica. In other words, the structure to be measured is replicated with a material that is better suited to the measurement

If, instead of drawing up individual lines or complexes, a large-area grid is created with periodic lines, then it is possible to measure its optical diffraction efficiency and hence assess the mean quality of a grid. Measurements can be made in reflection or transmission mode and can be compared with simulations.

2.1.5. State-of-the-art of the “Watermarking 3D graphical objects represented as a MeshGrid model”

Overview

Digital watermarking provides protection of intellectual property in the digital world, attempting to copyright the digital data, indifferent whether it is audio, visual or video. A digital watermark is designed to permanently reside in the host data. When the ownership of data is in question, the information can be extracted to completely characterize the owner. As opposed to traditional, printed watermarks, *digital watermarks* are transparent signatures. They are integrated within digital files as noise, or random information that already exists in the file. Thus, the detection and removal of the watermark becomes more difficult. Typically, watermarks are dispersed throughout the entire digital file such that the manipulation of one portion of the file does not alter the underlying watermark.

Characteristics of Watermarks

To achieve maximum protection of intellectual property with watermarked media, several requirements must be satisfied:

- **Imperceptible:** The watermark should be imperceptible in order to preserve data quality, so as not to affect the viewing experience of the image or the quality of the audio signal; and also for security reasons, because anyone who can locate the watermark can easily weaken or remove it.
- **Undeletable:** The watermark must be difficult or even impossible to remove by a malicious cracker, at least without obviously degrading the host signal.
- **Statistically undetectable:** A pirate should not be able to detect the watermark by comparing several watermarked signals belonging to the same author.
- **Robustness:** The watermark should be able to survive loss compression techniques like JPEG, which is commonly used for transmission and storage. The watermark should be retrievable even if common signal processing operations are applied, such as signal enhancement, geometric image operations and noise filtering.
- **Unambiguous:** Retrieval of the watermark should unambiguously identify the owner, and the accuracy of identification should degrade gradually in the face of attacks. Watermark detection should produce low false-alarm and false-rejection probabilities.

Types of Watermarks

Visible: Visible watermarks are designed to be easily perceived by the viewer, and clearly identify the owner. The watermark must not detract from the image content itself, however. Most research currently focuses on invisible watermarks, which are imperceptible under normal viewing conditions (figure 16).

Fragile: Fragile watermarks are designed to be distorted, or to be broken, under the slightest changes to the image. Semi-fragile watermarks are designed to break under all changes that exceed a user-specified threshold.

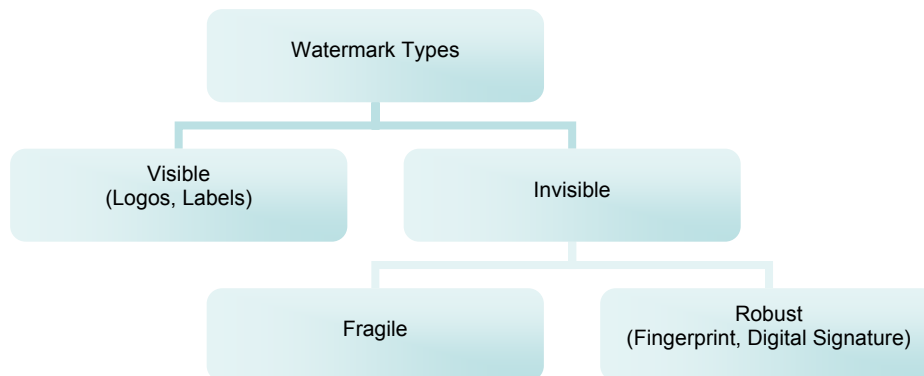


Figure 16: Types of watermarks

Embedding domain: The watermark can either be embedded directly in the spatial domain by properly modifying the content data, or in a transform domain, attempting to exploit the domain properties, mainly for watermark imperceptibility and robustness (figure 17). In the literature, there are papers that presented watermarking embedding methods in the Discrete-Cosine Transform (DCT), Discrete Fourier Transform (DFT), Discrete Wavelet Transform (DWT) or Fractal-based Coding Domain (FCD).

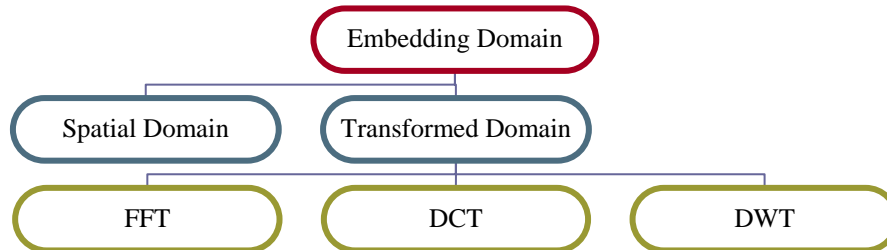


Figure 17: Watermarks embedding domains

Host signal adaptive: Recent methods exploit human auditory and visual system principles to attain improved watermark imperceptibility. Host signal adaptive watermarks are usually transform-based and very robust. They locally adapt the strength of the watermark to the audio or image content through perceptual models for human senses. These models were originally developed for image or audio compression.

Blind: Blind watermarking techniques can perform verification of the mark without use of the original image. Other techniques rely on the original to detect the watermark. Many applications require blind schemes; these techniques are often less robust than non-blind algorithms.

Public & private watermarking: In public watermarking, users of the content are authorized to detect the watermark while in private watermarking the users are not authorized to detect the watermark.

Asymmetric & symmetric watermarking: Asymmetric watermarking (also called asymmetric key watermarking) is a technique where different keys are used for embedding and detecting the watermark. In symmetric watermarking (or symmetric key watermarking), the same keys are used for embedding and detecting watermarks.

Steganographic & non-steganographic watermarking: Steganographic watermarking is a technique where content users are unaware that a watermark is present. In non-steganographic watermarking, the users are aware of the presence of a watermark. Steganographic watermarking is used in fingerprinting applications while non-steganographic watermarking techniques can be used to deter piracy.

For further details, the papers [18][19] provide an overview of existing multimedia watermarking methods.

Required Properties of 3D Watermarking Systems

A watermarking system designed for 3D model data should have the following properties at a minimum:

- **Capacity:** The system should allow embedding of nontrivial amounts of data. Embedding serial numbers that identify buyer or licensor identities requires at least 32 bits of capacity. Proving ownership requires enough capacity to store a hash value. Space requirements of information embedded in public watermarks range from a global model registration number of 32 bits up to a URL from which to get copyright- or licensing-related information, which could take 256 bits or more. A class of watermarking systems, called statistical approaches, hashes information of arbitrary length and feeds some sort of random number generator with it. This generator yields locations where data is modified in respect to some global statistical measures like mean value and variance. These systems

permit testing for the presence of watermarks whose contents are known in advance. While these systems might claim to have unlimited capacity, they have drawbacks.

- **Robustness:** As a matter of principle, private watermarks should exhibit resistance to all geometric or topological operations that don't substantially degrade the model's visual quality. Thus a watermarking system's primary goal is not robustness with respect to the following operations: shearing; non-uniform scaling along arbitrary axes; projections, as projection on a plane; global deformations. Several papers overview possible attacks and the limitations of many current watermarking approaches under such attacks [21][22].

Recommended Properties of 3D Watermarking Systems

In addition to the required properties, 3D watermarking systems would benefit from further capabilities, as follows:

- **Background processing and suitable speed:** Embedding and retrieving watermarks should be possible without user interaction. Automated search of Web sites and databases for watermarks performed by robots are an important application in monitoring the use of both legal and illegal copies and in enforcing the copyright. The ultimate goal in this respect is real-time monitoring. However, this puts heavy demands on watermarking systems' execution speed and storage requirements.
- **Embedding multiple watermarks:** Real-world applications might demand the possibility of embedding multiple watermarks. This occurs in the producer/resellers pipeline, in which producers embed a secret watermark identifying resellers and resellers embed one identifying customers or end licensees. Ideally, the watermarks should not interfere with each other even if producers keep the details of their embedding parameters secret.
- **Minimum knowledge of a priori data:** An ideal system requires only model data and knowledge of a key for watermark retrieval. The key may be specific to the model's creator or company, model class, model itself, and/or licensee. All necessary parameters, such as seed values for generators, derive from this key. In a public watermark system all of a creator's models may share a unique key. Alternatively, the system might use a key common to models from various creators. Unfortunately, a retrieval system may demand knowledge of more a priori data: Knowledge of the model itself, especially model-specific embedding locations to avoid synchronization problems; or/and Original model data or at least parts of it for reorientation, rescaling, and comparing features of a watermarked copy with the original. Such a retrieval system has reduced monitoring and background processing features. Decentralized retrieving of watermarks gets complicated, especially when it involves accessing large amounts of original model data organized in databases.
- **Minimum preprocessing overhead:** An ideal system should allow immediate access to embedded watermarks, without preprocessing model data. Such preprocessing might involve transforming the model data representation, recognizing the model, correcting surface normal, and reorienting and scaling with respect to the original.

General Watermarking Systems

Koch et al. [12] were one of the first to propose a general method for watermarking 2D images. They break up an image into 8x8 blocks and compute the Discrete Cosine Transform (DCT) for each of these blocks. A pseudorandom subset of the blocks is chosen, and in each such block, a triple of frequencies is selected from one of 18 predetermined triples and modified so that their relative strengths encode a 1 or 0 value. The 18 possible triples are created by selection of three out of eight predetermined frequencies within the 8x8 DCT block. The choice of the 8 frequencies to be altered within the DCT block is based on a belief that the "middle frequencies ... have moderate variance", i.e. they have similar magnitude. Therefore the relative strength of the frequency triples can be altered without being perceptually noticeable. Yet as the variance between the eight frequencies coefficients is quite small, their technique is quite sensitive to noise or distortions.

Cox et al. [13] developed later on the Secure Spread-Spectrum Watermarking (SSSW) algorithm, which is robust to common signal distortions and malicious attacks due to the fact that the watermark is placed in perceptually significant components of the signal. To avoid perceptual degradation of the signal, the watermark is inserted into the spectral components of the data using techniques analogue

to the spread spectrum techniques used in communication technology, hiding a narrow band signal (the watermark in our case) in a wide band channel, such that the signal energy present in any single frequency is imperceptible. Hence, the watermark is spread over many frequency bins so that the energy in any single bin is very small and certainly undetectable. Nevertheless, because the watermark extraction process knows the location and content of the watermark, it can concentrate these many weak signals into a single signal with a high signal-to-noise ratio.

In order to place a watermark with length n into an image, the DCT – although any frequency domain transform can be used – of the image is computed, and the watermark is placed into the n highest magnitude coefficients of the transform matrix, excluding the DC component. To insert X (the watermark data array) into V (the coefficients of the transformation matrix chosen to hold the watermark) to obtain V' , a scaling parameter α (in practice, around 0.1) is specified, which determines the extent to which X alters V . Different formulae for computing V' are possible:

$$v'_i = v_i + \alpha x_i \quad \vee \quad v'_i = v_i(1 + \alpha x_i) \quad \vee \quad v'_i = v_i(e^{\alpha x_i}).$$

For extracting the watermark, the similarity between the original watermark X and extracted watermark X' can be measured by: $\text{Sim}(X, X') = (X' * X) / \text{Sqrt}(X' * X)$ with $*$ representing the correlation operator. The watermark is robust to distortions such as: digital-to-analog and analog-to-digital conversion, resampling, requantization, including dithering and recompression, and rotation, translation, cropping and scaling.

Hong et al. [23] propose a blind watermarking algorithm that needs for the extraction procedure only the secret key and the original watermark data. The watermark is embedded in the middle frequency area (LH2 – low high frequency band of the second level) of the wavelet transform coefficients of the image. A secret key is used for choosing the coefficients that will store the watermark. The selected coefficients x_{ij} are modified according to the mean value m_{ij} of the neighboring coefficients. If $x_{ij} > m_{ij}$ then '1' is embedded using the formula $x'_{ij} = x_{ij}(1 + \alpha)$. If $x_{ij} < m_{ij}$ then '0' is embedded using the formula $x'_{ij} = x_{ij}(1 - \alpha)$. This watermark technique has proven experimentally to be robust to: JPEG compression, Noise addition, Collusion and Resize.

Solachidis et al. [17] developed an algorithm that embeds watermarks in polygonal lines describing image contours. These contours are usually described in vector format. This watermarking method slightly modifies the vertex coordinates of the polygonal line, and embeds the watermark in the magnitude of the curve's Fourier descriptors, which has location, scale, and rotation invariant properties. The watermark detection is also blind – that is, the watermark detection procedure doesn't need the original polygonal line. Let L be a closed polygonal line that consists of N vertices. Let also $[x(n), y(n)]$, $n = 0, 1, \dots, N-1$ be the Cartesian coordinates of each vertex. The complex signal $z(n)$ is defined as $z(n) = x(n) + j \cdot y(n)$, where $n = 0, 1, \dots, N-1$, and by randomly selecting a vertex as a starting point and tracing the vertices in a clockwise or counterclockwise direction. The watermark embedding and detection procedures do not require knowledge about the starting point or the traversing path. Let $Z(k)$ be the Fourier transform representation of the signal $z(n)$, called the *Fourier descriptors* of the polygonal line. In the Fourier descriptor representation, the $Z(k)$ coefficients around $Z(0)$ (DC term) describe low-frequency information, whereas the coefficients around $Z(N/2)$ describe high-frequency information. Low-frequency coefficients typically represent the general shape, whereas outline and high-frequency coefficients describe shape details and sharp corners. Using a pseudorandom generator, a bivalued ± 1 random sequence, which has zero mean value and unit variance, is created and used to produce a watermark. The watermarked polygonal line $|Z'(k)|$ is obtained via multiplicative embedding, which corresponds to a simple watermark masking (the watermark amplitude is larger in large Fourier descriptor coefficients). The correlation between $|Z'(k)|$ and the random sequence corresponding to the watermark W is used to detect the watermark's presence. The proposed method is robust to many geometrical transformations as well as to combinations of them: *Translation, Rotation, Scaling, Change of the starting point of the traversal, Traversal direction inversion, Mirroring*.

3D Geometry-oriented Watermarking Systems

Ohbuchi et. al [9] produced the first publication on 3D watermarking, in which they proposed a large variety of techniques. The techniques described fall roughly into mesh altering, topology altering, and visible pattern embedding methods.

The mesh-altering methods, especially the proposed Tetrahedral Volume Ratio (TVR) algorithm, show near-optimal properties with respect to capacity, execution speed, and monitoring capabilities. The significant drawbacks include vulnerability to re-meshing operations, polygon simplification, and point randomization. It is furthermore restricted to meshes consisting entirely of triangles; no planar polygons with more than three vertices can be processed. Nevertheless, the algorithm proves to be well suited for embedding public watermarks.

Topology altering methods, which basically embed information by cutting holes in a mesh, are trivially vulnerable against attacks that scan for these holes. The visible pattern embedding method, Mesh Density Pattern (MDP), is vulnerable to a re-meshing attack that generates patterns with mostly identical shapes (angles and size).

Boon-Lock and Minerva [10] published the first work concerned with the problem of authenticity and integrity protection for 3D polygonal models. Using their scheme, one can verify in knowledge of a *secret* verification key, if the model has been modified after embedding of a fragile watermark (geometric or topological modifications) if a constant reference watermark is used.

Oliver Benedens [8] proposes embedding watermarks by altering the distribution of mesh surface normal. The watermark data are embedded in the mesh by performing certain displacements of points, which in turn introduce specific changes in the mesh surface normal' distribution. This technique achieves robustness against: Randomization of points; Mesh altering (re-meshing) and Polygon simplification, but it requires a mesh representation of a 3D model consisting entirely of triangle patches as input.

Oliver Benedens and Christoph Busch describe in [11] another Digital Watermarking system dedicated for embedding watermarks into 3D polygonal models, named the Vertex Flood Algorithm (VFA), suitable for embedding fragile public readable watermarks with high capacity and offering a way of model authentication. The VFA algorithm modifies mesh vertices, so their distances to the center of mass of a designated start triangle encode the watermark bits. Except for the start face, the algorithm operates solely on vertices and does not take further topological relationships into account. It does not require connectivity of the faces in the input mesh. This technique is robust against more complex operations, most noticeably polygon reduction.

Ohbuchi [14] presents a robust watermarking method that adds a watermark into a 3D polygonal mesh in the mesh's spectral domain. The spectrum of the polygonal mesh is computed from connectivity and coordinates of the vertices of the mesh. Computation of mesh spectra involves eigenvalue decomposition of a *Laplacian matrix*, which is derived only from the connectivity of the mesh vertices. The decomposition produces a sequence of eigenvalues and a corresponding sequence of eigenvectors of the matrix. Approximately, smaller eigenvalues correspond to lower spatial frequencies, and larger eigenvalues correspond to higher spatial frequencies. Eigenvectors and spectral coefficients of the smaller eigenvalues represent global shape features, while eigenvectors and spectral coefficients of the larger eigenvalues represent local or detail shape features. Projecting the coordinate of a vertex onto a normalized eigenvector produces a mesh spectral coefficient of the vertex. A watermark is embedded by modifying the magnitude of the spectra. The watermark extraction is performed in the mesh spectral domain, comparing spectral coefficients of the watermarked and original meshes. Watermarks embedded by using this method are resistant to similarity transformations, random noise added to vertex coordinates, mesh smoothing, and partial resection of the meshes. The method is a private watermarking method, meaning that the watermark extraction requires both the watermarked mesh and the original, non-watermarked mesh.

2.2. Research description and results

2.2.1. Physical encoding

The first step in the project was the design of a secret pattern easily embeddable on a usual product and the development of a reading device. After the state-of-art study, the idea was to use a CD-like equipment. The CD technology is extensively developed, massively used (low cost) and very accurate for information retrieval at a micrometric level.

In the CD technology, the disc is the support of the data and the CD-player is the device for the signal processing. The goal of this task is to reproduce this process for our used: Retrieve hidden information on a product.

As the information on a CD is coded on a flat surface, we initially work on those kinds of surface. A disc is made of four layers. A protective lacquer coating where a printed ink can be added, a metalized pit surface for a better reflection and the disc substrate (figure 18).

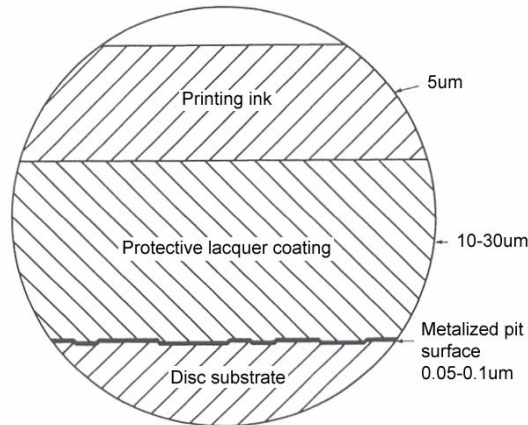


Figure 18: Layers of a disc

The data is physically contained in pits which are impressed on the substrate and are covered with a very thin metal layer. The physical method of accomplishing data storage in pits on a flat surface is not directly visible with naked eye. The disk contains a track of pits and lands arranged in a continuous spiral running from the inner circumference to the outer.

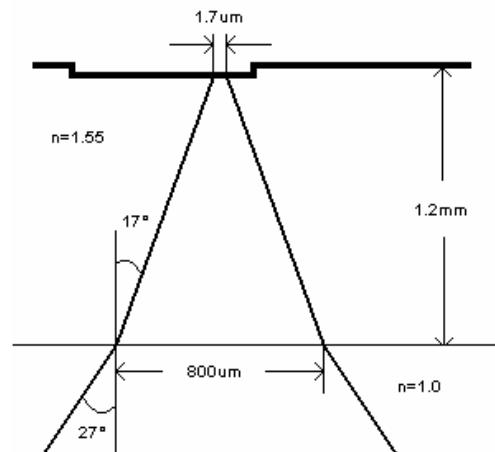


Figure 19: Modification of the incidence angle of the light inside the polycarbonate

When the CD is played the beam of the laser strikes the protective layer firstly. In the polycarbonate layer, the refractive index changes which contribute to the focusing of the laser beam (figure 19).

The protective layer is a polycarbonate substrate of 1.2mm and the laser's wavelength is 780nm in the air and 500nm in the substrate. The depth of the pits is 125nm (λ/4).

As it is noticed on the figure 20, the OPU is an interferometer. In theory, when the beam strikes a land, all of its light is reflected, and when it strikes a pit, all of its light is cancelled, so that none is reflected. In practice, the laser spot is larger than the pit width for a better tracking of the track.

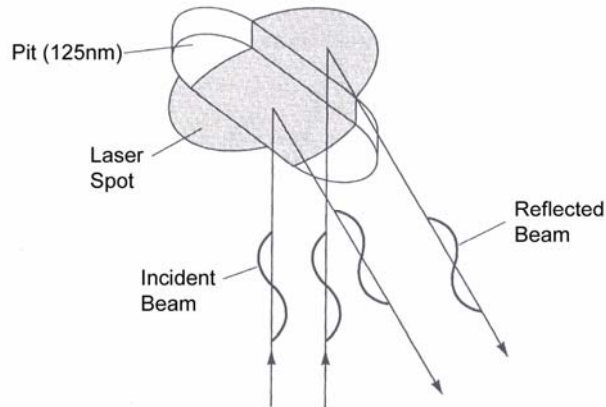


Figure 20: Reflected and incident beam

The data is encoded on the disc following a frame structure. The frame contains 27 bits of synchronization, 8 bits of subcode, 192 bits of data and 64 parity bits. The figure 21 shows how the pit's edge encodes logical channel bits.

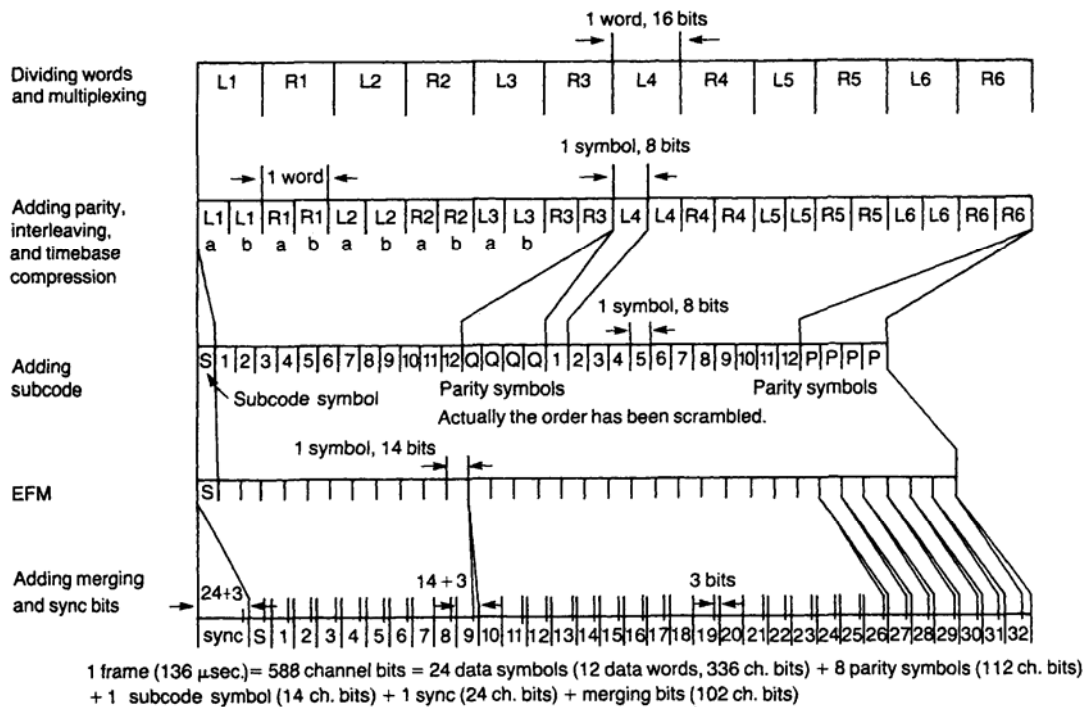


Figure 21: Frame format of the CD technology.

For our purpose, this encoding process is useless. Our work is slightly different even if we follow two principles :

- Stay close as possible to the CD technology for interoperability and robustness reasons,
- Keep the encoding and decoding process as simple as possible.

In the initial phase, the information length has been fixed to 144 bits. This number is chosen according to the Reed-Salomon error correcting code we plan to use against burst error. The code chosen is the RS(15, 9) which means that 9 data bits is encoded with 15 bits.

The code efficiency is : $\frac{9}{15} = 60\%$.

This code can correct up to 12 consecutive erroneous bits among 60 bits. This fixes error-correction capacity to : $\frac{12}{60} = 20\%$

After encoding, the 144 bits of pure information become $144 * \frac{15}{9} = 240$ bits of coded information.

The physical information is embedded on a plane surface. But, contrary to the CD technology, the protective layer of polycarbonate is removed. Consequently, the depth of the pits becomes $\frac{780}{4} = 195nm$, as the wavelength of the incident beam is $780nm$.

It appears that it is not possible to encode the information with the difference of the optoelectronic signal between a pit and a land. To encode the two binary digits 0 and 1, series of pits and lands are considered. Every pits and lands have a discrete length that are a multiple of T, where : $T = 0.325\mu m$

To encode a logical bit of “pure” information, symbols “a” and “b” are created whose correspond to the binary digits 0 and 1.

Symbol	Physical encoding	Total length
a	$\overline{6T} \ \underline{3T}$	$9T = 2.925\mu m$
b	$\underline{11T} \ \overline{11T}$	$22T = 7.15\mu m$
SYNCA0	$\overline{3T} \ \underline{3T} \ \overline{3T} \ \underline{3T} \ \overline{3T}$	$15T = 4.875\mu m$
SYNCA1	$\overline{6T} \ \underline{6T} \ \overline{6T} \ \underline{6T} \ \overline{6T}$	$30T = 9.75\mu m$
SYNCB0	$\underline{3T} \ \underline{3T} \ \underline{3T} \ \underline{3T} \ \underline{3T} \ \underline{3T} \ \underline{3T}$	$21T = 6.825\mu m$
SYNCB1	$\overline{6T} \ \overline{6T} \ \overline{6T} \ \overline{6T} \ \overline{6T} \ \overline{6T} \ \overline{6T}$	$42T = 13.65\mu m$

Figure 22: Symbols physical encoding

To ensure the shortest length of physical information, the symbols SYNCA0, SYNCB0, SYNCA1, and SYNCB1 are used for the synchronization. It is important to notice that the symbol “a” can encode the binary digit 0 if this digit appears more frequently in the message. Otherwise it will encode the binary digit 1.

The average length of each encode bit is : $\frac{9T + 22T}{2} = 15.5T$

Different synchronization patterns at the beginning and at the end are to help the reading device distinguish the beginning and the end of the data frame which enclosed the message. Of course, SYNCA0 and SYNCA1 are different in order to help the reader distinguish the two possible physical encoding of both digits 0 and 1 (figures 23 & 24)

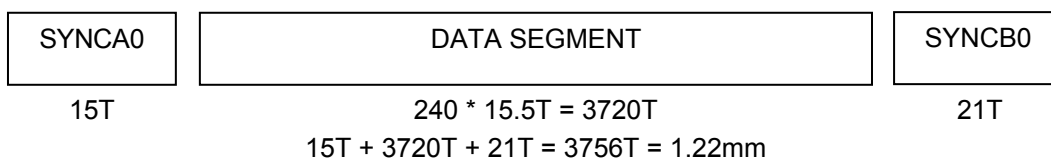


Figure 23: Frame when the symbol a encodes the digit 0

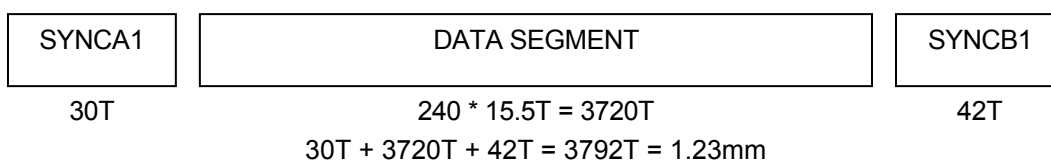


Figure 24: Frame when the symbol a encodes the digit 1

In the CD technology, the encoding information is on a circular track. It appears that this solution is not useful for our purpose. Two constraints would be satisfied:

- The possibility of reading the information from any point on the surface and in any direction (no synchronization and no track alignment as in CD technology),
- The information has to be read linearly (in one dimension).

Supposing the reading device is placed randomly on the surface, at least, one pattern must be swept by the reader. Some patterns of pits and lands with a particular tiling were considered (figure 25).

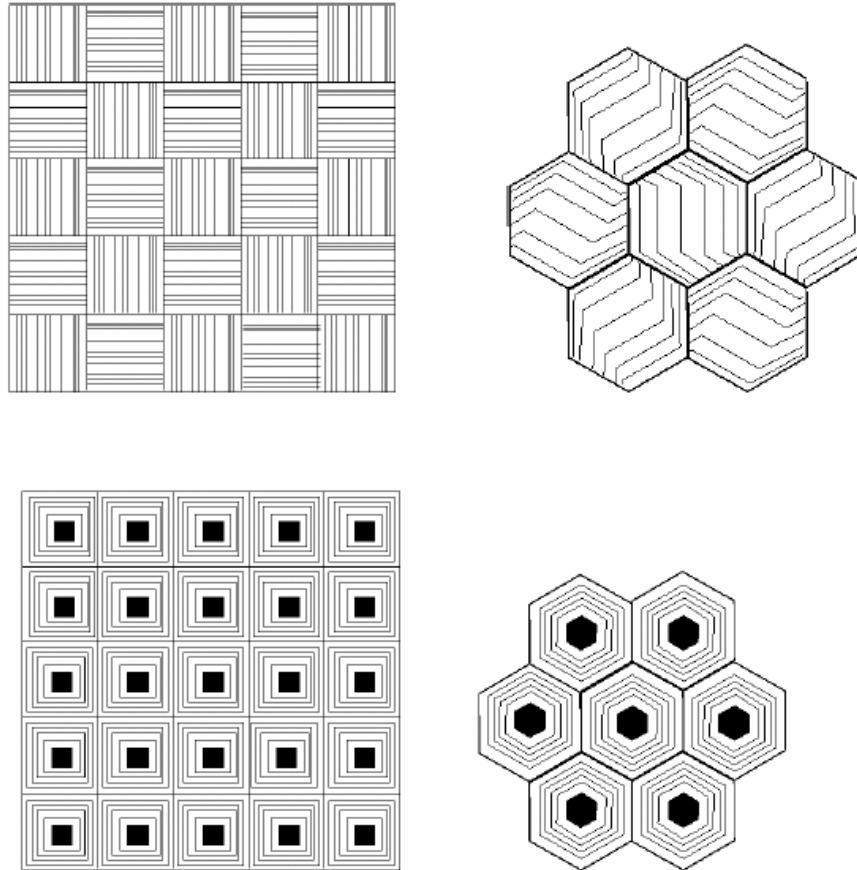


Figure 25: Tiling proposed.

The study shows that the best solution to encode the information on the surface is a tiling of squares of parallel furrows of pits and lands (left up corner of figure 25). As the optical reading device must sweep a whole pattern, the HF signal study helps to go further in the way to encoded information. The HF signal is the electrical signal obtained at the output stage of the photodetector device in the optical pickup unit. If v denotes the linear velocity of the scanning beam in $m.s^{-1}$, the frequencies of all elements of the HF signal are:

Symbol	Frequency	Freq. for $1.3m.s^{-1}$
a	$f = \frac{v}{9 * 0.325} 10^3 kHz$	$f = 444kHz$
b	$f = \frac{v}{22 * 0.325} 10^3 kHz$	$f = 182kHz$
SYNCA0	$f = \frac{v}{6 * 0.325} 10^3 kHz$	$f = 666kHz$
SYNCA1	$f = \frac{v}{12 * 0.325} 10^3 kHz$	$f = 333kHz$
SYNCB0	$f = \frac{v}{6 * 0.325} 10^3 kHz$	$f = 666kHz$
SYNCB1	$f = \frac{v}{12 * 0.325} 10^3 kHz$	$f = 333kHz$

Figure 26: Symbols frequencies

The speed of the $1.3m.s^{-1}$ is chosen according to the rotating speed of the disc in the CD technology. The frequency of each symbol is used to distinguish the symbols.

Remember that the encoded information is the “pure” information with an error-correction code. Then, this encoded information is set into a frame which is made of synchronization symbols and of symbols which are a series of pits and lands. This frame is encoded physically on the surface. We call the frame a MAP (Micrometric Authentication Pattern). The MAP is the physical way of the encoded information.

2.2.2. Production of the master with MAPs

The second important step in the project that has to be realized is the production of a master plate with a pattern on its surface at the micrometric scale. Among the methods cited above two were chosen to be conducted in parallel: microdroplets and photolithography. The microdroplet array is a technique that is partly available at UMH. Some modifications of the visualization system already available have to be performed in order to control and visualize the droplet produced. Beside this aspect the resolution achievable with the microdroplet technique is rather low compare to the photolithography. The focus was thus put on the photolithography technique and on the implementation of this technique in the UMH laboratory.

The next step in the process of making patterned goods is to replicate this master (MAP) by means of nickel electroforming (as for CD fabrication technique). Material was bought and adjusted to perform photolithography at microscopic scale at a reasonable price. So it was important to choose what was necessary to perform photolithography without the expensive parts of the steppers available. The mask aligners (or steppers) are expensive mainly because they focus the light on a small part of the mask to be able to reduce the pattern to a smaller scale without any defect due to light diffraction. This needs a precise and expensive optic system. Beside this aspect once the image is reproduced on the wafer on a particular part the light has to be focused on another part of mask. All this process is often automatically. Then this whole process can be replicated. All this adjustments need to visualize and control precisely where the light is arriving. The movement of the mask and the wafer respectively to the light have to be controlled. All this processes make a masks aligner a very expensive tool. But principally what is needed for our research application is: a UV light source, a mask, a photoresist and chemicals. The technique of the photolithography can be done by direct contact between the mask and the wafer. Then the necessity to align is no more necessary. But of course the pattern replicated will be of the size of the mask no more and not smaller. So without the reduction facility and the precise alignment of features the process can be executed with a rather inexpensive tools.

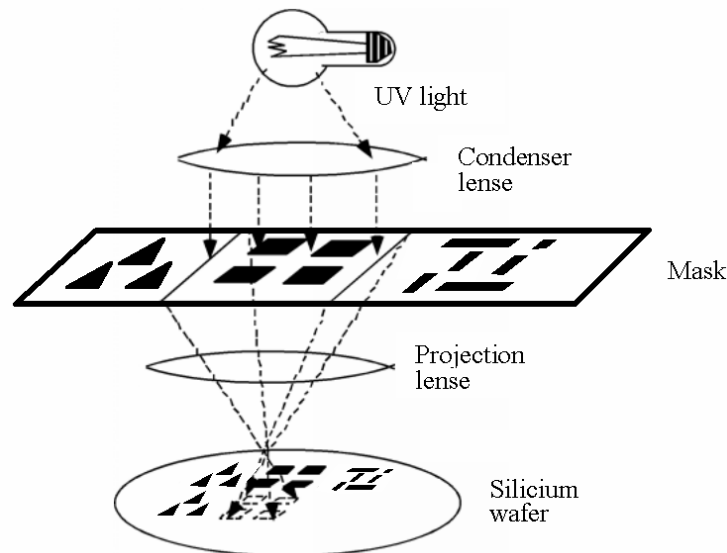


Figure 27: Projection illumination schema of a mask aligner. Alignment and reproduction need precise control and movement of wafer, mask and optics.

A positive photoresist has been chosen (SU8-2xxx). The polymer will reticulate only on the place where the UV light is applied.

With a specific chemical developer the reticulated part becomes solid. A solvent is used to remove the rest of the non-reticulated polymer. Only the reticulated part sticks and stays to the surface. In this way structures on the micrometer scale can be created. These structures are of 0/1 type, this means that the solid surface will present two possible heights (top/bottom and only that) on demand, depending on the place where the light has been applied.

A spin-coater is available at the UMH laboratory. In this way the thickness of the photoresist layer (so the height of the bottom part respect to the wafer) can be adjusted. The control of the concentration of the photoresist, the velocity and time of spinning will enable to adjust the thickness to the desired one. Structures can be controlled through optical microscope and measured via an optical profilometer (Wyko NT1100) present in the CRMM.

The following equipments were chosen to make the photolithography equipment:

- A CAO software to design the masks.
- Masks.
- Chemical products (SU8-2002; SU8-2025; SU8-developper; SU8-2000 Thinner; Omnicoat; Remover PG).
- A special UV lamp.
- Small material to mix products, heat, etc.



Figure 28: UV-400 lamp system for photolithography.

Then masks are ordered to specialized companies that produce on special glass plate desired patterns.

The masks have been designed to improve and test the necessary amount of redundancy in order to be able to read the coded message. In this direction two different pattern have been designed:

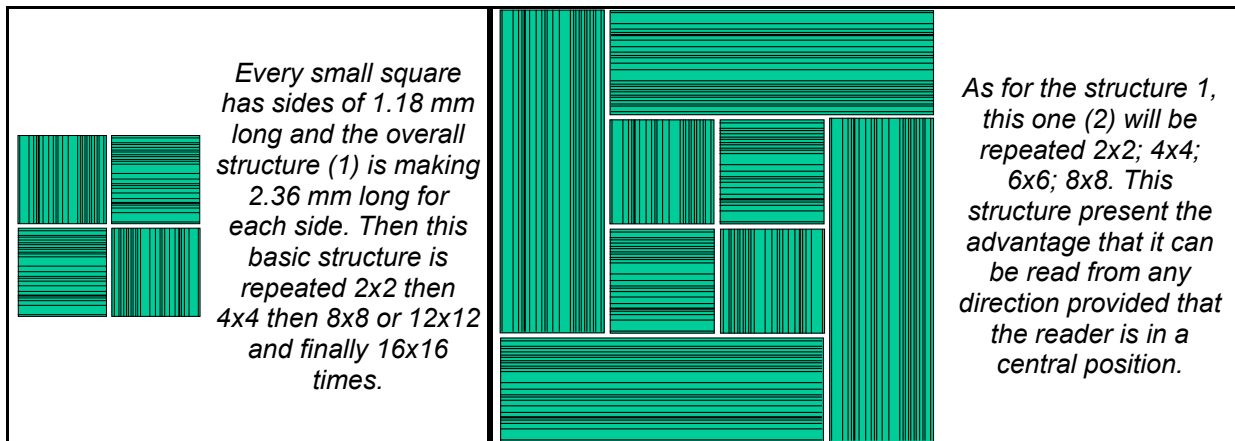


Figure 29: Drawing of the two basic structures (1 and 2) that are reproduced on the masks in different amount (2x2; 4x4, etc) depending on the necessary amount of redundancy.

The first tries for the photolithography consisted in getting familiar with the technique and establish the sensibility of the product (SU8-2002) and the key parameters to get good structures on the surfaces.

Figure 30 presents the standard procedure to make the structures on the photoresit polymer surfaces.

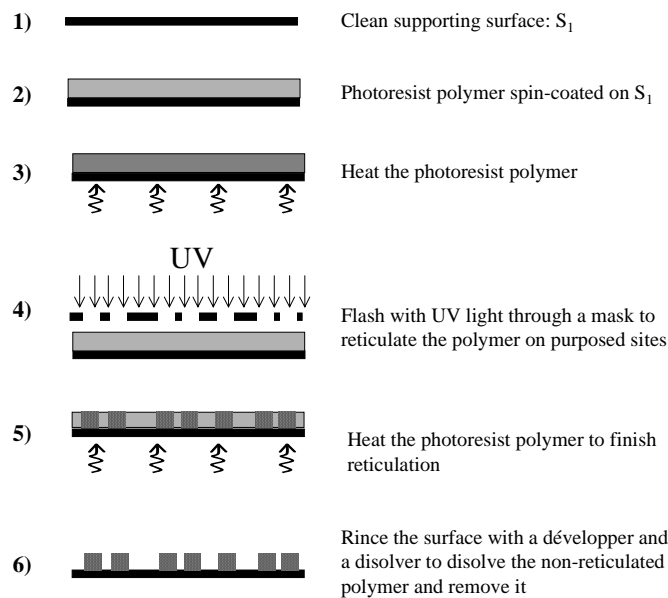


Figure 30: Adapted photolithography procedure.

The adjustment of all parameter showed that the contact between the mask and the polymer should be well performed (minimize the distance) in order to improve the quality of the image on the photoresist. Another important point was to perform the spin-coating with perfectly cleaned and filtered mix of SU8-2002 and SU8-2000 thinner to get homogeneous surfaces. Several months were needed to implement the system and adjust the parameters. Nevertheless several MAPs were produced with variable quality. An example is given on the Figure 31.

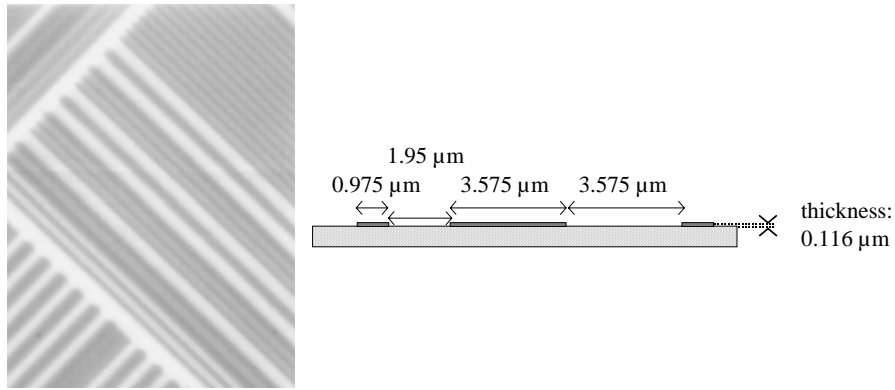


Figure 31: Zoom on a part of the first MAP (photoresist on a silicium wafer with a message encoded). Left: a photograph of approx. 80 μm large; Right: Transversal cut scheme of the wafer with the different thicknesses and band stretches that we desired.

All the stages of the Figure 30 require to be performed in clean conditions in order to avoid dust on the surface. But as our pattern are replicated and has a predictor-corrector encoding one can think that small defects on the surface will not affect the readability of the information. But stage 4 on Figure 30 required perfect contact between mask and surface. Figure 32 explains the detail of the problem.

The sketch a1 and a2 present the UV illumination with the mask. In practice, without clean room facilities, some dust particles are always deposited on the surface. Even particles which are about few microns or tens of microns prevent to have perfect contact between surface and mask. The resulting illumination in the bulk of the photoresist produces a decrease in precision. If the distance between two adjacent illumination places is small this effect is enhanced as can be seen in Figure 32-a2). This problem leads to heterogeneities in the low level of the surface. The distance between the top and the bottom of the surface is not anymore constant. Ideally it is necessary to have $\frac{1}{4}$ of the wavelength of the laser light to get a complete and perfect transition from white (intensity=1) to black (intensity=0) when passing from the top to the bottom of the surface (figure 32-c1). If the surface has a thickness value different from $\frac{1}{4}$ of the wavelength of the laser light, the result in intensity will be different (values between 0 and 1) as can be seen in figure 32-c2.

The decoding of the signal will then be very difficult as the threshold in intensity will probably be difficult to find.

In the defined process, the resulting MAP has to go to CRIF for Nickel electroforming. Then from the master in Nickel, surface replication was needed on the suitable polymers (see following part on the polymer tests). All these stages will probably add some deteriorations of the quality of the initial pattern.

Adding to these problems the usual inherent noise problem in signals, it was rather probable that the resulting surface would not be correctly decrypted. So it was decided to change the mask to a mask with a larger pattern.

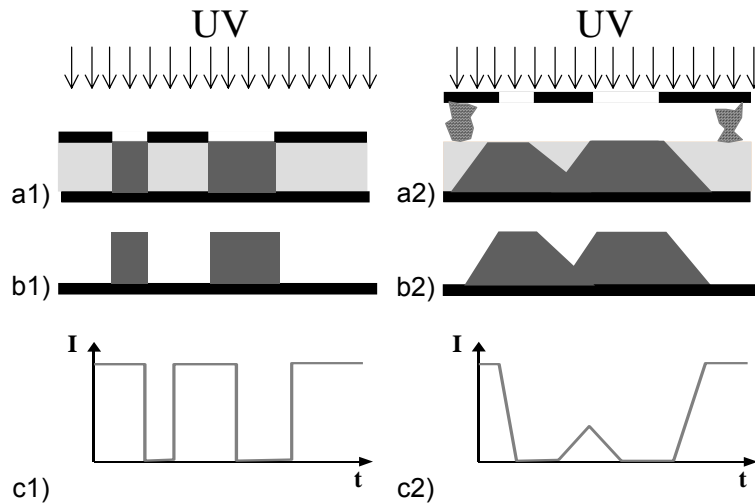


Figure 32: Stages of the photolithography in theory (left) and in practice (right). a) UV lightning; b) Resulting surface; c) Result in term of light intensity with the laser reader.

In the first mask the size of the smallest features were $0.975\mu m$. Beside this aspect it was also necessary to change the size of the wafer used as a MAP. The CRIF needed wafers of at least 6" diameter when in a first time the technique was developed with 3" wafer. The spin-coating adjustments had to be adjusted for this new diameter. It is important to notice it is much more difficult to spin-coat on large wafer that on small ones.

Beside the spin-coating problem, one has to notice that larger is the wafer stronger is the probability to get big dust particle on the wafer with all the problems that this implies (increased distance between mask and wafer with photoresist).

Figure 33 shows a sketch of the design of the mask. On the right the mask is divided in four regions (top-right, bottom-right, top-left, bottom-left). On each region the basic information is replicated a maximum number of time within the place allowed by the size of the wafer. The two left regions are simply different from the two rights by the fact that they are mirrored in terms of white/black lines or top/bottom lines. In other words, the design is exactly the same except that what are supposed to be black lines (with reticulated photoresist ie top features) will be white lines (without reticulated photoresist ie bottom features) and vice-versa. This is done to see the influence of the inherent problem explained before (figure 32). "White" and "black" lines have not the same size (figure 33 left). The two top regions are similar to the two bottom region except that every size is multiplied by two.

In this way this mask will allow us to cover a wide range of lengths in order to study and prevent the effect of the problem seen in figure 33.

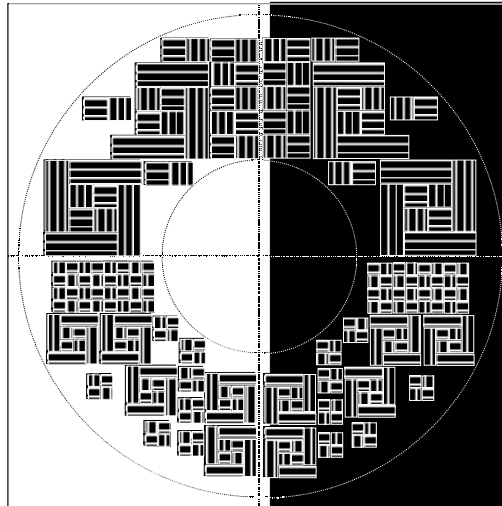
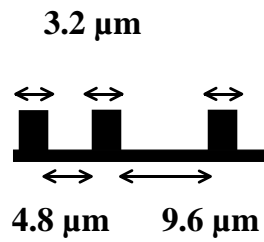


Figure 33: Left: dimensions of the lines for the two bottom quarter of the mask. Right: design of the mask. Results on the mask are taken with a microscope and presented in Figure 34 & 35.

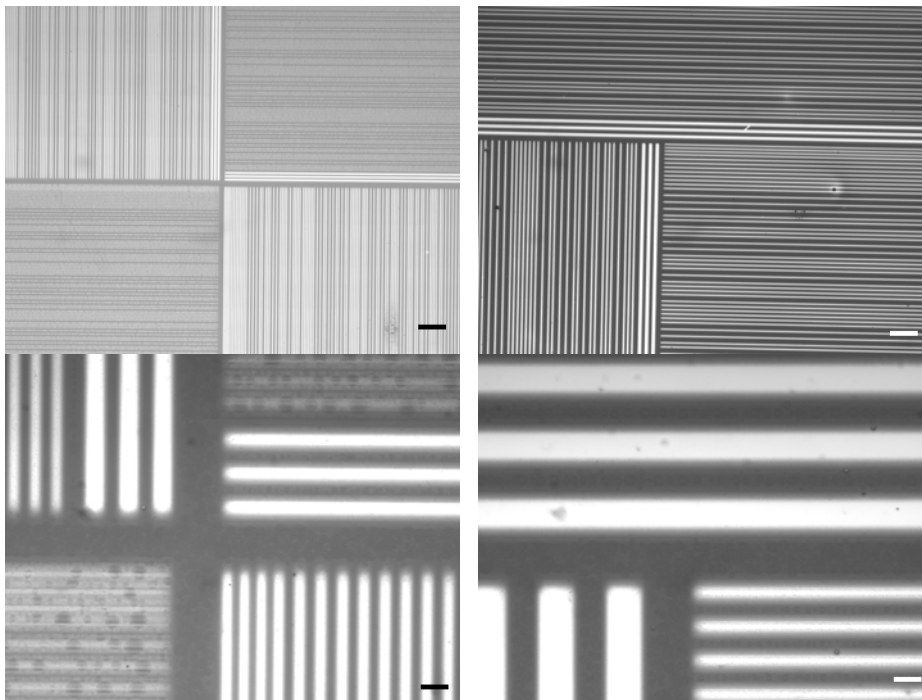


Figure 34: Photographs of details of the left part of the MAP (black background). Top: magnification 50x (bar is 100 μm); Bottom: magnification 500x (bar is 10μm). Left: features are 3.2 μm at smallest; Right: features are 6.4 μm at smallest.

On figure 34 grey zone shows a height which is between top (black) and bottom of the wafer (white). It is clear that when features are bigger the problem presented in figure 35 is less important and will probably not prevent from reading.

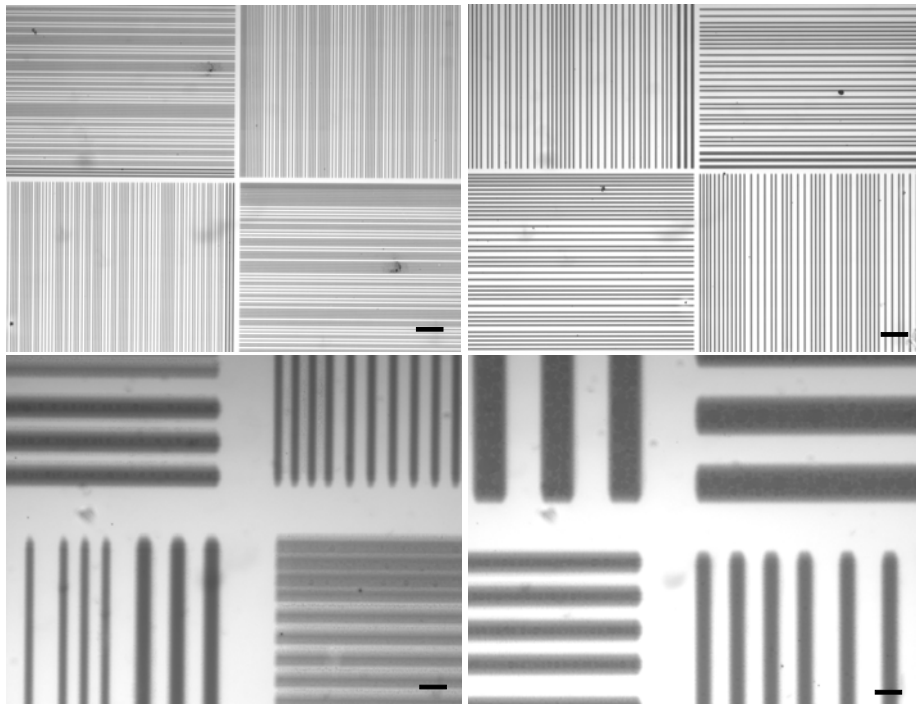


Figure 35: Photographs of details of the right part of the MAP (white background). Top: magnification 50x (bar is 100µm); Bottom: magnification 500x (bar is 10µm). Left: features are 3.2 µm at smallest; Right: features are 6.4 µm at smallest.

Figure 35 shows that the white background (corresponding to the black background of the mask) gives better results than the black. This makes sense since this corresponds exactly to the situation of figure 34-left with dimensions multiplied by two. While the one in figure 34 represents the exact inverse of this situation. In other words in figure 35 the smallest features are holes (more problematic) while on figure 34 the smallest features are hills (easier).

The spin-coating produces thicknesses with gradient from the centre to the border of the wafer. As the size of the wafer is too big it is not possible to get perfectly homogeneous thicknesses on the entire wafer. Ellipsometric measurements on the resulting wafer have been performed to get the value of the thickness with very high precision (Angstrom precision). The resulting thicknesses are given in figure 36-bottom-left. From the centre to the border the thickness passes smoothly from 103, 108 to 130nm.

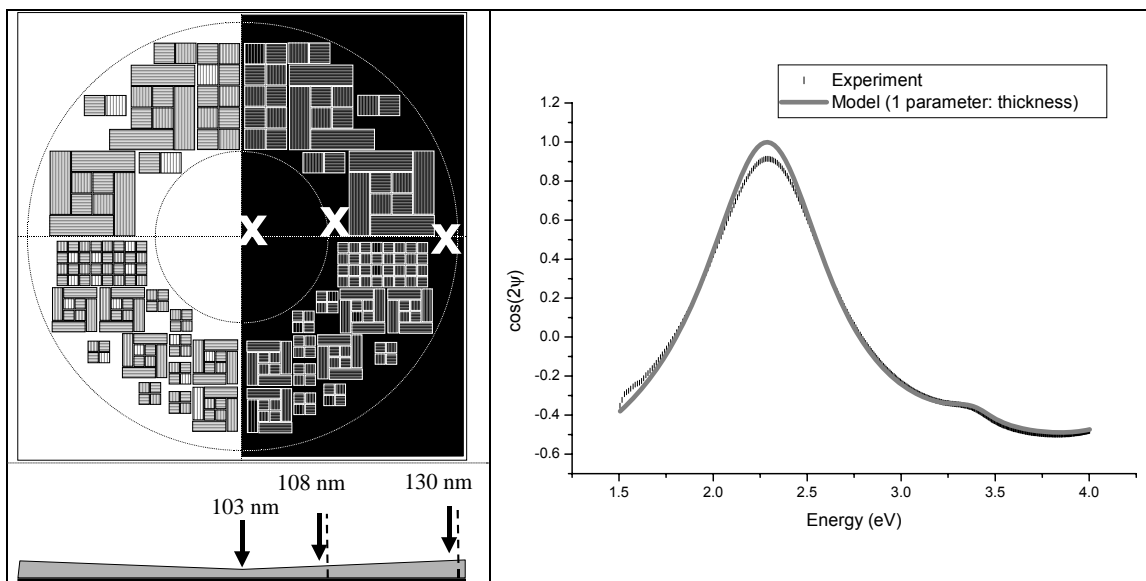


Figure 36: Thickness of the layer on the MAP. Top-left: positions where measurements were performed; bottom-left: thicknesses measured; Right: example of result in terms of ellipsometric parameters.

Thus it is expectable that there is on the MAP a place where the thickness is exactly or very close to $125nm$, the value necessary to have the best results in terms of reading ($1/4$ of the wavelength).

2.2.3. MAPs replication

As the type of micro-structuration to be embedded in the object is chosen, it is necessary to propose different ways of embedding which are feasible at the industrial scale and to check the replication capabilities of the different techniques.

As previously stated, the information encrypted and embedded in the parts are included in MAPs. A MAP is a set of parallel grooves similar to a micro bar-code. Each MAP is identical and holds the same information. As the number of these MAPs is high, the redundancy of the information is high and allows some degradation of the MAP during the life-time of the part.

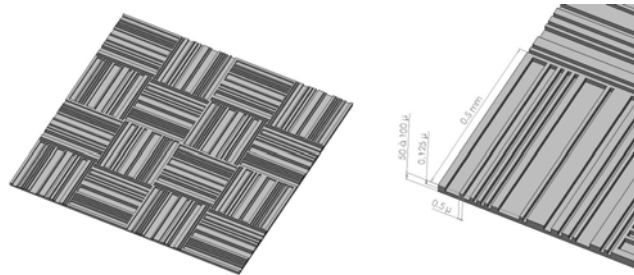


Figure 37: Patch and grooves.

The dimensions of the grooves are a width of $500nm$ and a depth of $125nm$. These dimensions are the typical dimensions used in the CD's industry. The main role of CRIF in this task was to find and to validate a technological and economical way to put these patterns onto the surface of a thermoplastic part. The ways proposed by CRIF are the following:

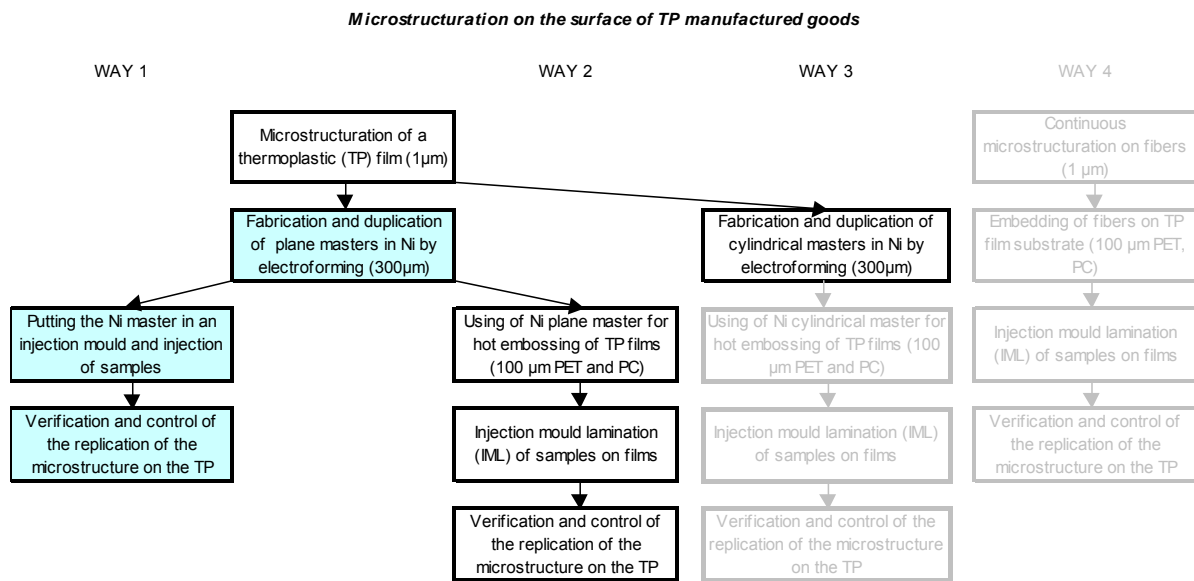


Figure 38: Different ways to embed the information

The first way is the most classical. The second way is more innovative. Both require manufacturing a negative pattern in metal which is used in an injection mold (way 1) or in a hot-embossing press (way 2).

The first way requires putting the negative pattern of the micro-structuration, which is called a "master", in an injection mold. This master is made by electroforming of Nickel on a "premaster" in resin (lithography on photoresist). The photoresists were made by UMH.

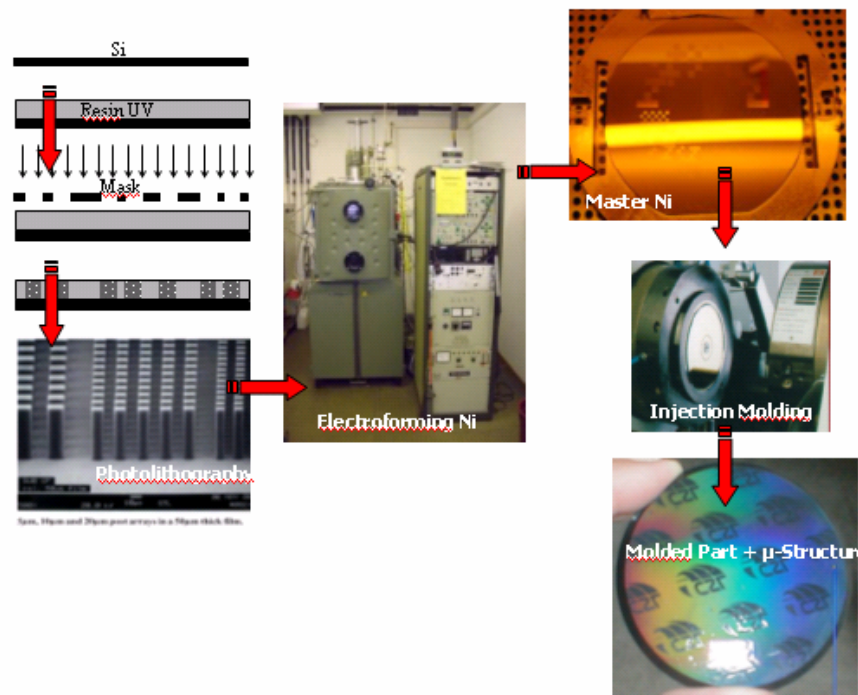


Figure 39: Replication technique: from the photo-resist to the replicated structure on a thermoplastic molded surface.

Before getting the first trials of photoresists from UMH, CRIF made first tests trials with an existing Nickel master with nearly the same characteristics than used: The widths of the grooves are $500nm$ and the depth $175nm$ (thus higher than the final product).

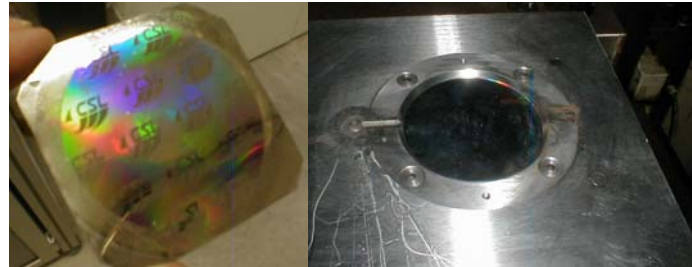


Figure 40: “Test” Ni-master and insert in the injection mold

This master was put in a mold and different materials were tested: PC/ABS, PMMA, ABS, HiPS, PC, PP and PA6.



Figure 41: Replication by direct injection molding (PC/ABS)

The first tests showed that the capability of replication was good with PC, PC/ABS and PMMA. The figure 42 shows the height of peaks/valleys on the PC/ABS sample in comparison with the initial depth on the Ni master (Distance between the two dark lines). The replication level is more than 70 %.

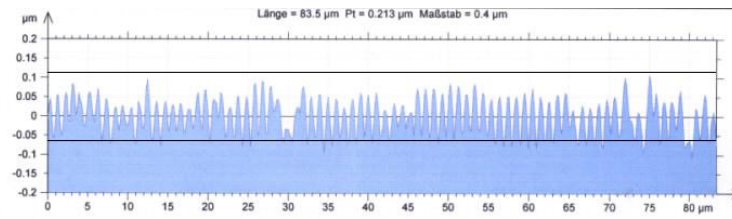


Figure 42: Results on PC/ABS

ABS and HiPS showed poor results due to the elastomeric phase of the materials (butadiene). Some TPE (thermoplastic elastomers) were tested too and showed very bad results. After these first trials, Multitel and CRIF decided to embed the microreplication on a part able to be read on a modified CD reading device. A CD mould was acquired to perform this.

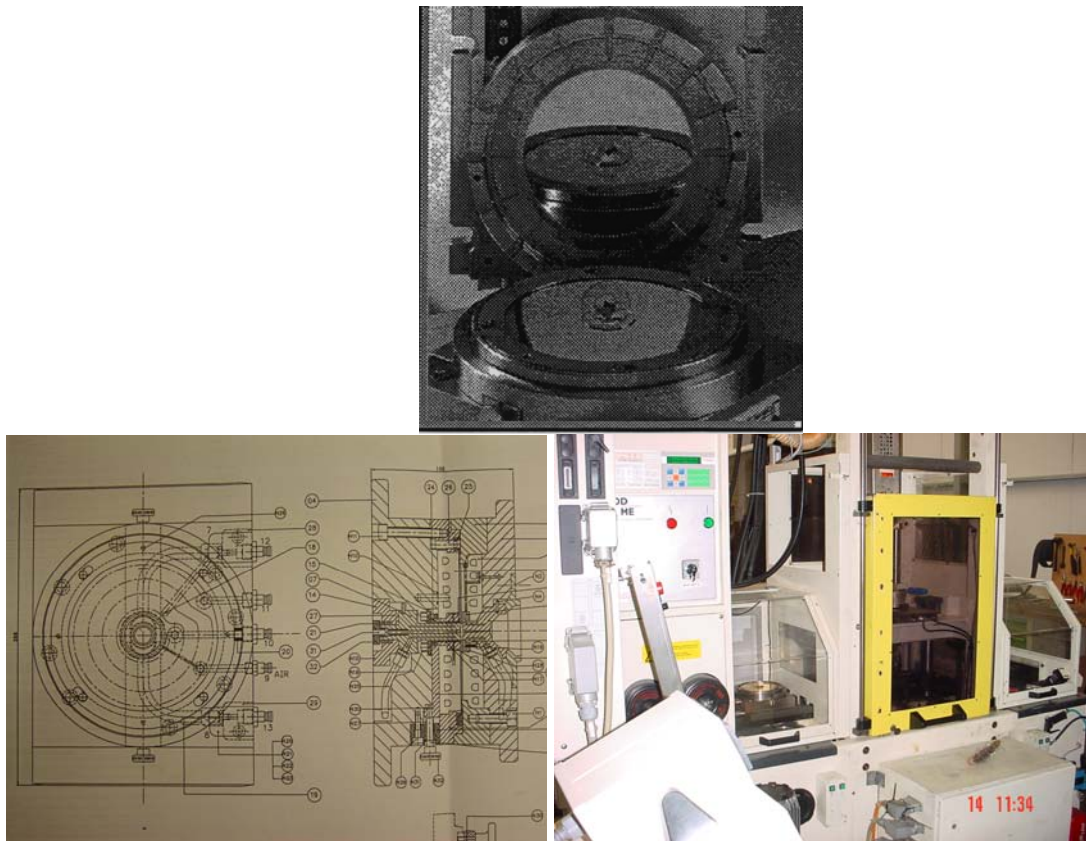


Figure 43: Mold for CD

CRIF has worked on two different kinds of masters provided by UMH and corresponding to two different kinds of SU-8 patterns on a silicone wafer (diameter 6”).

The AFM technology used by CRIF to check the replication capabilities and also the quality of the SU-8 patterns, is the Easyscan™ AFM from Nanosurf®. The EasyScan™ AFM is the perfect tool for routine surface analysis measurements. It allows fast in-situ non-destructive high resolution process control. A break-through in scanning technology is the new electromagnetic scanner. Problems with nonlinearity, creep or aging of piezo actuators which are usually used in standard SPMs are things of the past.

The EasyScan™ AFM is the perfect tool for:

- Surface quality control,
- Corrosion investigations,
- Controlling surface finishing,
- Determining impurities,
- Entering the submicron world with ease.

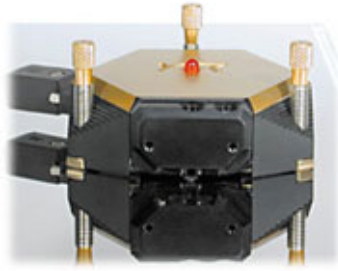


Figure 44: EasyScan™ AFM

EasyScan™ AFM operating features are:

- A portable, compact system, fully computer controlled,
- Can be operated using a laptop computer,
- Stand-alone suited for small and large samples,
- Motorized automatic sample approach,
- Connects to standard computer serial port (no interface card needed).

Main specifications are:

- Maximum scan range $100\mu m$,
- Maximum Z-range $20\mu m$,
- Resolution-XY $1.5nm$,
- Resolution-Z $0.3nm$,
- Z-noise level (RMS) $< 1nm$,
- Sensor radius $< 50nm$,
- Scanner mass $350g$,
- Feedback loop bandwidth $3kHz$,
- Motorized automatic sample approach,
- No dangerous high voltage used.

EasyScan™ AFM has been used to perform checking on two types of silicone wafers with SU-8 patterns provided by UMH.

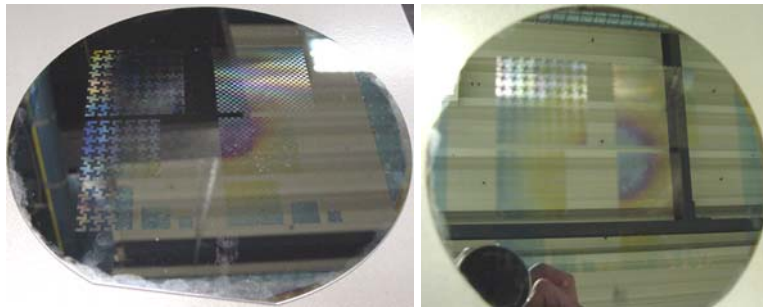


Figure 45: Wafers.

Investigations were performed with the AFM positioned directly on the wafer, keeping the target zone away from the AFM structure. All components were placed on an anti-vibration table.

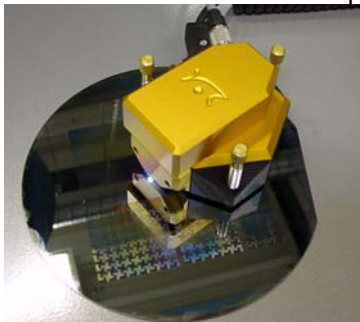


Figure 46: AFM on the wafer.

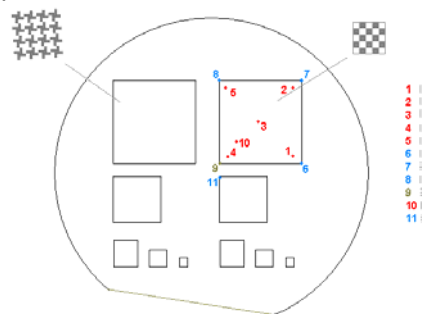
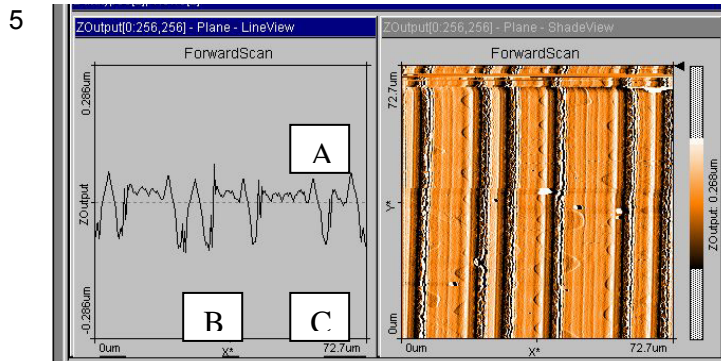


Figure 47: Locations of the measurement points.

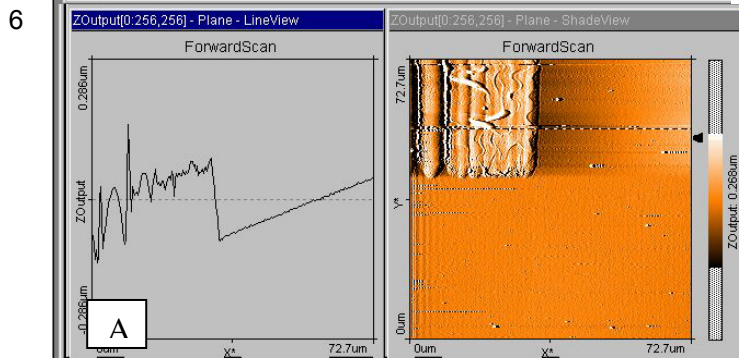
The most relevant results are given on the following table. These results have oriented the decision to ask to UMH to provide an improved wafer, due to the average low values of the depth of the existing μ structure

1		<p><u>Remarks :</u> Positive waves only</p> <p><u>Measurement :</u> Height A: 60nm Period A: 3.12μm Height B: 123nm Height C: 300nm</p>
2		<p><u>Remark :</u> Positive and negative waves</p> <p><u>Measurement :</u> Height A: 36nm Period A: 3.1nm Height B: 177nm Period B: 6.55nm</p>
3		<p><u>Remark :</u> Negative waves only</p> <p><u>Measurement :</u> Height A: 50nm Period A: 2.9nm Height B: 187nm</p>
4		<p><u>Remark :</u> Negative waves only</p> <p><u>Measurement :</u> Height A: 68nm Height B: 271nm Period B: 9.65nm</p>



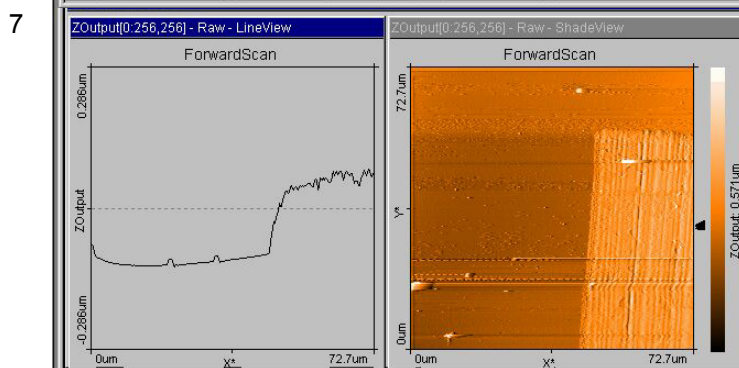
Remark :
Negative waves

Measurement :
Height A: 21nm
Period A: 3.03nm
Height B: 162nm
Period B: 6.82nm
Period C: 19nm



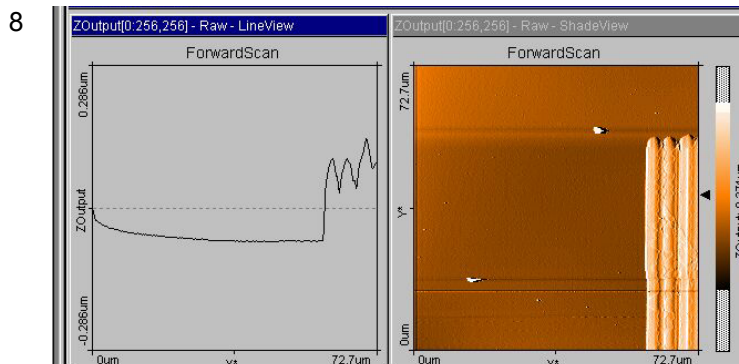
Remark :
Surface defects

Measurement :
Height to flat bottom: 178nm
Height A: 121nm



Remark :
Waves low level

Measurement :
Height to flat bottom: 143nm



Measurement :
Height to flat bottom : 169nm
Height: 69nm
Period: 3.98nm

AFM Checking of Wafer 2

The locations of the measurement points on the new wafer provided by UMH are summarized on the picture 49.

Point	Orientation	Zoom	distance between grooves	heights of main peaks
			μm	nm
1		No zoom	25	40
		Zoom 23	-	52
2		No zoom	25	94
		Zoom 25	-	109
3		No zoom	8 & 12,5	54
		Zoom 38	-	55
4		No zoom	-	19
		Zoom 30	-	19
4b		No zoom	12.5	21.8
		Zoom 30	-	21.4
5		No zoom	8 & 13	92.5
		Zoom 30	-	106
6		No zoom	8 & 13	103
		Zoom 30	-	103
7		No zoom	16 & 25	110
		Zoom 20	-	109
8		No zoom	15 & 25	100
		Zoom 25	-	102

Figure 48: Results of the measurement are given on following table.

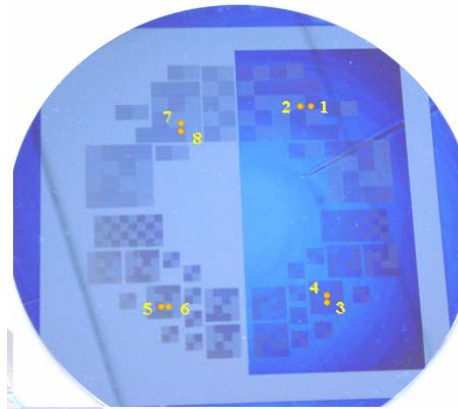


Figure 49: Points of measure.

Main conclusions:

For measurement points 1 to 4:

- Quality of the results is depending on the position but also on the orientation (for a given position)
- Distances between hills are easily measurable, depths are more difficult to measure precisely
- A zoom technique allows to improve the quality measurement of the depths
- point 4 presents some defects

For measurement points 5 to 8:

- Quality is highly better and the depth of the hills are reaching the target of 125nm

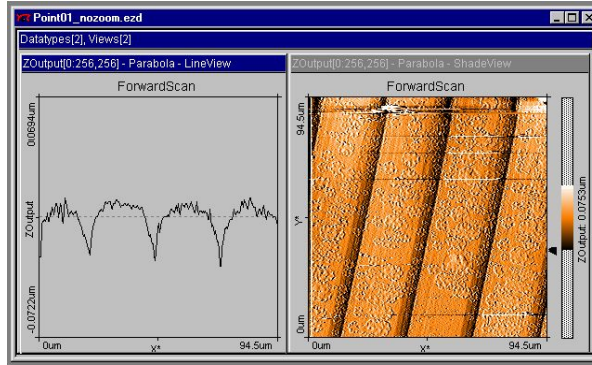


Figure 50: Point 1

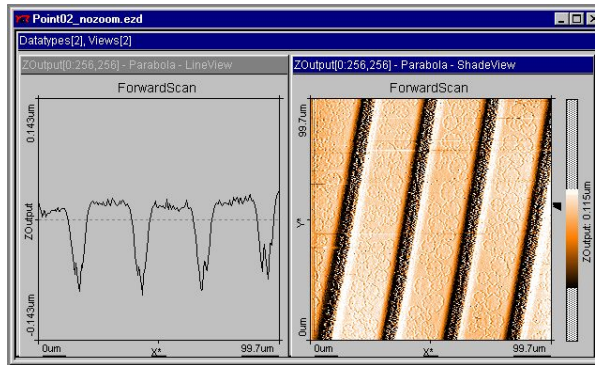


Figure 51: Point 2

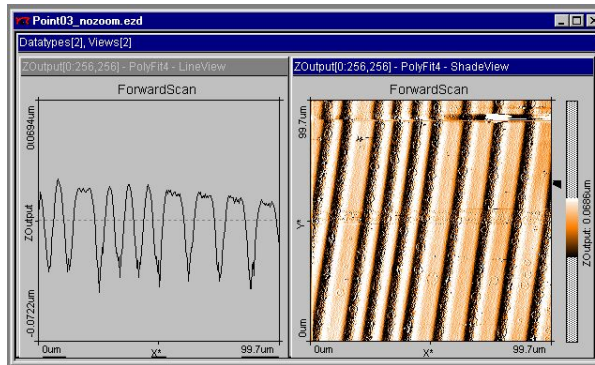


Figure 52: Point 3

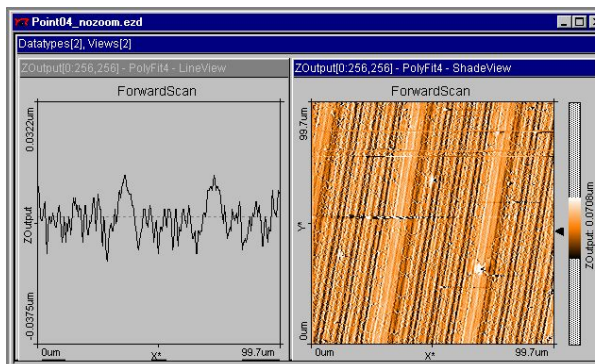


Figure 53: Point 4

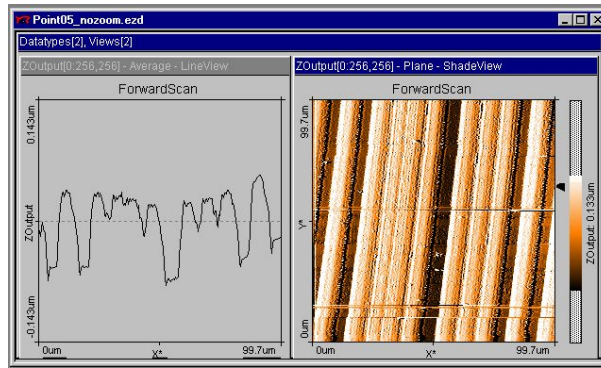


Figure 54: Point 5

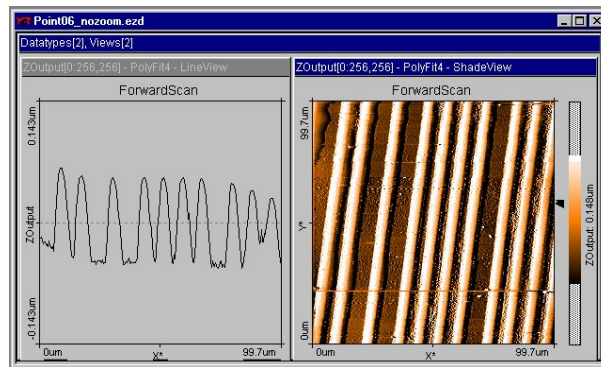


Figure 55: Point 6

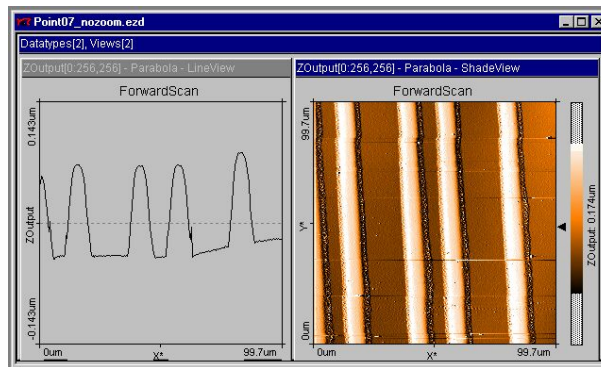


Figure 56: Point 7

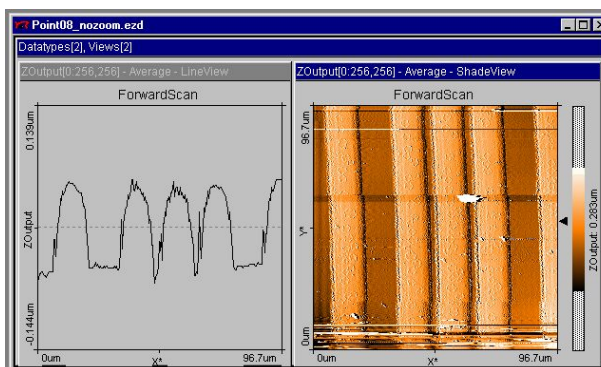


Figure 57: Point 8

Starting from the Wafer 2 provided by UMH (highest quality), CRIF has subcontracted the manufacturing of a Nickel shim compatible with the dimensions of an existing CD injection mold. Most important steps of the manufacturing process are illustrated below. Separation of the Ni shim from the silicone wafer has resulting on residual SU-8 photoresist on both Ni shim and silicone wafer but not affecting the nickel pattern. Further cleaning of the Ni shim was performed using ultrasonic bad

(isopropanol, acetone, MEK)

Ni-Start layer deposition by CVD process



Figure 58: Resulting silicone wafer Ni Shim separation



Figure 59: Ni Shim

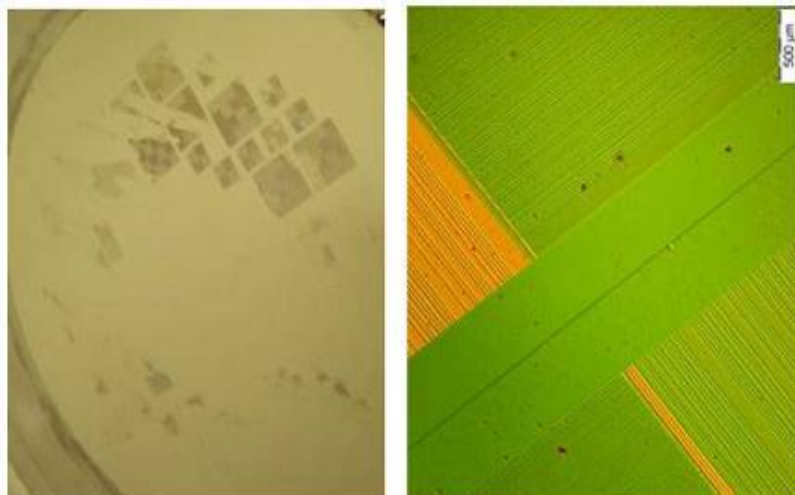


Figure 60: Pictures of the MAP.

Concurrently with the Ni shim manufacturing, CRIF has optimized the setup of an existing CD injection mold modified and customized to be compatible with the Ni shim.

A fully operational mold has been developed and able to produce high quality CD-like plastic substrates (initially in polycarbonate) with embedded micro-structuration.

2.2.4. Optical reading device

The optical reading device is based on a CD-player. The OPU is used to retrieve the signal from the photodiodes without removing the focus system. An electronic card is connected to the OPU. The signal of the photodiodes is amplified and processed in order to distinguish the pits and the lands and so to distinguish the logical bits and retrieve the information.

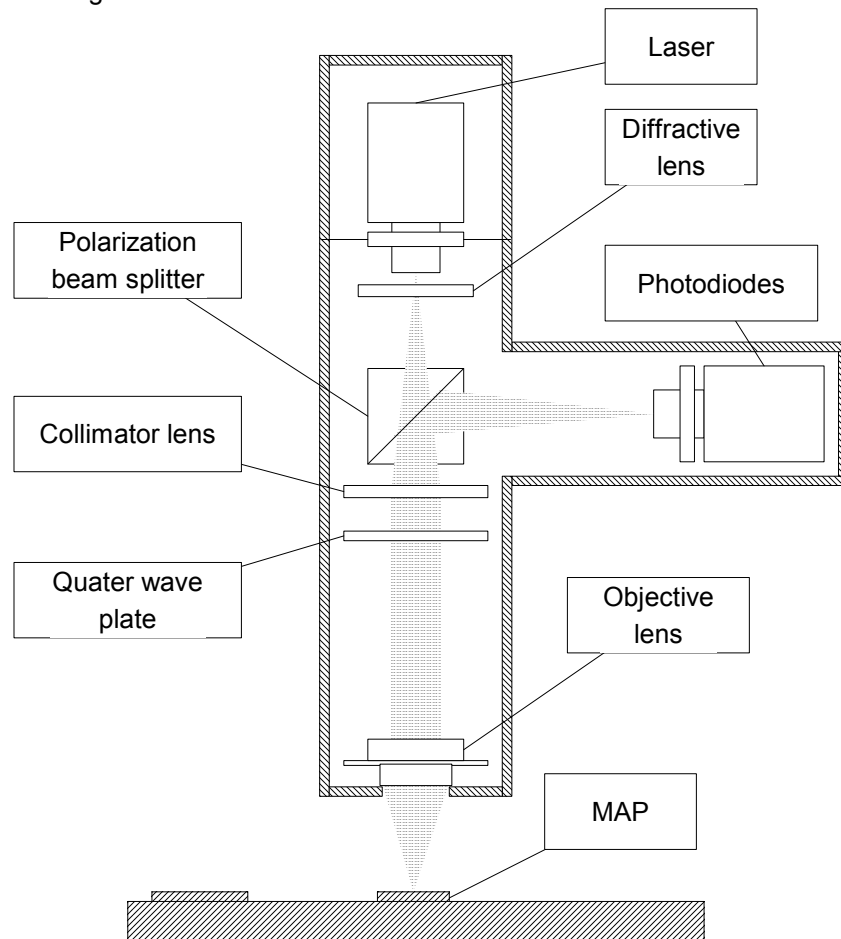


Figure 61: Schematic of an optical pickup unit.

The reading device must sweep at least one MAP. We can consider two modes of reading: circular or linear. The study shows that the circular mode is the most adapted (figure 62). For a tiling of square MAP, the reader can sweep 2.82 MAPs with the linear mode but 9.85 MAPs with the circular mode.

Also, considering the mechanical aspect, it is easier to control the speed of a rotary unit. Consequently, the circular mode is selected, the optical pickup-unit moves along a circular trajectory on the surface with a fixed radius at a constant speed.

The first approach to design the optical reading device is to use a CD-player and to remove its electronic card. For the first prototype, the reader is fixed but the object is mobile, like a disc and a CD-player. Instead of using a disc with music or data, a disc with a tiling of MAP is "read". The disc has only one layer. The metalized and the polycarbonate layers are removed because it is not possible to add such layers on a real object (a metalized layer reflects light and changes the aspect of the object).

Linear mode		Circular mode	
Length of reading	Average numbers of swept squares	Diameter of reading	Average numbers of swept squares
4	0.63	4	3.16
6	1.07	6	5.05
8	1.51	8	6.42
10	2.14	10	8.14
12	2.82	12	9.85
14	3.19	14	11.41
16	3.78	16	13.14
18	3.85	18	14.8
20	4.95	20	16.58
22	5.17	22	18.08
24	6.38	24	19.85
26	6.45	26	21.41
28	7.01	28	23.09
30	6.81	30	25.02
32	7.76	32	26.43
34	8.3	34	28.05
36	8.8	36	29.76

Figure 62: Study of the reading mode

The new electronic card is made of three blocks: Focus control, signal RF and motors and actuators control. A classical CD player is summarized by the following functional diagram:

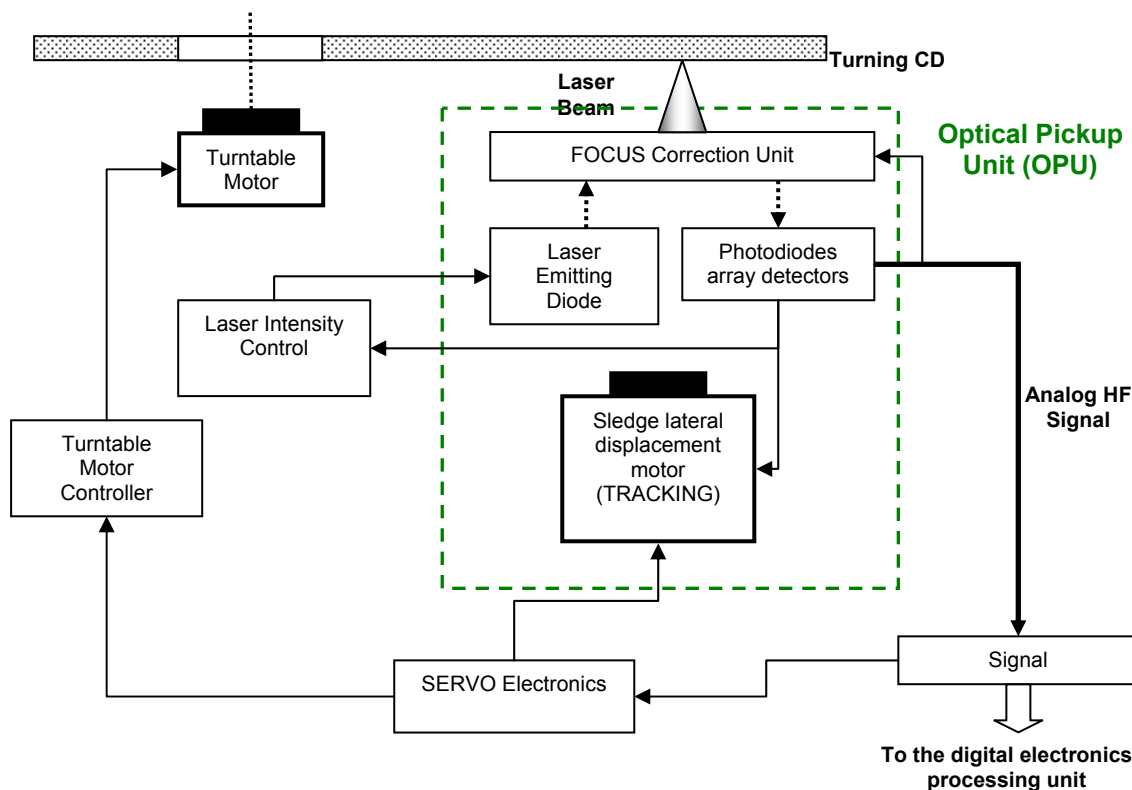


Figure 63: Principle of an optical pickup unit.

The signal processing unit is removed. The servo control loops for the turntable motor controller and the sledge lateral displacement motor are replaced by a user configurable device. The new signal processing unit is a HF signal normalizer and equalizer.

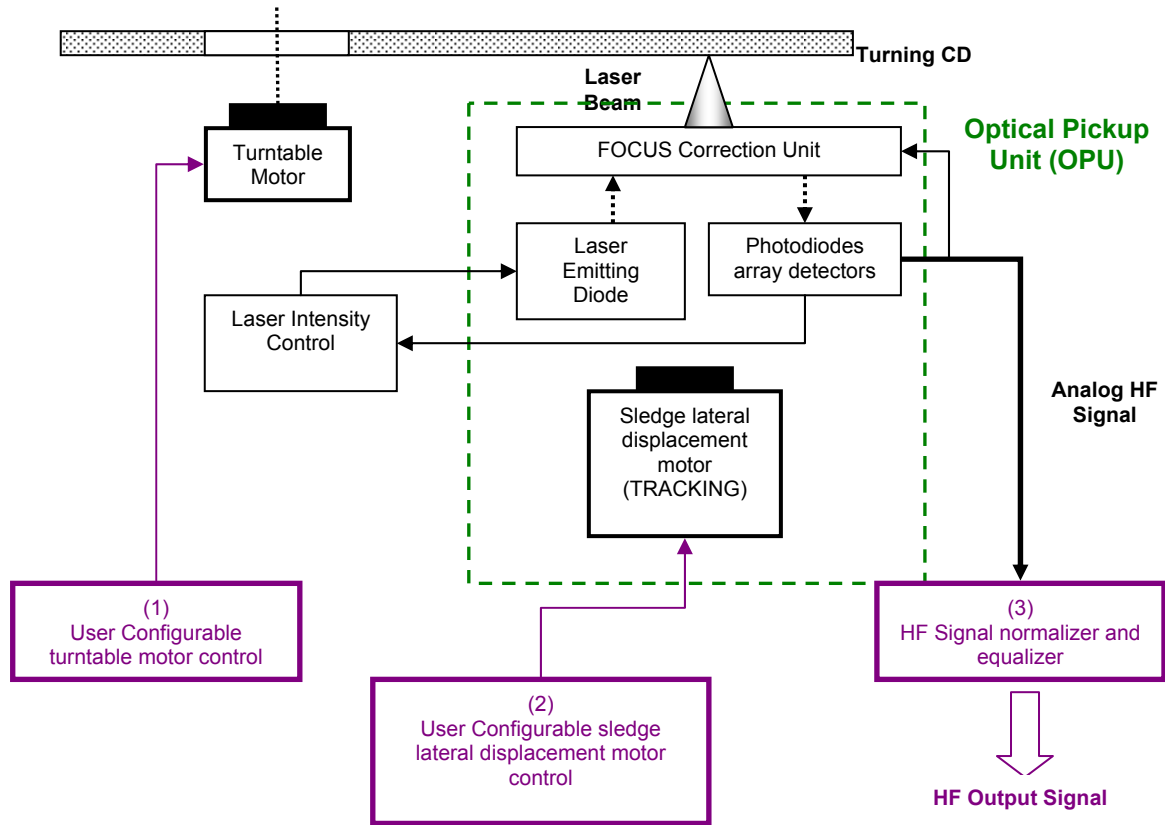


Figure 64: Principle of the new optical pickup unit.

The focus control depends widely from the conception of the OPU itself. The OPU used is a VAM1201 from Philips (figure 65).

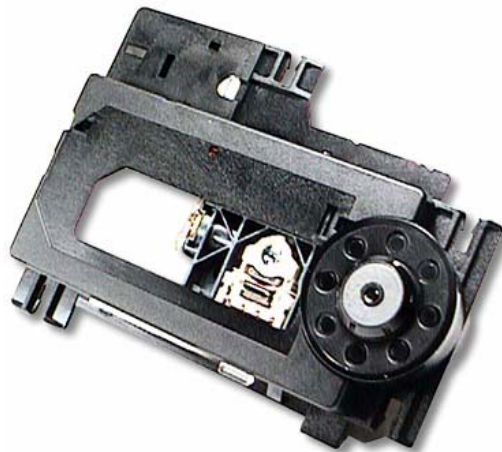


Figure 65: VAM1201 OPU.

The focus is control thanks to the photodiodes signal. A feedback loop sends the focus error to the focus actuator which moves the lens of the OPU upwards or downwards. The focus error is obtained by applying the single edge Foucault knife.

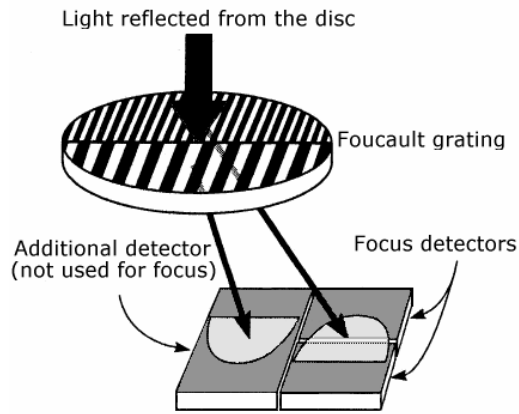


Figure 66: Edge Foucault Knife's principle.

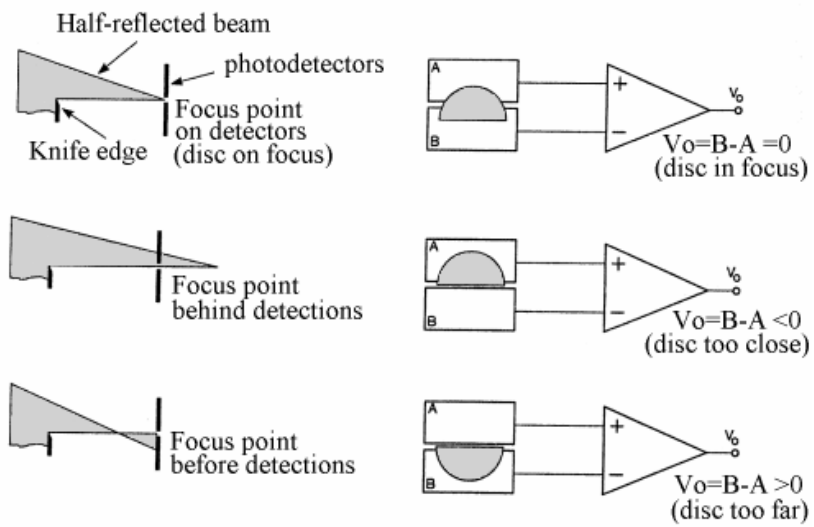


Figure 67: Focus control.

The focus control always keeps the lens of the optical pickup unit at the same distance from the surface of the disc. On the VAM1201, the lens can move between -0.8mm to 0.8mm. A test CD is used to detect if the electronic card works correctly.



Figure 68: Test CD.

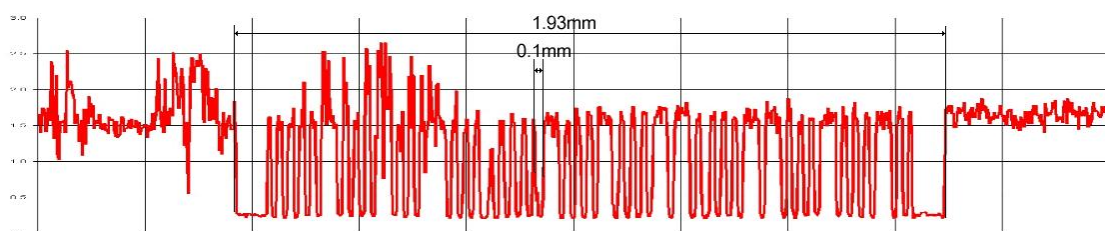


Figure 69: Signal of the photodiodes

The lands and pits are easily recognizable. The noise on the top of the signal comes from the surface of the CD. These tests succeed but the depth of the pits is 0.5mm and the disc with the tiling of MAP has a pit's depth of 125nm .

From the reading test of the replicated surfaces (MAP) the resulting surface had pattern but it was not possible to read with the adapted CD reader we produced.

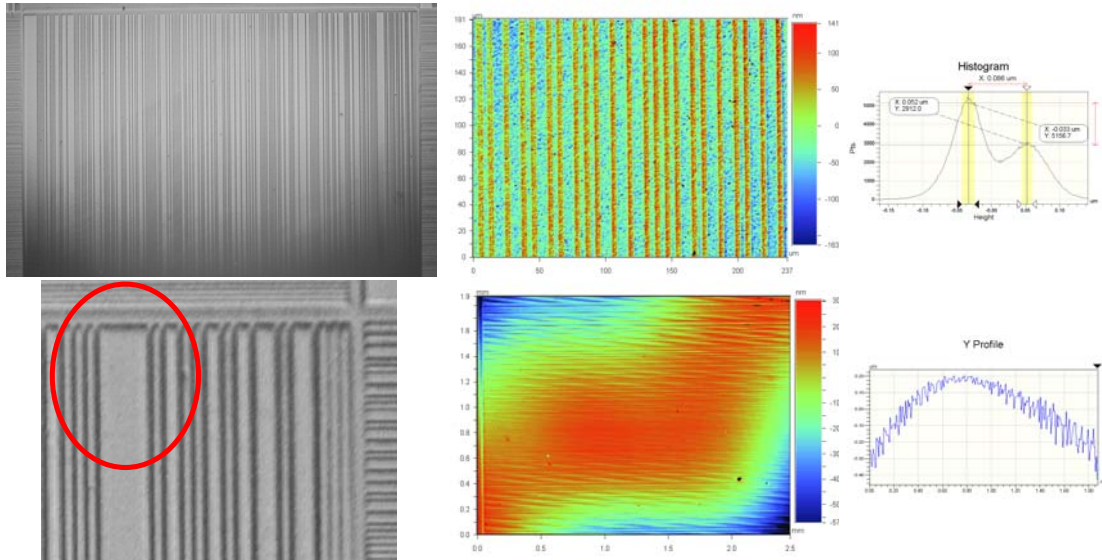


Figure 70: Problem related to the concept of linear MAP. Left: picture of a linear MAP (top: whole picture with apparent detailed features; bottom: zoom in a zone where various lines should be present); Middle: topographic profile at different scale: Top (size: 0.23mm) and bottom (size: 2.3mm) and the measurement related to those (Top right: histogram showing 2 distinctive heights; bottom right: transversal cut to the lines on the surface showing the variation in height).

Figure 70 shows the inherent problems of the linear MAP conception. First of all very small features were difficult to reproduce for the smallest scales. This means that to reproduce the message large MAP where necessary jeopardizing the anti-counterfeiting argument to make the features as small as possible, ie in the micrometer range. Second, even when reproduction was good (Figure 70-middle top) the mean height of the surface is varying a lot (Figure 70-middle bottom).

Due to several technical problems, the disc with MAPs can't be scanned. The main problem is the poor quality of the photodiodes signal. As the metalized layer is removed, the power of the reflected light's beam is not enough powerful to interfere with the incident light. Consequently, the RF signal cannot be visualized and the focus cannot be controlled.

To reduce this problem, the best solution is to add a metalized layer on the MAP. But, this deteriorates the aspect of the protected object.

Finally the amount of information available in a linear MAP is much smaller than on one designed on a 2D basis. Thus the whole MAP size could be increased with a better designed, a 2D designed.

2.2.5. Design of the new MAP

From this point on, examination of the surface allowed noticing that with simple camera devices and right illumination it was possible to detect and recognize feature on the surface by means of imaging instead of reading with a CD-like system.

Thus the decision to move the project from a CD-like technology designed to a 2D basis was adopted (but always keeping the technological point of view of creating the surface with the MAP).

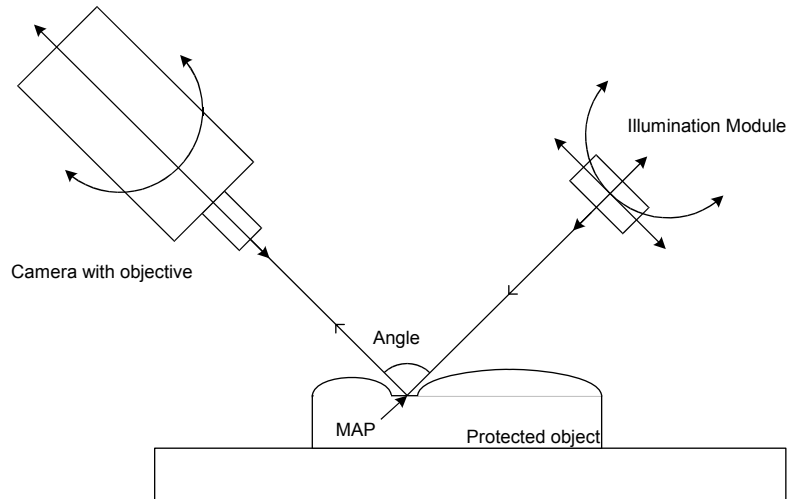


Figure 71: Schematic of the new reader

The new MAP is now a 2D barcode (Datamatrix). Datamatrix is a public domain 2D barcode developed by RVSI Acuity CiMatrix. This matrix symbology is able to pack a lot of information into a very small space. An error correction code is used (Reed-Solomon) to guarantee accurate information decoding even under difficult reading conditions. The symbol can store between 1 and 3116 numeric or 2335 alphanumeric characters.

According to the authentication protocol, the MAP's size is 44x44 dots where you can embedded 144 data bytes and 56 bytes of error-correction code (figure 72).



Figure 72: Example of Datamatrix

2.2.6. Photolithography of the new MAP

Nothing was changed and the photolithography technique was kept as nice features at tens of microns were possible.

The success of the new designed, in terms of creation of the surface, replication of the surface on the right polymer support and the reading of the message on the surface at a micrometric scale allowed the consortium to start a patent registration procedure. Thus some sensible details which are unnecessary to the understanding of the work done will not be mentioned in the present report also due to space constrains.

On a CD shape and size basis (due to electroforming constrains) several Datamatrix were replicated at various dimension (Figure 73).

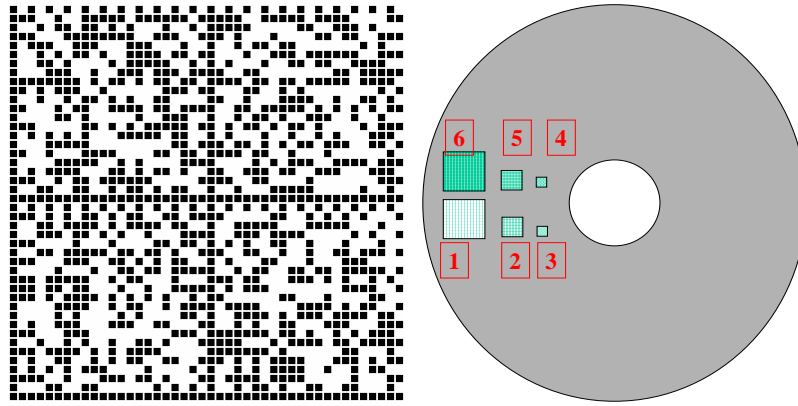


Figure 73: Datamatrix pattern that had to be replicated at different scales on a CD (left).

The patterns 1, 2 & 3 are the negative of respectively the patterns 4, 5 & 6 (all hole of 1 are pit on 6 and vice versa). The two patterns 1 & 6 are twice bigger (in all dimensions except the height which is uniform all along the CD) than the 2 & 5 which are themselves twice bigger than the patterns 3 & 4. The resulting examples of image of the whole CD are given in figure 74. When measuring precisely the topography of the patterns the result can be seen on Figure 75. It can be seen that the best features are the biggest one. The patterns 3 & 4 even if much less well reproduced than the other present almost enough right points of the Datamatrix well reproduced to keep the message. In fact due to redundancy of the message the quality of the pattern has not to be perfect to be useful for the reading and recognition of the message.



Figure 74: Picture of the CD at different illumination. Left: classical illumination; Right: illumination with the right angle that allow to see the patterns at different scales.

To be readable the pattern has to be taken from an easy and cheap device and not an optical profilometer which cost more than 80000 euros. Thus the pattern has to be recognized with a simple still camera.

Results of this can be seen on figure 76. As expectable the images 1 & 6 are the best while the 3 & 4 are not readable with the objective and camera we used. This allows us to determine the limit in term of size of pattern.

The whole pattern with the necessary amount of redundancy and replication (the pattern is then reproduced several times on the surface) has a size below $1mm^2$. With such size almost any plastic good (using the right plastic as surface polymer, see below) can be stamped (mobile phones, sunglasses, etc). It is sufficient that the good present a zone of $1mm^2$ which is flat (or almost) to be secured by this method.

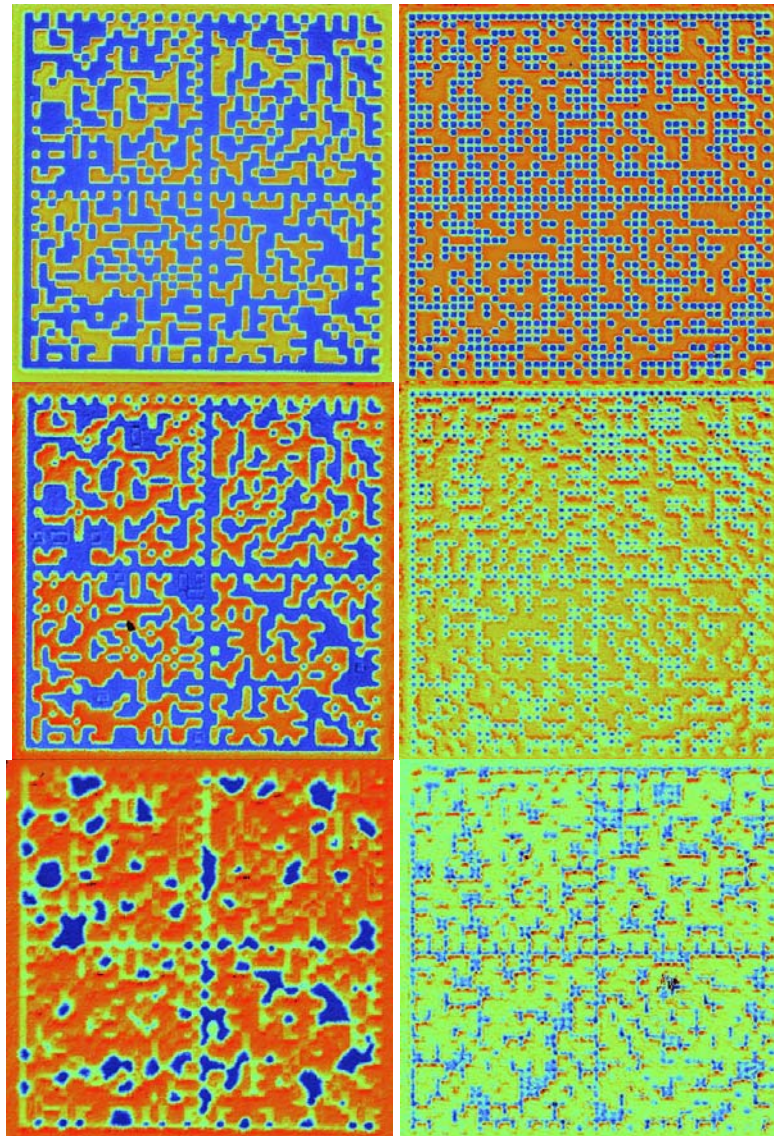


Figure 75: Topographies of the 6 patterns at different scale (from top to bottom: each feature is divided by 2; top 1 & 6; middle 5 & 2; bottom: 3 & 4). Left row is negative of right row.

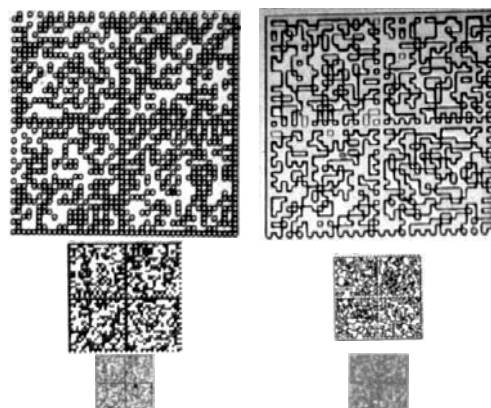


Figure 76: Images of the 6 patterns at different scale (from top to bottom: each feature is divided by 2; top 1 & 6; middle 5 & 2; bottom: 3 & 4). All images are made with the same objective.

2.2.7. Polymer tests for replication

The CRIF performed replication of a sinusoidal ($1\mu m$ wavelength) pattern on various polymer surfaces in order to see which polymer could be used for the final product. Imaging of the replicated structures

for each polymer were performed at the CRMM with the optical profilometer. The measurements were performed on 5 different points of each polymer plate in order to verify the homogeneity of the results. Seven polymers were thus tested: HIPS (polystyrene), PC (polycarbonate the one used for CD), ABS, PMMA (polymethylmetacrylate), PA (polyamide), PP (polypropylene), PC/ABS. Figure 77 are showing two examples and a table with a summary of the results of the quality of the replication.

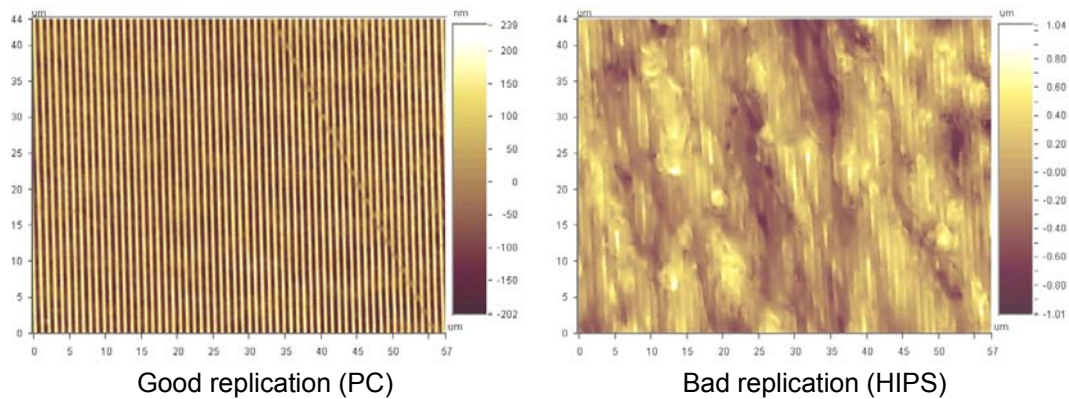


Figure 77: Example of replication.

Polymer	PP	PMMA	ABS	HIPS	PC/ABS	PC	PA
Quality	Medium	Very bad/Good	Bad	Null	Very bad/Good	Medium/Excellent	Very good

Figure 78: From this table the preferred polymer to replicate the message encoded in the MAP is in order of preference: PC, PA, PMMA. The HIPS and ABS should be avoided.

From this result all the replication on CD were performed on PC in order to better evaluate the sizes and technologies suitable for the application foreseen in this study

A new Ni shim were manufactured corresponding to the new MAP and similar microreplication tests were performed (with ABS material). Geometrical details about the Ni-shim, original mask frame, Si wafer and plastic molded substrate are given in figure 79.

During the manufacturing process of the Ni-Shim, solutions were founded for solving the problem of adherence between Ni and Su-8 using an Au-layer. Details about the manufacturing process are given below

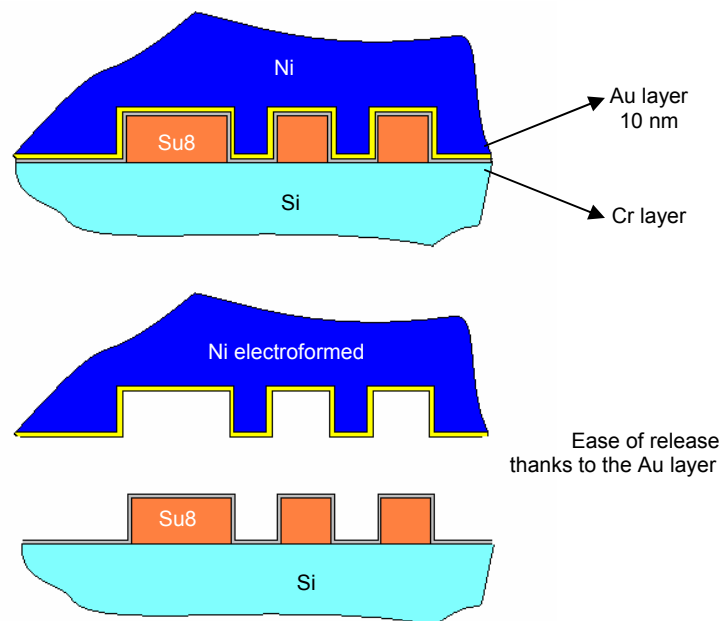


Figure 79: Manufacturing schematic

Resulting Ni-shim is illustrated at the following picture



AFM and SEM measurements were performed on the Ni-Shim and the micro-structured ABS parts. A very good replication capability has been demonstrated

Main conclusions are given below :

- Approximate drop of the details depth due to manufacturing of the SU8 master:.,
- The replication technique (injection moulding) is reliable to produce a legible pattern (drop of ~ 30% in details depth),
- The medium size of pattern is a good compromise :
 - Difficult to detect to the naked eye,
 - But legible with low cost optical device.

The second way consists in using a Ni-master to perform the hot embossing. The hot embossing allows printing the micro-structuration on a thermoplastic film by pressing the master on it. Once the film is printed, it can be used as an insert in an injection mold. The advantage should be to embed the micro-structuration inside the material itself instead of the top surface of the part. The result is briefly described on following picture:

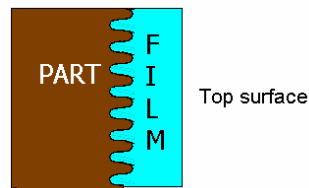


Figure 81: Micro-structuration inside the material.

First tests of micro-structurations by hot embossing were performed on PC films with the test Ni master. The thickness of the films is $250\mu\text{m}$. The results showed the good capability of replication

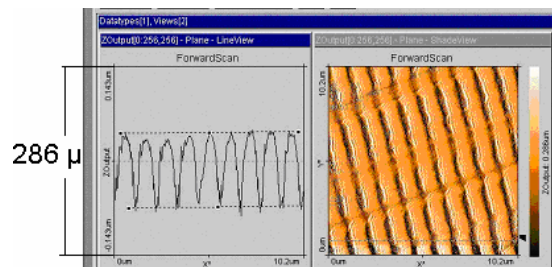


Figure 82: Microreplication by hot embossing: Ni master: 175nm / film: ~140nm

The next step consists in putting these films in the test injection mold and to evaluate the capability to avoid the destruction of the grooves during the overmolding process.

The actions are summarized here below

- Manufacturing of hot-embossed microstructures starting from an existing Ni master and polycarbonate films coming from the In Mold Injection technology
- Characterization of the hot-embossed microstructures

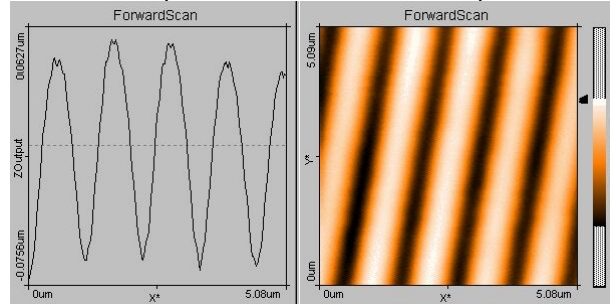
- In-Mold Injection trials using the hot-embossed PC films oriented respectively with the microstructure on the side of the mold, and on the side of the overmoulded polymer
- Characterization of the resulting microstructure after In-Mold Injection

The main observations issued from these actions are listed below.

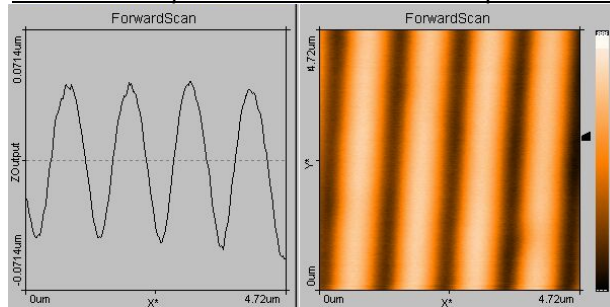
Hot-embossing and embedding of microstructures have been proven possible using existing commercial version of PC In-Mold Labeling technology (supplier: GE Structural Products) and this, independently with the initial thickness of the IML films (respectively $250\mu\text{m}$, $375\mu\text{m}$ and $500\mu\text{m}$).

Starting with an existing Ni master with uniform microstructure (period 1100nm – depth 125nm), excellent results have been obtained with hot-embossing, resulting on a quite perfect replication.

PC film – $250\mu\text{m}$ / Period $\sim 1100\text{nm}$ / Depth $\sim 110\text{nm}$



PC film – $500\mu\text{m}$ / Period $\sim 1100\text{nm}$ / Depth $\sim 90\text{nm}$



The hot-embossed PC films have been used as insert into a mold for In-Mold Labeled samples manufacturing. Different thickness of films have been considered, as different type of overmoulded polymers and the possible orientation of the hot-embossed microstructure into the cavity of the mold (respectively mold side or polymer side)

Considered data are listed below :

- Film thickness : $250\mu\text{m}$, $375\mu\text{m}$, $500\mu\text{m}$
- Polymers : PS (molded at 230°C), PC/ABS (molded at 270°C) and PC (molded at 290°C)
- Orientation of the hot-embossed film into the cavity : A (micro-structure on polymer side), B (micro-structure on mold side)

Basic results are given on following table. Qualitative evaluation of the conservation of the integrity of the microstructure after overmoulding has been roughly performed referring to the observation or not of light diffraction on the sample (visibility of the colored network)

	250 μ	375 μ	500 μ
PC-A-1	coloured network NON visible	coloured network +/- visible	coloured network NON visible
PC-A-2	coloured network NON visible	coloured network NON visible	coloured network NON visible
PC-A-3	coloured network NON visible	coloured network +/- visible	coloured network NON visible
PC-B-1	coloured network +/- visible	coloured network visible	coloured network +/- visible
PC-B-2	coloured network visible	coloured network NON visible	coloured network visible
PC-B-3	coloured network +/- visible	coloured network NON visible	coloured network visible
PC/ABS-A-1	coloured network NON visible	coloured network NON visible	coloured network NON visible
PC/ABS-A-2	No film	coloured network NON visible	coloured network NON visible
PC/ABS-A-3	coloured network NON visible	coloured network NON visible	coloured network NON visible
PC/ABS-B-1	coloured network +/- visible	coloured network visible	coloured network +/- visible
PC/ABS-B-2	No film	No film	coloured network visible
PC/ABS-B-3	coloured network visible	coloured network visible	coloured network visible
PS-A-1	coloured network visible	coloured network visible on unmatched film	coloured network visible on unmatched film
PS-A-2	coloured network visible	coloured network visible	Coloured network NON visible
PS-A-3	Coloured network NON visible	coloured network visible on unmatched film	coloured network visible on unmatched film
PS-B-1	coloured network visible	coloured network visible	coloured network visible
PS-B-2	coloured network visible	coloured network visible	coloured network visible on unmatched film
PS-B-3	coloured network visible	coloured network visible	coloured network visible on unmatched film

The most important observations are the following ones:

- Better results with lower temperatures (PS >> PC/ABS, PC),
- Lower adherence of PS (only due to the use of PC films !),
- Better results with thinner films,
- Better results with micro-structure on mold side (lower temperatures),
- Micro-structure on polymer side: possible to maintain the microstructure after direct contact with the melted polymer when using a low temperature moldable polymer.

These qualitative results have been confirmed by Easyscan AFM analysis (only the B-family samples).

2.2.8. Vision system and software decoder

The new reader for the decoding of the new MAP is a machine vision system. Multitel worked on the development of software which is able to detect and to decode the 2D pattern containing information (like Datamatrix as in the picture below) in the picture taken from the reader.



Figure 83: Datamatrix detection.



Figure 84: Datamatrix after the threshold.

The Datamatrix has a very strong contrast. The software detects the L shape of the Datamatrix to define the orientation of the Datamatrix. Then, a threshold is applied to determinate the dots and so define the

pixels 0 and 1 (figure 84). The last step is to create the grid with synchronization pattern which is around the Datamatrix. This grid helps to decode the Datamatrix. The information retrieved is the MAP.

2.2.9. Textiles and fibers studies

In the same time, the first investigations on marking of textiles were conducted by Centexbel in collaboration with Signatiss (located in Mouscron). This enterprise manufactures of a broad range of PES labels including secured labels and was ready to lend us machinery for test purpose.

Centexbel and CRIF developed a method to put markings on textile labels, especially the models manufactured by Signatiss. Several meetings and discussions took place about the best way to apply the MAP (Micrometric Authentication Pattern) on PES labels. Two possibilities emerged:

1. Moulding method:
 - Elastomers work badly
 - PA and PP give good results
2. Hot embossing:
 - Shall allow for thinner layers
 - Still to be investigated further



Figure 85: Polypropylene

Furthermore, during the second year of the project, Centexbel developed an automated instrument to measure fibre diameter along textile fibres.

This device named hereafter “profile meter” gives the following results:

- Measurement on individual fibres
- Simultaneous length and diameter characteristics
- Correlation between length and diameter
- Detailed diameter profile along the fibres

A diagram of the instrument is shown hereafter. The principle is to move a single fibre at constant speed under a high magnification electronic CCD camera which observes the image of a narrow line perpendicular to the fibre axis. By sliding the fibre from one end to the other slightly tight under the camera, the extended length (i.e. uncrimped) of the fibre is measured. Simultaneously, the transverse dimension of the fibre is computed by analysing the video signal from the camera. Successive signals are analysed at a high rate, corresponding to successive sections of the same fibre. In this way, short term as well as long term variations of the diameter along the fibre can be observed, and corresponding parameters computed. The instrument is under control of a software code which also allows to collect the measurements from successive fibres and hence to compute statistical data about length and diameter characteristics for a sample of fibres.

The instrument operates in a semi-automatic mode: the fibre is drawn manually from a sample and held at one end by means of tweezers. The measurement then proceeds automatically by pulling the fibre at a constant speed under the camera until the fibre end is detected.

A specially designed light source illuminates the fibre through a narrow slit and allows a sharp image of it to be obtained. The instrument also comprises electronics for camera control, signal processing and power supplies. Dedicated software controls and synchronises the different steps of the measurement cycle and computes the parameters and statistical data.

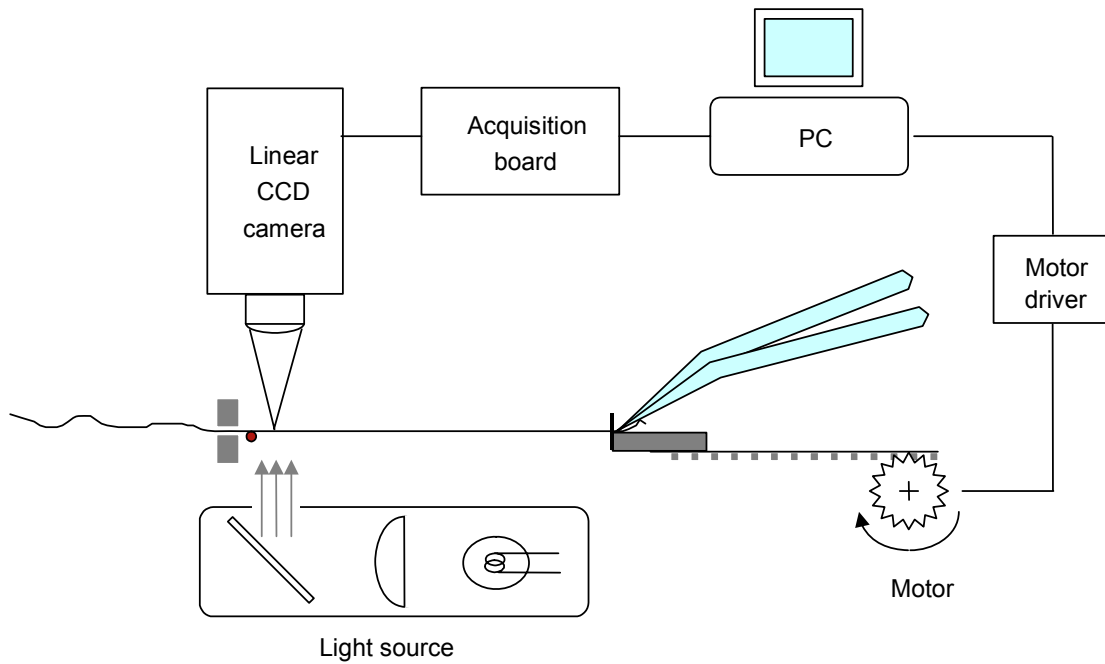


Figure 86: Profile Meter Diagram



Figure 87: Example of the acquired data

In the final year of this project, some enhancements were investigated by Centexbel and UMH:

1. Marking of individual fibres:
 - possible with current means BUT far from easy,
 - Should be possible in an extension of the project.
2. Interwoven fibres:
 - redundancy information to deal with hidden parts,
 - Narrow depth needed of field to “isolate” fibres.

However, there was not enough manpower left to implement these improvements before the end of the project.

2.2.10. Watermarking 3D graphical objects

VUB-ETRO and its subcontractor University of Ghent-IPI worked respectively on Watermarking 3D graphical objects represented as a MeshGrid model and on texture and morphology analysis.

VUB-ETRO investigated how graphical models described as a 3D MeshGrid Surface Representations could be copyright protected by a digital watermark. MeshGrid is a compact, multi-scalable and animation-friendly 3D object representation method, that has been designed at VUB-ETRO, and which has been recently standardized and adopted by MPEG as part of **MPEG4-AFX** (Animation Framework Extension) [1].

After an extensive literature study, the two most powerful blind watermarking systems that were appropriate to be applied on MeshGrid models, were withheld and adapted/implemented and tested.

In order to keep the local errors resulting from embedding a watermark within a certain bound, a novel approach based on the concept of MAXAD (maximum local error in the spatial domain - L_∞), introduced originally in the context of image coding at our department [28]-[29], has been worked out. More precisely, L_∞ or MAXAD encoding of MESHGRID models requires finding the optimal truncation threshold for each sub-band in the Wavelet domain, such that the minimal overall bit-rate is obtained subject to a MAXAD user-defined upper-bound. In other words, this technique orders the bit-planes of each sub-band from the wavelet transform according to the visual impact they have on the reconstructed 3D model. Thus, it is possible to distribute the strength of the watermark accordingly to the visual impact each bit-plane has, permitting to embed the hidden signature at the maximum power while preserving the imperceptibility. On the other hand, the control of the local errors introduced by the encoding process can be exploited also to limit the maximum error introduced by embedding the watermark, so guaranteeing a certain level of distortion. The MAXAD process will be presented in more details in section 0 and its application to a MeshGrid model in combination with the *Spread-Spectrum Embedding* technique is shown in section 0. The MAXAD encoding for MeshGrid has been published in [33].

Besides focusing on watermarking, further, development work has been performed to extend the MeshGrid representation for elevation surfaces and cylindrical surfaces, since they were playing beside 3D objects, an important role in the Tracing project: i.e. respectively for coding of patterns on flat surfaces and textile fibers. These changes were also introduced as amendments to the MPEG 4 standard [34]. VUB-ETRO has continued to follow the MPEG4-AFX standardization activities and further updated/optimized its implementation. A result of the project was also the successful completion of the PhD-thesis of Alexandru Salomie [3].

For the purpose of understandability, first a short introduction to the MeshGrid surface representation format is given in the next section.

An introduction to MeshGrid

Supporting real-time visualization of three-dimensional (3D) data for a wide range of target devices is becoming an important issue for various applications such as virtual reality, and e-commerce. In this context, it is mandatory to adapt on-the-fly the data representation to the characteristics of both the network (bandwidth) and the user terminal (processing power and rendering capabilities). To meet these requirements, a data representation that simultaneously supports scalability and view-dependent decoding needs to be employed.

A 3D surface representation method that has been designed at VUB-ETRO with these requirements in mind, is MESHGRID, which has been recently standardized and adopted by MPEG as part of **MPEG4-AFX** (Animation Framework Extension) [1]. MeshGrid [2]-[6] is a compact, multi-scalable and animation-friendly 3D object representation method, providing three types of scalability: resolution scalability, shape precision, and vertex position scalability. These scalability modes can be enabled at an ROI-level, allowing for ROI-based transmission, decoding and visualization of the visible parts of the mesh at the appropriate resolution and quality levels. This makes the MeshGrid representation also highly suitable for view-dependent decoding scenarios. MeshGrid is a hierarchical multi-resolution object representation which differentiates itself from existing multi-resolution representations (e.g. Wavelet Subdivision Surfaces [7]) by the fact that it not only preserves the surface description of the object, but also its volume description and the relationship between these two. To be more precise, the surface description is specified as the union between 1) a connectivity-wireframe (CW), describing the connectivity between the vertices, and 2) a regular 3D grid of points, the reference-grid (RG), characterizing the space inside and outside the CW. The MeshGrid representation is compact and progressive and is based on a 3D extension of a Freeman-like chain-code to encode the connectivity description in the CW.

The particularity of the MeshGrid surface representation lies in attaching the vertices of the connectivity-wireframe (CW) to the reference-grid (RG) points. The decomposition of a MESHGRID object into its components is illustrated in figure 88 for a multi-resolution humanoid model, obtained by applying a custom-made surface extraction method: i.e. the TriScan method. Figure(a) shows the MeshGrid representation of the model, which consists of the hierarchical CW (figure(b)) and the hierarchical RG (figure(c)). The different resolutions of the mesh are shown in (figure(d)). The RG is defined by a hierarchical reference-system as shown in figure(e). The RG (see figure(c), (e)) is the

reference system upon which the MeshGrid model is built, and is defined by the intersection points between three sets of reference-surfaces S_U, S_V, S_W .

Based on the fact that each reference-surface (RS) has a certain ordering inside the set, the following constraints are imposed at the surface of the object: 1) the RSs from one set keep their ordering, 2) they do not self-intersect, and 3) the RSs from any set intersect at least some of the RSs from the other two sets. The discrete position (u, v, w) of a reference-grid point, illustrated in Figure(a) by the white dots, represents the indices of the RSs $\{S_U, S_V, S_W\}$ intersecting in that point, while the coordinate (x, y, z) of a reference-grid point is equal to the coordinate of the computed intersection point.

Figure 89 illustrates the relationship between the vertices of the CW and the RG points. A RG line (curve) L , drawn in green in the 3D view of the object (figure(a)), is defined by the intersection between two RSs S_1 and S_2 from two different sets. As shown in the 2D cross-section (inside a reference-surface) through the object (figure(a)), line (curve) L , identified by label 1, passes by definition through a series of RG points (labels 2, 3) resulting from its intersection with the RS S_3 belonging to the third set. In the MESHGRID representation the vertices are part of the CW, and each vertex V is located on a reference-grid line between two adjacent grid points G_1 and G_2 . Considering that G_1 is the reference-grid position inside the object, respectively G_2 outside the object, vertex V stores the discrete reference-grid position (u, v, w) of G_1 .

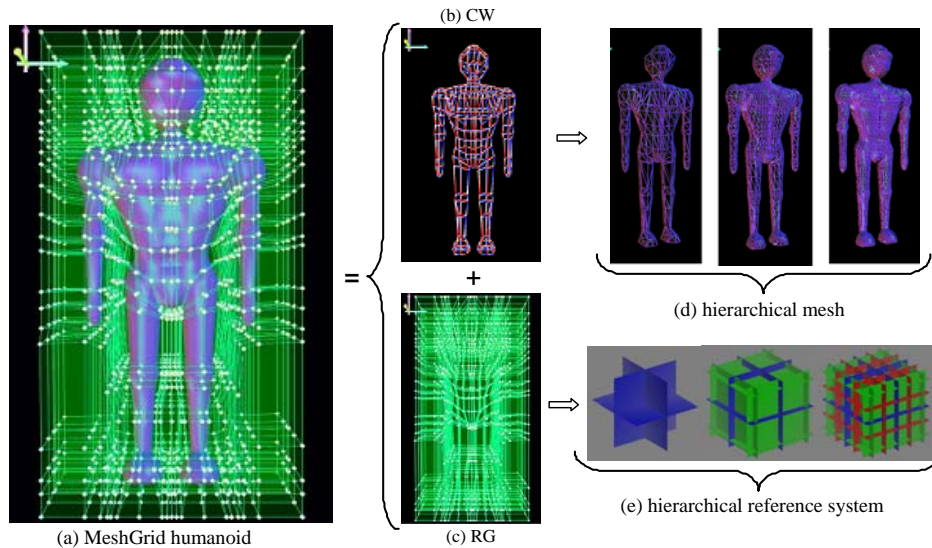


Figure 88: MESHGRID representation of a humanoid model.

The coordinates $C_{x,y,z}^V$ of vertex $V(u, v, w)$ are given by the intersection point between reference-grid line L and the object's surface (label 4), and are computed as:

$$C_{x,y,z}^V = C_{x,y,z}^{G_1} + \text{offset} \cdot (C_{x,y,z}^{G_2} - C_{x,y,z}^{G_1}), \quad (1)$$

Where *offset* (label 5) is a scalar in the range $[0,1)$. The coordinates of V are updated each time the *offset* or one of the coordinates of G_1 and G_2 change, for example during the animation (figure 91).

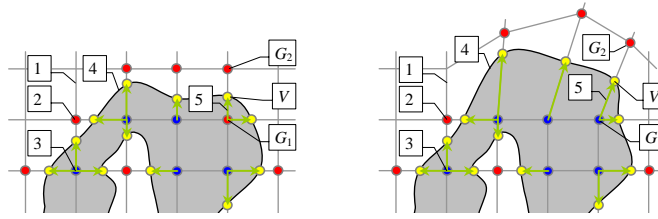


Figure 89: A cross-section through a 3D object, illustrating the contour of the object, the reference-grid, and the relation between the vertices (belonging to the connectivity-wireframe and located at the surface of the object) and the grid points.

In order to allow efficient encoding and unambiguous triangulation, the connectivity-wireframe has to satisfy particular connectivity constraints:

1. Each vertex has to be connected to four adjacent vertices (less if the mesh is open).
2. Two connected vertices are related to the same or adjacent reference-grid points.
3. Two connected vertices cannot have discrete border directions with opposite orientations
4. Distinction between back and front faces is necessary for a consistent triangulation.

The connectivity-wireframe can be obtained with a custom-made surface extraction method, called TriScan, which is a contour-oriented method, since it scans the object in the three directions defined by the reference-system coupled to the object.

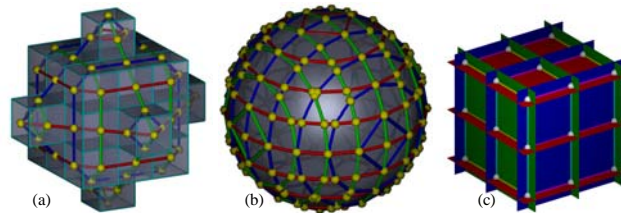


Figure 90: (a) Contouring a discrete sphere by means of a binary decision function and (b), a continuous sphere by means of a scalar decision function. The reference-surfaces and reference-grid points are shown in (c).

The method is automatic once the discrete 3D reference-system $\{u, v, w\}$, lying at the basis of the RSs and the RG has been defined. Yet an appropriate local coordinate system $\{x'=x'(u, v, w); y'=y'(u, v, w); z'=z'(u, v, w)\}$ needs to be defined and should take into account the desired density and distribution of the vertices. It will be in general curved and non-uniformly distributed, and may be arbitrarily oriented with respect to the global coordinate system $\{x, y, z\}$. Once the global transform is established, the coordinates of the RG can be defined either (1) explicitly by specifying the coordinates (x, y, z) of each point (u, v, w) from the lattice, or (2) implicitly when the points are by default equally spaced.

The reference-grid itself is coded using a multi-resolution progressive coding algorithm based on a combination of a 3D wavelet transform and an intra-band octree-based wavelet coder [2]. The 3D wavelet decomposition is applied separately to each of its coordinates $x(u, v, w)$, $y(u, v, w)$ and $z(u, v, w)$. The transform uses the same one-dimensional (1D) analysis low-pass ($H(n)$) and band-pass ($G(n)$) filters for each of the u , v , and w directions. At each resolution level p , a signal f is decomposed into its discrete approximation $A_j^d f$ (low-frequency subband) and detail information $D_j f$ (high-frequency subband), as expressed below:

$$A_j^d f(n) = A_{j+1}^d f(2n).$$

$$D_j f(n) = A_{j+1}^d f(2n+1) - 0.5(A_{j+1}^d f(2n) + A_{j+1}^d f(2n+2)).$$

The wavelet reconstruction is the inverse of the formula above, given by:

$$A_{j+1}^d f(2n) = A_j^d f(n).$$

$$A_{j+1}^d f(2n+1) = 0.5(A_j^d f(n) + A_j^d f(n+1)) + D_j f(n).$$

The analysis/synthesis filters are as follows:

$$H(n) = \{1 \mid n = 0\}; \quad G(n) = \{-0.5, 1, -0.5 \mid n = -1, 0, 1\}.$$

Error! Objects cannot be created from editing field codes.

Watermarking Systems Implemented for MeshGrid

For copyright protection purposes, blind watermarking is the most desirable method, since they can perform verification of the watermark without use of the original model. Next, are presented the two most powerful blind watermarking systems that were appropriate to be applied on MeshGrid models.

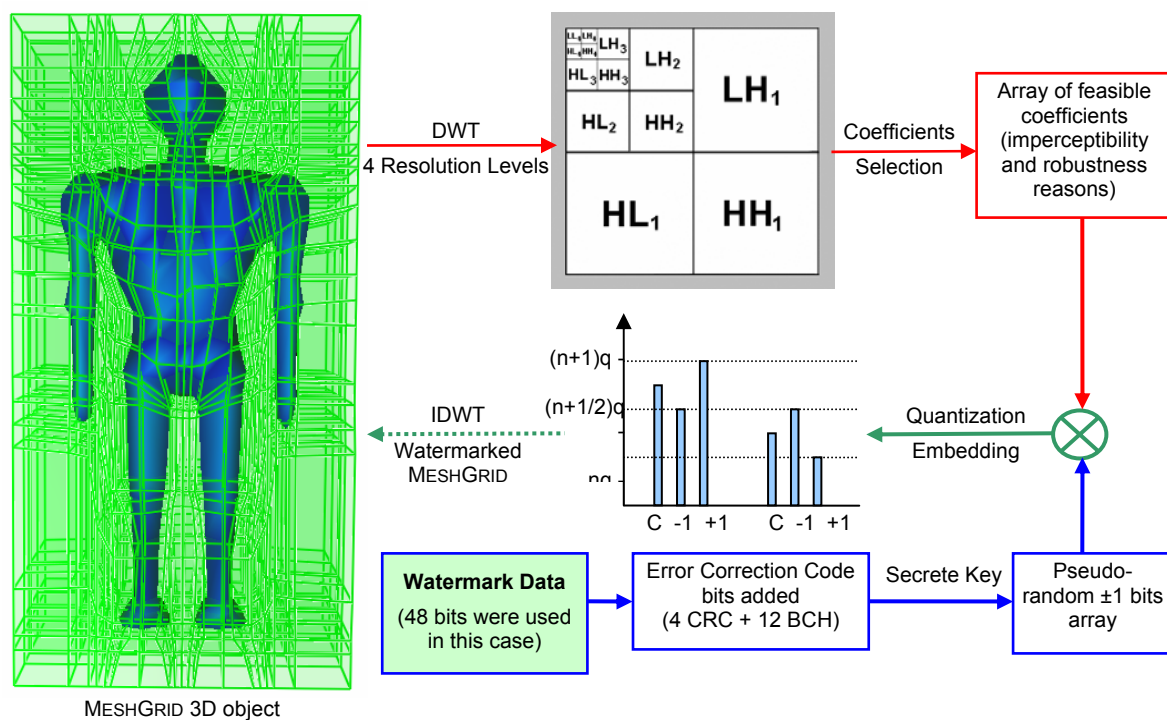


Figure 91: The Quantization watermark embedding algorithm

Quantization Embedding

Yasein et al. [16] and also Yongliang et al. [15] propose a blind watermarking embedding process based on quantization of the transformed data coefficients. The original 2D image is split into a set of non-overlapping blocks of 32x32 pixels. Each block is used to embed one bit of the watermark. A 3-level DWT decomposition of each block of the original 2D image is performed using Daubechies-8 filters. The embedding of the watermark is done by quantizing the magnitude of selected wavelet coefficients of the LL₃ sub-band. The algorithm has proven to be robust against image compression, filtering, noise addition and sharpening.

We adapted this algorithm to match the MESHGRID's [2][3][4][5] surface representation structure, the scalable 3D content encoding standard, part of the MPEG-4 [1] framework. The embedding of the watermark is done by modifying the magnitude of the wavelet coefficients of the grid (figure 93). The coefficients to be modified are selected to be within certain range, i.e. large enough, such that the distortion introduced by the quantization process is negligible.

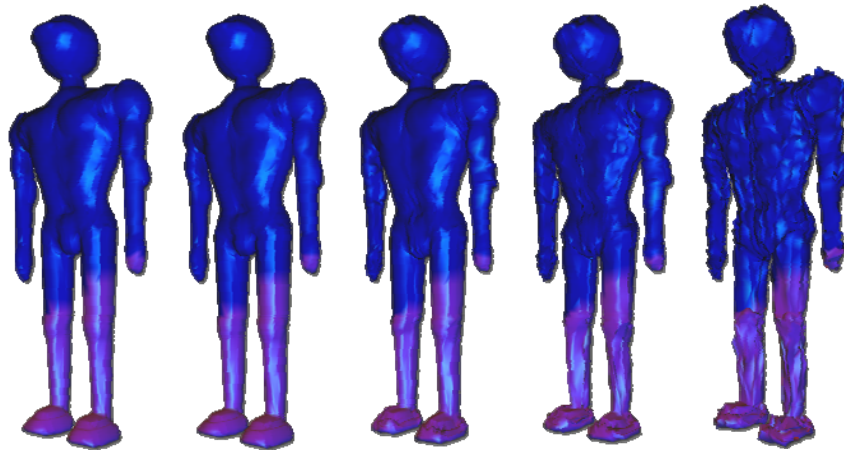


Figure 92: Different watermark embedding strengths

The watermark extraction is reversing the embedding process. In order to increase the robustness, the watermark data is first formatted. Cyclic Redundancy Check (CRC) coding is used to construct a signature that is a function of the watermark data bits and is appended to the watermark. In the watermark extraction process, the appended CRC signature is used to check whether the embedded watermark was extracted correctly. The watermark bits and the appended CRC signature are then encoded using Error Correcting Code (BCH), which is used for its capability to correct a certain number of errors that may have happened due to the manipulation of the watermarked object.

The strength with which the watermark is embedded in the 3D model can be adjusted in order to meet the desired robustness and imperceptibility. In the case of fragile watermarks, the quantizing coefficient q is chosen small enough such that if the model is degraded beyond a tolerable threshold, the watermark signature is lost. Figure 92 shows different watermark strengths. The watermark was embedded in the right models with an extreme strength just to visually demonstrate the process.

Spread-Spectrum Embedding

Guzmán et al. present in [24] a Wavelet-based watermarking algorithm, in which the Discrete Wavelet Transform (DWT) is used for embedding and detecting a watermark in 2D images. The detection process is based on the cross-correlation between marked image and pseudorandom sequences. In this process the original image is not required, hence it is also a blind watermarking method. The computer simulation results demonstrate the robustness and perceptual invisibility of the algorithm. We adapted this method for 3D MESHGRID models. The next figure presents the implementation of this method for 2D images.

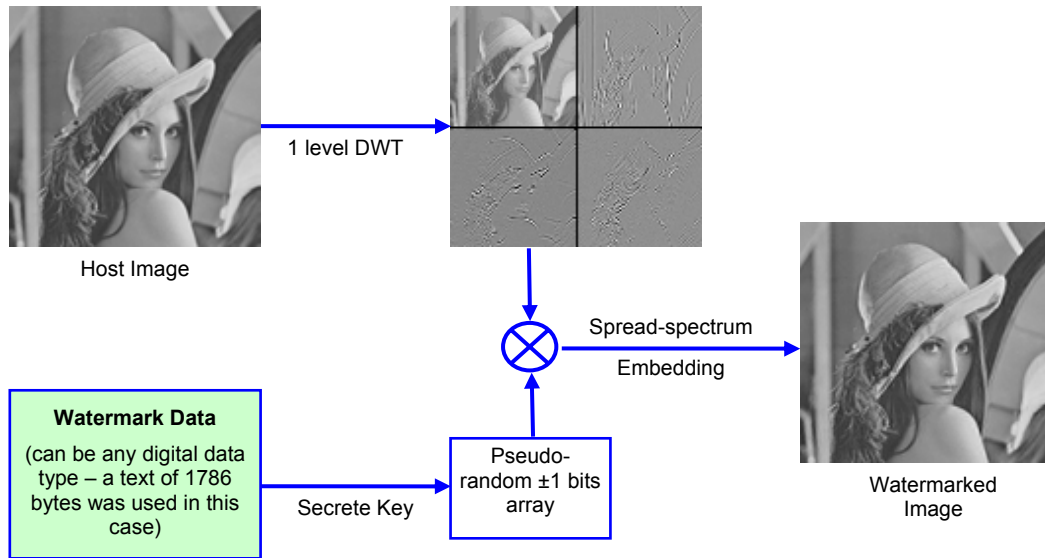


Figure 93: The Spread-spectrum watermarking algorithm for 2D images

The watermark is embedded along the band in the detail matrices of the resolution level 0 (LH_0 , HL_0 and HH_0), modifying the wavelet coefficients of these matrices. The embedding equation is given by (1).

$$Y_0^{\tau}(i, j) = Y_0^{\tau}(i, j) + \alpha G^{\tau}(i, j) W^{\tau}(i, j) \quad (1)$$

Where:

- $Y_0^{\tau}(i, j)$ is the original wavelet coefficient of the τ -th detail matrix in level 0 (i.e. LH_0 , HL_0 and HH_0);
- $Y_0^{\tau}(i, j)$ is the marked coefficient of the τ -th detail matrix in level 0;
- W is the pseudorandom binary sequence (± 1);
- α is a constant which controls the watermark embedding energy, and it was set in this experiment by 0.3;
- G is a weight function, which is proportional with the absolute value size of the wavelet coefficients;
- τ is the orientation {0 – vertical, 1 - horizontal, 2 - diagonal}.

The binary pseudorandom sequence $W = \{-1, 1\}$ is generated from a binary data vector which is as large as the three detail matrices in level 0, using a secret key. Once the watermark is embedded in the sub-band of level 0, the Inverse Discrete Wavelet Transform (IDWT) is computed to obtain the watermarked image.

For the detection process, the DWT is applied on the watermarked image. The detection is based on the cross-correlation between the watermarked DWT coefficients and the possible watermark code, as given by (2).

$$\rho = \frac{1}{3MN} \sum_{\tau=0}^2 \sum_{i=0}^{M-1} \sum_{j=0}^{N-1} Y_0^{\tau}(i, j) W^{\tau}(i, j) \quad (2)$$

The result is compared with a threshold determined by an adjustment of Neyman–Pearson criterion [25], to minimize the error probability in the detection process (3).

$$T_{\rho} = 3.97 \sqrt{2\sigma_{\rho B}^2} \quad (3)$$

where $\sigma_{\rho B}^2$ is estimated in practice by:

$$\sigma_{\rho B}^2 \approx \frac{1}{(3MN)^2} \sum_{\tau=0}^2 \sum_{i=0}^{M-1} \sum_{j=0}^{N-1} Y_0^{\tau}(i, j)^2 \quad (4)$$

Hence, it is possible to calculate the threshold of the watermark, without using the original image and without knowing the energy related value α , with which the watermark was inserted.

To analyze this method, we evaluated the robustness of the embedded watermark by applying various attacks to the watermarked image. The tested attacks were: compression, noise addition, clipping, geometrical distortion, luminosity modification and multiple watermarks embedding. The method proved to be robust, especially in the cases where a very large number of coefficients were used for the cross-correlation process. Yet, the practical consequence is that the image, and respectively the 3D model, should have a moderate to large grid size.

Spread-Spectrum Embedding applied to MESHGRID models

The Spread-Spectrum Embedding algorithm described above was adapted for 3D MESHGRID models. In figure 94, the user interface for embedding watermarks in the MESHGRID's editor, is presented. The efficiency of the algorithm, as well as the results, are comparable with those obtained for the experiments with images. The powerfulness of the approach is illustrated by figure 96: no visual differences can be noticed between the original 3D surface and the watermarked one, although the strength of the watermark was chosen four times bigger than the threshold.

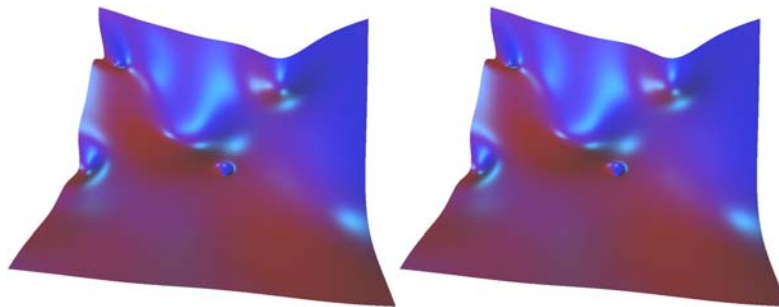


Figure 94: The original MESHGRID model (left) and the watermarked model after Spread Spectrum embedding (right)

The correlation values resulting from the detection process are shown in figure 95. The authentic key used to generate the watermark that was embedded in the original model has index 500. Its correlation value has been compared with 1000 random keys; the red line is the threshold value.

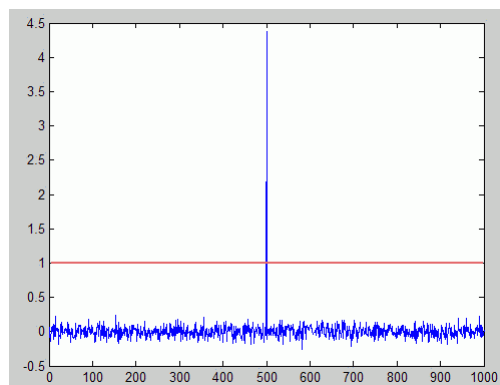


Figure 95: Spread Spectrum watermark detection values

Further, we have tested the robustness of the watermark in the presence of noise. In our experiment, the spatial grid values of the watermarked model were significantly altered by additive

Gaussian random noise was, which can be easily observed in figure 96. The detection process was still successful (see figure 97), yielding a correlation score of 1.12, still above the threshold.

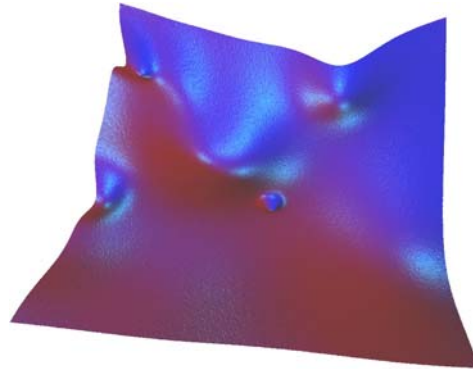


Figure 96: The watermarked MESHGRID model after Spread Spectrum Watermark embedding and noise degradation

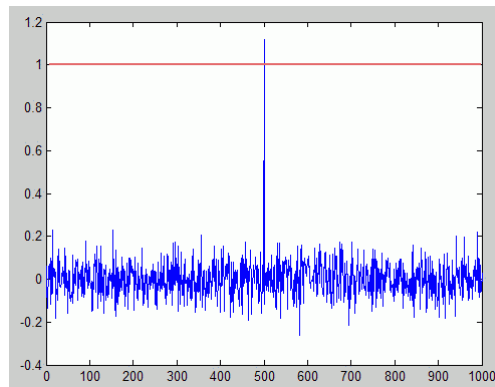


Figure 97: Spread Spectrum watermark detection values after noise degradation of the watermarked model

Error-bounding MeshGrid models using MAXAD

Introduction

Visualization of 3D information is widely used in various applications. In addition, the increasing trend of user mobility has led to a proliferation of heterogeneous terminals. Since the requirements vary from extremely high to very-low realism, the models need to be scaled in resolution and quality accordingly. A coding scheme for 3D models that optimally addresses such application scenarios should generate an embedded bit-stream going up to lossless reconstruction that could be progressively transmitted, would allow to be truncated at any bit-rate and would guarantee a given distortion at several bit-rates, according to the end-user requirements.

Yet, since it represents an encoder issue, the MPEG-4 AFX standard does not cover the rate-allocation aspects for none of these codecs. Traditionally, the L_2 norm is used in lossy coding literature. For instance, the L_2 distortion depends on the number of bits used to quantize the prediction errors in 3DMC, the refinement details in WSS [7], or the wavelet coefficients in MESHGRID. In general, designing optimal rate-allocation techniques for lossy coding of meshes may follow approaches similar to those employed in image coding – e.g. [31]. However, although the overall L_2 distortion at a certain rate might be practically small, the presence of error-spikes (large vertex-position errors) translates into visually distorted object reconstructions, making the lossy decoding at that rate unusable. That is, the L_2 norm (or the mean-square-error) might not be the most appropriate distortion measure in coding of 3D models, due to its global nature. Hence, limiting the L_∞ distortion – denoted as the maximum absolute difference (MAXAD) between the original and reconstructed vertex positions – to a user-defined upper-bound is a strong requirement in order to favor realistic lossy decoding of 3D

models. In this sense, it is important to point out that none of the schemes contained within MPEG-4 are capable of providing scalable L_∞ -oriented coding of 3D models.

Therefore we tackled this problem for our MESHGRID representation and have addressed the following combined problem: targeting L_∞ coding of 3D models while preserving the embedded nature and the scalability functionalities provided by MESHGRID.

Scalable L_∞ coding has been recently introduced in the context of image coding in recent work done at our department [28], [29]. These papers describe a wavelet-based compression scheme that is capable of providing embedded L_∞ -oriented functionalities, while retaining the coding performance and scalability options of a wavelet codec. In this project we followed the approaches of [28], [29] and designed optimal scalable L_∞ coding for MESHGRID models. The obtained stream remains embedded, and, additionally, one guarantees that a minimal bit-rate is achieved for any imposed MAXAD, or alternatively, a minimal MAXAD is attained for any user-specified target bit-rate.

As explained in section 0, the R-G is a smooth vector field defined on a regular discrete 3D space, which is efficiently compressed by using an embedded 3D wavelet-based multi-resolution intra-band coding algorithm, allowing for lossy to near lossless encoding, and yielding a multi-scalable bit-stream. The employed intra-band coding algorithm is a variant of the SQP coding algorithm of [30], extended to 3D. The algorithm operates in resolution-scalable mode and encodes the wavelet coefficients of the wavelet transformed reference-grid coordinates in a bit-plane by bit-plane fashion, using a depth-first coding strategy. For each bit-plane b , the associated threshold is computed as $T(b) = 2^b$ ($b = 0$ is the lowest bit-plane). When encoding the coordinates in a lossy manner, the main issue to be tackled is then the decision of what bit-planes to truncate, and from which decomposition levels, in order to obtain a minimal bit-rate for an imposed MAXAD or vice-versa.

Optimal L-infinity-oriented compression of MeshGrid models

The smallest upper bound of the MAXAD

It has been shown in [28] that in the two-dimensional case, the smallest upper bound M of the MAXAD can be written for any non-integer lifting-based wavelet transform as:

$$M = \frac{D_{LL}^{(L)}}{2} (K_{LL})^J + \sum_{l=1}^L \frac{D_{LH}^{(l)}}{2} (K_{LL})^{J-1} K_{LH} + \frac{D_{HL}^{(l)}}{2} (K_{LL})^{J-1} K_{HL} + \frac{D_{HH}^{(l)}}{2} (K_{LL})^{J-1} K_{HH} \quad (1)$$

where $D_s^{(l)}$ is the bin-size of the scalar uniform quantizer applied on the subbands s of the decomposition level l , $1 \leq l \leq L$, L is the total number of decomposition levels, and K_s is a weight factor derived from the predict and update lifting coefficients. A generalization of (1) to N dimensions and embedded dead-zone uniform scalar quantizers leads to [29]:

$$M = 2^b \left(1 - \frac{1}{2^{b+1}} \right) \left[(K_{S_1})^L D_{S_1}^{(L)} + \sum_{l=1}^L \sum_{s=1}^{S_1-1} (K_{S_1})^{J-1} K_s D_s^{(l)} \right] \quad (2)$$

where S_1 is the total number of wavelet subbands obtained for one level of decomposition and $b \in \mathbf{Z}_+$ represents the number of discarded bit-planes; for any s , l and b , the dead-zone bin-size is given by $(2^{b+1} - 1)D_s^{(l)}$, respectively the other bin-sizes are given by $2^b D_s^{(l)}$.

The lifting factorizations using the filters employed for the wavelet transform of the MESHGRID R-G coordinates lead to the one-dimensional forward and inverse transforms, expressed by equations (3) and (4) respectively:

$$\begin{aligned} s_i^{(0)} &= x(2i), \quad d_i^{(0)} = x(2i+1) \\ d_i^{(1)} &= d_i^{(0)} - \frac{9}{16} (s_i^{(0)} + s_{i+1}^{(0)}) + \frac{1}{16} (s_{i-1}^{(0)} + s_{i+2}^{(0)}), \quad s_i^{(1)} = s_i^{(0)} \end{aligned} \quad (3)$$

$$\begin{cases} x(2i+1) = d_i^{(0)}, x(2i) = s_i^{(0)} \\ d_i^{(0)} = s_i^{(1)}, d_i^{(1)} = d_i^{(1)} + \frac{9}{16}(s_i^{(0)} + s_{i+1}^{(0)}) - \frac{1}{16}(s_{i-1}^{(0)} + s_{i+2}^{(0)}) \end{cases} \quad (4)$$

Further, following a similar approach as in [28], [29], it can be shown that starting from the one-dimensional filter instantiation (3) and (4), for $N = 3$ and $b = 0$ relation (2) leads to:

$$M = \left(\frac{125}{64}\right)^L \frac{D_{LLL}^{(L)}}{2} + \sum_{l=1}^{L-1} \left(\frac{125}{64}\right)^{L-l} \frac{1}{2} D_{HHH}^{(l)} + \frac{5}{8} (D_{HHL}^{(l)} + D_{HLH}^{(l)} + D_{LHH}^{(l)}) + \frac{25}{32} (D_{HLL}^{(l)} + D_{LHL}^{(l)} + D_{LLH}^{(l)}) \quad (5)$$

which is the expression of the smallest upper bound of the MAXAD for L wavelet-decomposition levels for the R-G coordinates in MESHGRID models.

MAXAD-bounded Rate Optimization

L_∞ compression of MESHGRID models requires finding the optimal truncation threshold for each subband, such that the minimal overall bit-rate is obtained subject to a MAXAD user-defined upper-bound. This constrained-optimization problem is solved by using a Lagrangian multiplier method similar to the approach used for instance in JPEG2000 [31]. The following distortion-rate slopes are computed, in which the distortion is related to the L_∞ norm, in other words the MAXAD:

$$l^{(l)}(b_k) = \frac{D^{(l)}(b_k + 1) - D^{(l)}(b_k)}{L^{(l)}(b_k) - L^{(l)}(b_k + 1)} \quad (6)$$

where $b_k \in \mathbb{Z}_+$ is the bit-plane corresponding to the truncation threshold $T(b_k)$. Notice that only the bit-planes having an associated threshold $T(b)$ ($b > b_k$) higher than $T(b_k)$ are encoded. The distortion-rate slope l in (6) is defined as the ratio between the decrease of the distortion (D) associated to the increase of the bit-stream length (L) when an additional bit-plane b_k is encoded. The slope (l) is assumed to decrease monotonically when decreasing the truncation threshold (i.e. increasing the rate). If some of the truncation points do not follow this constraint, they do not lie on the convex-hull defined by the discrete set of distortion-rate points, hence, will not be considered as feasible truncation points. To find the order in which the bit-planes corresponding to the subbands from all decomposition levels should optimally be truncated, the $l^{(l)}(b_k)$ from all decomposition levels l are sorted in a monotonically decreasing order. The order in which the $l^{(l)}(b_k)$ are sorted indicates the order in which the subbands are encoded. This corresponds to a global distortion-rate curve for which the slopes are monotonically decreasing.

In addition to equation (5) (*theoretic* approach), two additional methods have been considered to determine the distortion D used to compute the l ratios. In the second method, called the *absolute* approach, instead of employing equation (5), the distortion D is determined by effectively encoding and reconstructing the model, and computing the real MAXAD with respect to the original model. The third method (*progressive*) is similar to the second approach in the way it computes the distortion. The difference is that the MAXAD is recomputed for each candidate truncation threshold (from each decomposition level) again after each truncation. This is because the real distortion introduced by truncating the subbands of a certain decomposition level depends on the order in which the subbands of the other decomposition levels are truncated. Hence, the distortion-rate curve is built progressively while encoding.

Results MAXAD

Figure 98 depicts the order in which the bit-planes of the subbands of each decomposition level are truncated by each of the three methods described in the previous section. We illustrate in figure 103 the results obtained by each method for three MESHGRID models at various MAXAD values. The MAXAD is expressed in percentages relative to the size of the bounding box containing the model. Compared to the *absolute* approach, the *theoretic* method always achieves better or equal compression ratios and is in average twice as fast. The *progressive* method is slightly better than the

absolute approach, and worse than the *theoretic* method. As expected, the *progressive* method is much slower than the other two, due to the fact that it computes the MAXAD at each truncation step. We illustrate in figure 103 and figure 104 the reconstructed MESHGRID models compressed using the *theoretic* method. Notice that for the rightmost model all the bit-planes are truncated; therefore the reconstructed reference-grid is uniformly distributed, leading to the altered shape of the model. The comparison between the *theoretic* L_∞ method and the coding approach wherein the rate is optimally allocated using an L_2 distortion metric are given in figure 105, visual results being reported figure 107. Note that the models have been encoded here at high compression ratios in order to visually emphasize the differences between the two techniques. As expected, the results of figure 107 indicate that optimization with respect to the L_2 norm lays no claim on minimization of the local distortion, in this sense having the potential of introducing large local error-spikes (i.e., large vertex-position errors) that would otherwise not be present in an L_∞ -oriented framework. This phenomenon can be most clearly witnessed on the Tangle Cube model of figure 108, in which the second “lobe” of the cube (counting clockwise from the upper-left corner) appears over-peaked and distorted in the L_2 case. Overall, the results shown here indicate that optimizing the rate for an L_∞ distortion metric outperforms the results obtained when using the traditional L_2 norm.

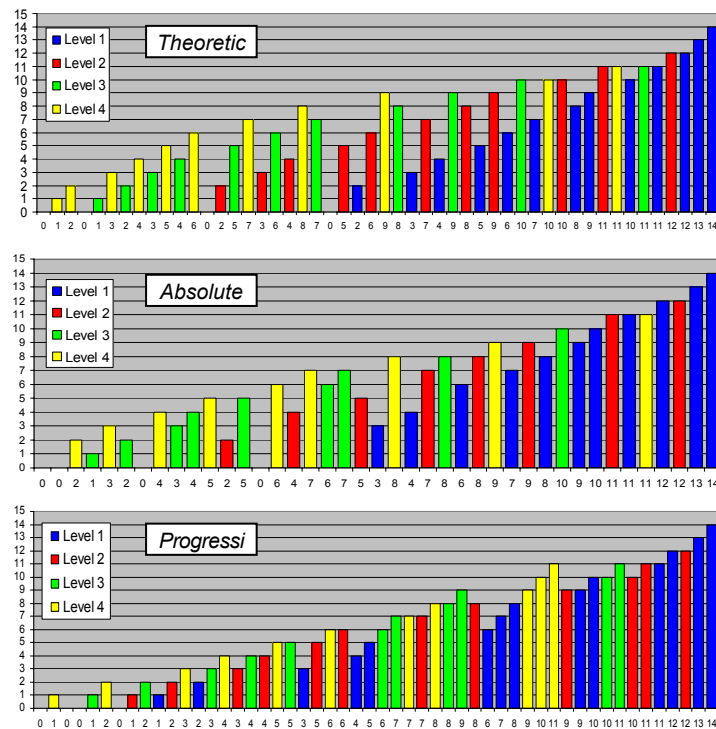


Figure 98: Cutting order of the bit-planes from the different subbands displayed each in a different color. Horizontal/vertical axes indicate the bit-planes with associated threshold T(b).

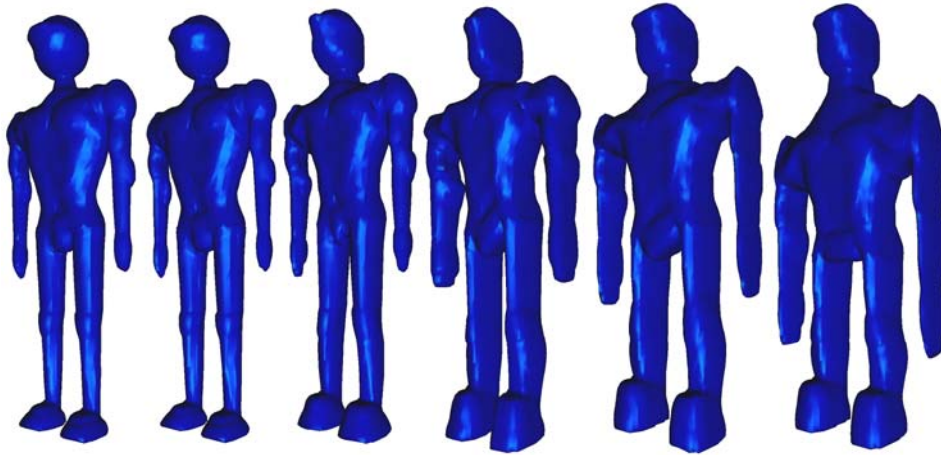


Figure 99: Lossy compressions of the Humanoid model obtained for MAXAD values (from left to right): 0, 0.5, 1.5, 5, 20, 100 (%).

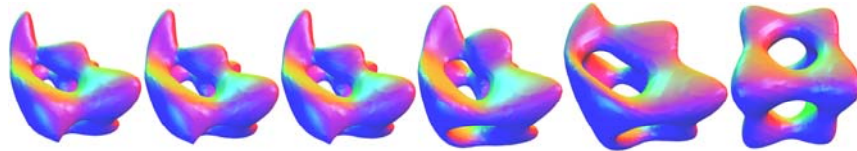


Figure 100: Lossy compressions of the Tangle Cube model obtained for MAXAD values (from left to right): 0, 0.5, 1.5, 5, 20, 100 (%).



Figure 101: Lossy compressions of the Torus Heart model obtained for MAXAD values (from left to right): 0, 0.5, 1.5, 5, 20, 100 (%).

Model	Method	MAXAD	Time	Grid CR
Humanoid	Theoretic	20.00%	0.48	5971
Humanoid	Absolute	20.00%	2.79	5971
Humanoid	Progressive	20.00%	8.8	5971
Humanoid	Theoretic	5.00%	0.86	296
Humanoid	Absolute	5.00%	3.05	296
Humanoid	Progressive	5.00%	8.89	274
Humanoid	Theoretic	0.50%	2.72	11
Humanoid	Absolute	0.50%	4.13	11
Humanoid	Progressive	0.50%	8.67	11
Tangle Cube	Theoretic	20.00%	0.34	6867
Tangle Cube	Absolute	20.00%	0.7	6867
Tangle Cube	Progressive	20.00%	1.85	6867
Tangle Cube	Theoretic	5.00%	0.45	385
Tangle Cube	Absolute	5.00%	0.83	385
Tangle Cube	Progressive	5.00%	1.82	385
Tangle Cube	Theoretic	0.50%	0.86	21
Tangle Cube	Absolute	0.50%	1.02	19
Tangle Cube	Progressive	0.50%	1.45	21
Torus Heart	Theoretic	20.00%	1	6411
Torus Heart	Absolute	20.00%	3.91	6411

Torus Heart	Progressive	20.00%	12.7	6411
Torus Heart	Theoretic	5.00%	1.68	1261
Torus Heart	Absolute	5.00%	4.17	1261
Torus Heart	Progressive	5.00%	12.61	1261
Torus Heart	Theoretic	0.50%	4.54	40
Torus Heart	Absolute	0.50%	5.76	40
Torus Heart	Progressive	0.50%	12.23	33

Figure 102: Lossy compressions for several MAXAD constraints (Time in seconds and CR - grid Compression Ratio).

Model	MAXAD - L ₂	MAXAD - L _∞	Grid CR
Humanoid	30.00%	20.00%	5971
Tangle Cube	17.50%	5.00%	385
Torus Heart	5.60%	5.00%	1261

Figure 103: MAXAD values obtained when optimizing for the L_2 and L_∞ norms respectively, for the same grid compression ratios.

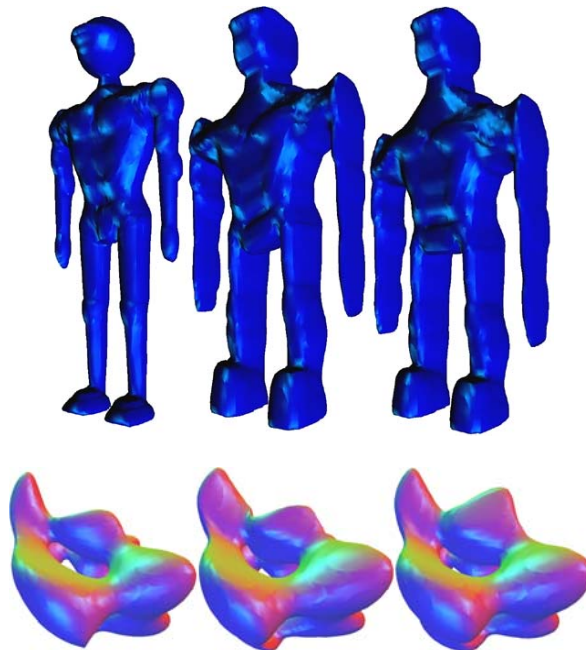


Figure 104: Original models (left); visual results obtained when optimizing for the L_2 (middle) and L_∞ (right) norms respectively, for the grid compression ratios given in Table 2.

Finally, we wish to point out the fact that the procedure described in this paper is not limited solely to static models, but rather can be extended a step further to dynamic models. Although this is still ongoing research, we would like to already illustrate here some preliminary results. Thus, the animation of the “Humanoid” depicted in figure 109 was realized by keeping the C-W unchanged for the entire sequence and modifying only the vertices’ coordinates. Given that the vertices are attached to the R-G and their coordinates are derived from the coordinates of the R-G points, animation of the R-G points can be used to obtain the same effect as direct animation of the vertices. The advantage of using the former technique is that the animation can now be defined in a hierarchical and more straightforward manner [6]. The sequence has been encoded as follows: the full model, i.e. the mesh C-W and the R-G, was encoded only once (i.e. for the first frame), while for each of the following frames only the changes in the R-G with respect to its previous frame were encoded. The differences in the R-G coordinates between successive frames have been encoded in the same way as for the static model discussed above.

Figure 110 illustrates the visual results of one frame from the “Humanoid” sequence of 109, which has been coded lossy at several MAXAD constraints. In addition, figure 111 shows the rate/distortion curve of the experiments. The results depicted here show that the proposed technique can also be applied with success in the compression of dynamic models. Indeed, in figure 111, the bit-rate can be dropped from 900kbits/s to 100kbits/s (corresponding to a MAXAD of 1%) with hardly any visual penalty on the model (see figure 110).

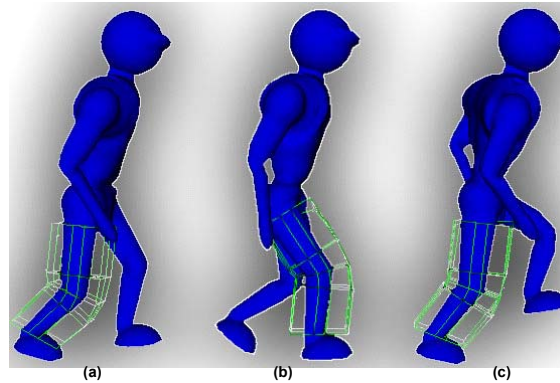


Figure 105: Volumetric animation of a “Humanoid” by altering the positions of the R-G points

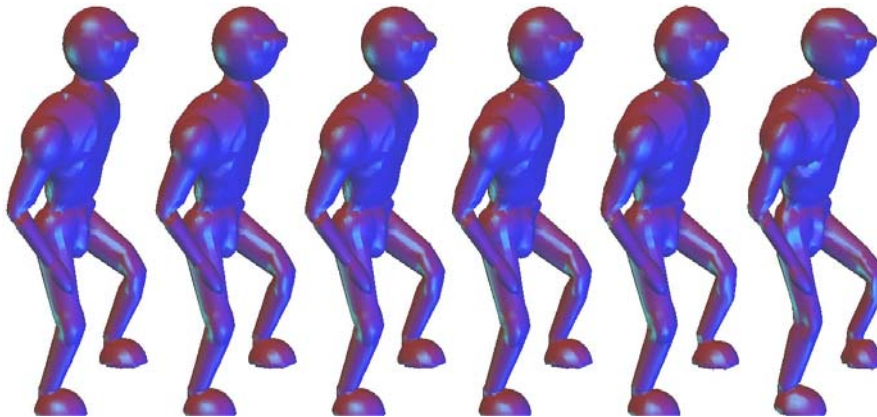


Figure 106: Frame of volumetric animation of the “Humanoid” coded at MAXAD values (from left to right): 0, 0.01, 0.1, 0.5, 1, 2 (%)

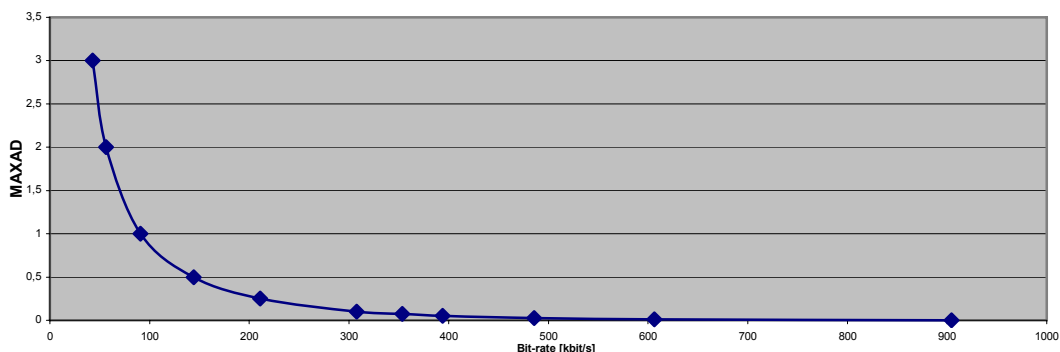


Figure 107: The rate/distortion curve for the “Humanoid” sequence coded at different MAXAD values

Spread-Spectrum Embedding applied to MESHGRID models using MAXAD

In order to keep the local errors, introduced by the spread-spectrum embedding of a watermark within a certain bound, one can adjust the weight function G - which is proportional with the absolute value size of the wavelet coefficients - in formula (1) of section 0, according to the distortion-rates computed via formula (6) in section 0. The user interface (see figure 112) for embedding watermarks in the

MESHGRID's editor offers the choice to either apply spread spectrum embedding with a static weight or with weights that are automatically computed for a certain specified MAXAD tolerance.

Representing elevation and cylindrical surfaces using MESHGRID

In order to represent elevation and cylindrical surfaces, the MeshGrid format has been adapted to support also open surfaces (see figure 114). In that case, an elevation surface can be represented as an open surface (connectivity-wireframe) sandwiched in between two reference surfaces. The shape of the reference surfaces can be chosen in such a way that all offsets are equal to the default value 0.5 (see figure 115(a),(b)), which enables an efficient coding, since only the reference grid, consisting of the two surfaces needs to be coded, which is accomplished on the basis of a wavelet transform. In order to further compact the coding of the elevation surface, the definition of the reference grid has been adapted to allow the representation of the elevation surface (connectivity-wireframe) in terms of one reference surface only (see 115(c)). A similar approach, i.e. the usage of only one reference surface, has been followed for the representation and coding of cylindrical objects. Further enhancements were made to allow that two parallel sides of the open surface (connectivity-wireframe) can be connected to each other and a special interpolation scheme was devised to enable the efficient wavelet-encoding of a cylindrical grid. Two wavelet high-pass filters are supported, and are derived from Dyn's filtering scheme shown in figure 113. The synthesis filter is given by equation (1), while the reconstruction filter is defined in equation (2). The "short" first-order filter is obtained for the weighting factor $w = 0$ while a third-order "smooth" filter is defined when $w = 1/16$. The choice of the filter depends on the shape of the object and the distribution of the grid points. In case of cylindrical objects the smooth filter gives the best compression result. When applying the smooth filter on an open cylindrical object, i.e. that is non-cyclic, efficient encoding of the points at the borders of the open mesh can be achieved, by estimating the positions of the missing samples at the edges with formula (3).

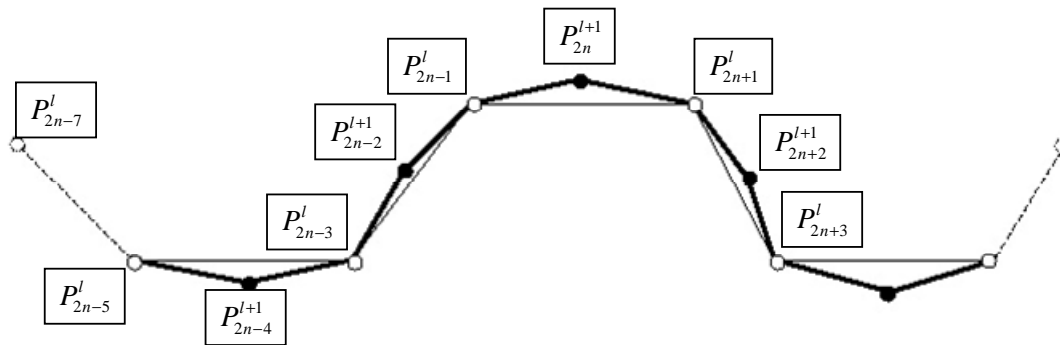


Figure 108: Dyn's four-point scheme for curves applied to the hierarchical MeshGrid

According to Dyn's formula, the reconstructed position of a reference grid point P_{2n}^{l+1} (shown in figure 113) at the resolution level $(l+1)$ is computed as follows:

$$\Delta P_{2n}^{l+1} = \left(w \cdot P_{2n-3}^l + 0 \cdot P_{2n-2}^l - \left(\frac{1}{2} + w \right) \cdot P_{2n-1}^l + P_{2n}^{l+1} - \left(\frac{1}{2} + w \right) \cdot P_{2n+1}^l + 0 \cdot P_{2n+2}^l + w \cdot P_{2n+3}^l \right), \quad (1)$$

$$P_{2n}^{l+1} = \left(-w \cdot P_{2n-3}^l + 0 \cdot P_{2n-2}^l + \left(\frac{1}{2} + w \right) \cdot P_{2n-1}^l + \Delta P_{2n}^{l+1} + \left(\frac{1}{2} + w \right) \cdot P_{2n+1}^l + 0 \cdot P_{2n+2}^l - w \cdot P_{2n+3}^l \right), \quad (2)$$

where l represents the hierarchical level of the grid point, P the coordinate of a grid point, and ΔP denotes the computed detail of P .

$$P_{2n-7}^l = P_{2n-1}^l + (2k+1) \cdot B, \quad \text{where } k = (\vec{B} \cdot \vec{A}) / B^2, \quad B = P_{2n-5}^l - P_{2n-3}^l, \quad A = P_{2n-3}^l - P_{2n-1}^l \quad (3)$$

Some results:

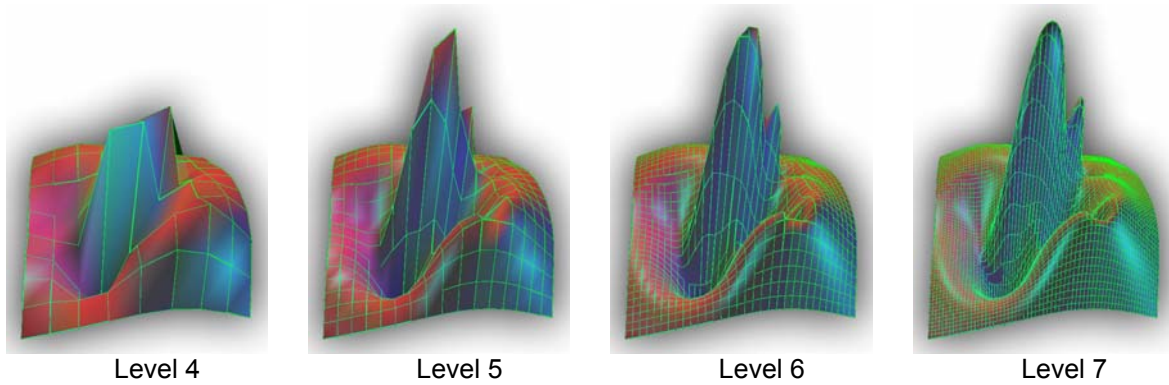


Figure 109: Different resolution levels of an elevation object.

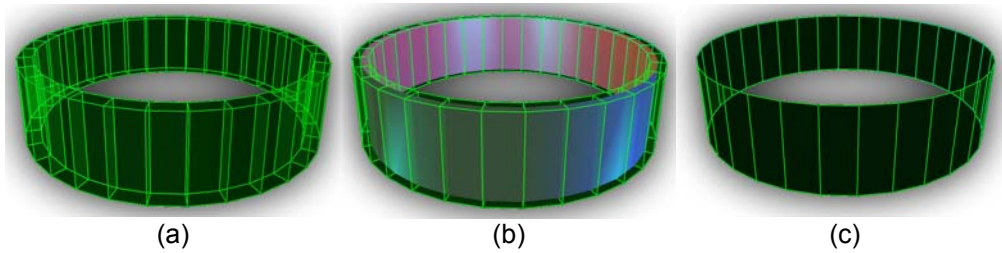


Figure 110: Two-layered and single-layered reference-grid designed for a cylindrical object

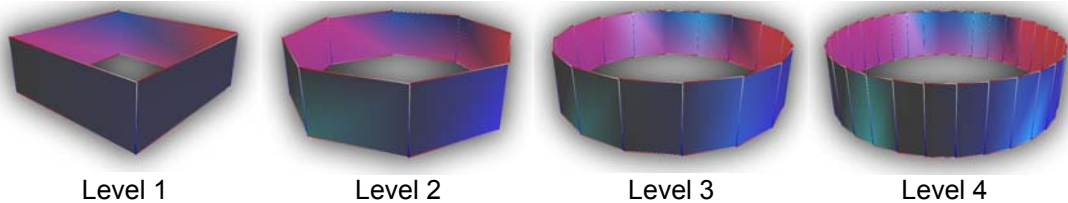


Figure 111: Different resolution levels of a cylindrical object

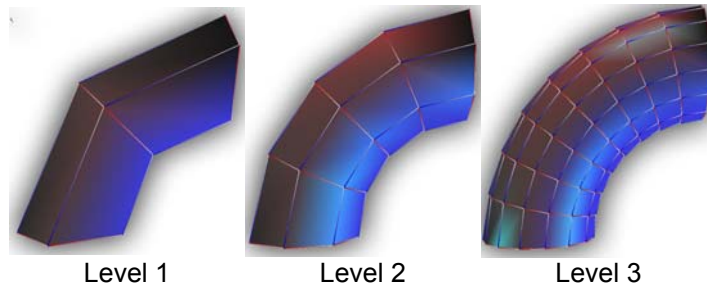


Figure 112: Different resolution levels of a bended cylindrical object. Note the change in topology between the levels 1 and 2.

2.2.11. Texture and morphology analysis

Introduction

The working goal was formally defined as to provide a technical and experimental overview of low-level image processing techniques within fiber watermarking and analysis tasks and applications. The subtopics within the scope of the project we selected were:

- Fiber segmentation
- Detection of structural irregularities (possibly caused by watermarking)
- Textile texture segmentation

We selected and implemented some low-level image processing techniques from the state of the art to tackle these topics.

The state of the art of the relevant low-level image processing techniques will now be summarized:

- General image segmentation:

- Clustering: adaptive threshold techniques [1], k-means [2], hierarchical clustering [3], parametric density estimation [4], non-parametric density estimation [5].
- Edge based techniques: active contours (snakes) [6], edge operators like for example the Canny edge detector [7].
- Region based techniques: recursive growing [8], split-and-merge [9], watershed segmentation [10].
- Graph based techniques: graph merging [11], graph splitting like for example the normalized cut [12].
- Other methods: level sets [13], markov random fields [14].
- General texture analysis:
 - Gabor filters [15], wavelet filters [16], markov random fields [17], co-occurrence matrices [18], run-length matrices [19].

The respective image processing techniques and corresponding applications within the scope of the project we selected were:

- Watershed segmentation and region merging to perform fiber segmentation.
- Gabor filtering for the detection of structural irregularities. The Gabor filter can easily be tuned to detect irregularities with very specific characteristics.
- Wavelet based texture gradient for generic (textile) texture segmentation. The non-decimated complex wavelet decomposition proves to be a descent method to perform multi-scale unsupervised texture segmentation in a well defined way.

Watershed segmentation

Explanation of the technique:

Image segmentation is the process of partitioning a digital image in meaningful segments, i.e. segments that show a certain degree of homogeneity. Image segmentation can be interpreted and implemented in many ways. The division into edge detection and region growing algorithms could be a rough classification of segmentation algorithms. The watershed transform can be attributed properties of both classes, i.e. it tries to find the homogeneous closed regions by using an edge indication image as input. An edge indication image is loosely defined as an image with for each pixel a value that indicates the probability of an edge on that pixel. In case of intensity segmentation, the edge indication map can be created by calculating the gradient magnitude of the input image. The watershed transform then regards the edge indication map as a topographic landscape in which “valleys” correspond to the interior of segments, whereas the “mountains” correspond to the boundaries of segments. Figure 113 illustrates these first steps of the process for an example photographic image.

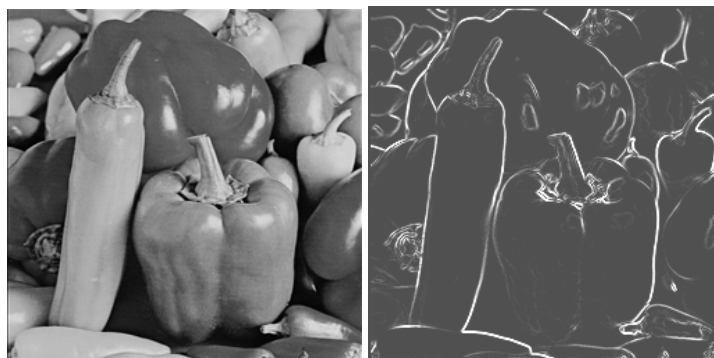


Figure 113: The image PEPPERS and its corresponding edge indicator image

The watershed algorithm derives the “mountain rims” from the topographic landscape and those mountain rims then delineate the segments in the image. This is shown in Figure 121 for a 2D slice of a 3D topographic landscape.

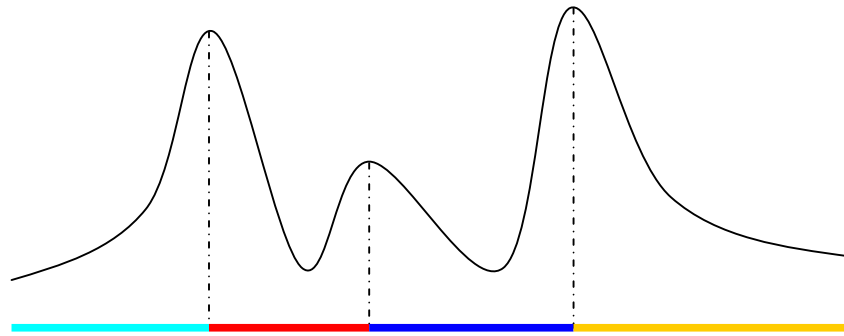


Figure 114: Delineated segments for a 2D slice

Watershed algorithms can be divided in two classes depending on the method that is used to extract the mountain rims from the topographic landscape. The first class contains the flooding watershed algorithms. These algorithms extract the mountain rims by gradually flooding the topographic landscape. The points where the waterfronets meet each other constitute the mountain rims. The second class contains the rainfaling watershed algorithms.

We used a rainfaling watershed algorithm that works as follows. For each point on the topographic landscape the algorithm tracks the path that a virtual droplet of water would follow if it would fall on the topographic landscape at that point. All droplets or points that flow to the same local minimum constitute a segment. This concept is depicted in Figure 115 for the two-dimensional case. However, an inherent problem of this method is that even the smallest dent or puddle in the topographic landscape will generate segments that do not correspond to real and important edges and objects. Hence, we have applied a simple method to try and solve this problem. By creating a ground-water level drowning threshold, before the real watershed results are computed, we can successfully merge all the image regions that only contain relatively weak edges. All the mountains below a certain drowning threshold will not be taken into account. This is shown in Figure 115.

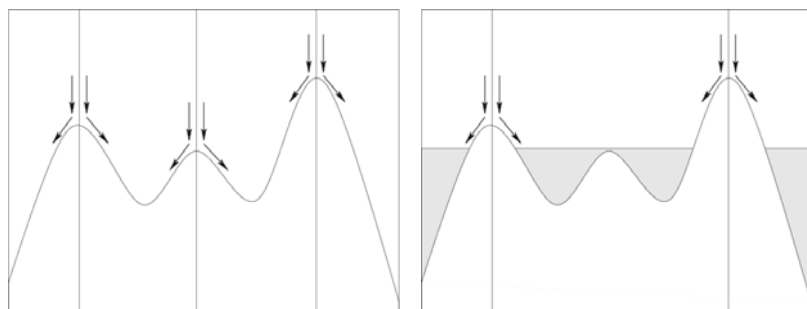


Figure 115: Rainfaling concept; Drowning threshold

Experimental results of the technique:

We used the raw rainfaling watershed technique combined with the drowning threshold method to perform fiber segmentation.



Figure 116: Example fiber image segmentation result (microscope)

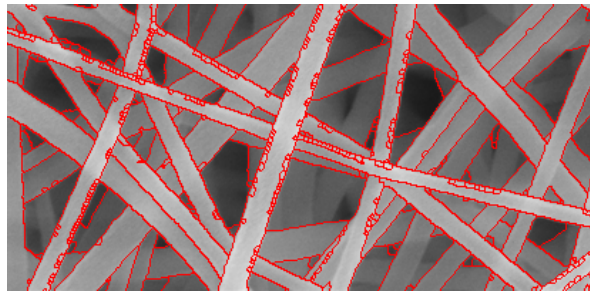


Figure 117: Example fiber image segmentation result (SEM)

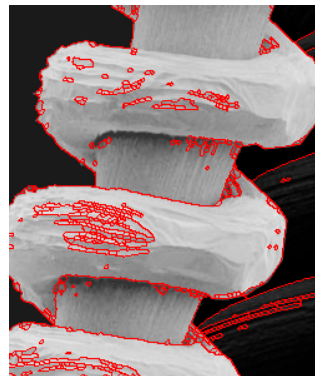


Figure 118: Example fiber image segmentation result (SEM)

As we can see on these images, there is still a lot of small undesirable irrelevant segments. In fact if we would not have used the drowning threshold method described above, the quality of the obtained segmentation results would be very poor.

We thus still need an additional, more advanced technique to reduce the over segmentation. A few solutions are possible:

- Pre-processing: changing the input image or the gradient of the input image.
 - Linear diffusion or Gaussian smoothing: smoothing the image by convolving it with a Gaussian mask of a certain sigma and size.
 - Non-linear diffusion: smoothing the input image by applying an iterative diffusion process steered by the sharpness of the edges.
 - Any noise filter.
- Post-processing: use the statistics of the segments to make certain decisions about them.
 - Region merging: iteratively merge the 2 neighboring segments that are the least dissimilar according to a certain criterion. A very simple criterion could be the mean intensity of a segment.
 - Graph splitting: construct a graph out of the segmentation given by the watershed with costs that represent the similarity between segments or nodes. Then iteratively split this graph with a graph split algorithm like for example minimum cut.

Region merging

Explanation of the technique:

After obtaining the basic watershed segmentation result, we create a data structure called the region adjacency graph (RAG). In this type of graph, each node represents a distinct segment of the image partition and an edge connecting two nodes represents the fact that the two segments associated with those nodes are adjacent or neighbors. Then we associate a cost to each node, the cost indicates the similarity between the two nodes or segments in question following a certain criterion. There are a lot of choices possible to quantify the similarity between two neighboring segments:

- Region based: difference in the statistics of the intensity, color, texture, ...
- Border based: statistics of the gradient along the common border.

Now the actual merging of segments starts using the calculated similarity values. For each merging step, we look for the pair of adjacent regions in the current image partition who are the least dissimilar. In other words we look for the edge in the current RAG with the lowest cost. Then we merge those two segments by removing the connecting edge and recalculating the costs of the edges in the

neighborhood. We repeat this process till a maximum cost is reached or a certain amount of segments is reached.

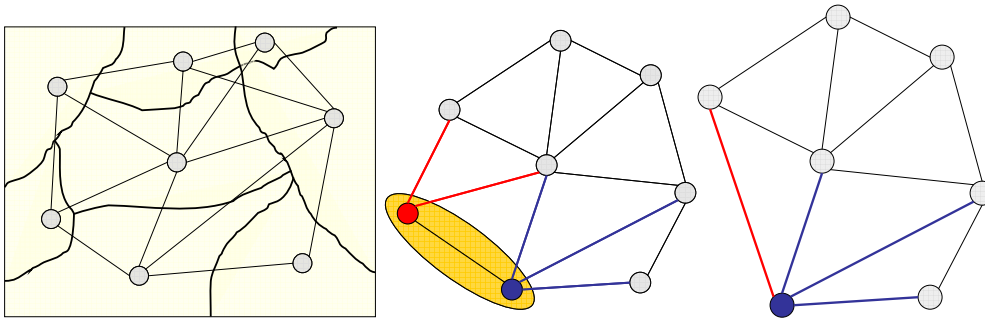


Figure 119: The RAG and an exemplary merge of two segments

Experimental results of the technique:

We used the region merging technique to remove the over segmentation on the segmentation results obtained with the basic watershed technique.

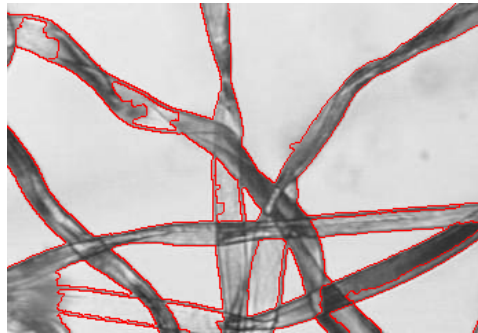


Figure 120: Example fiber image segmentation result (microscope)

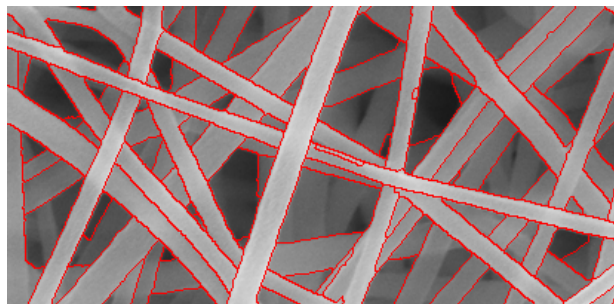


Figure 121: Example fiber image segmentation result (SEM)

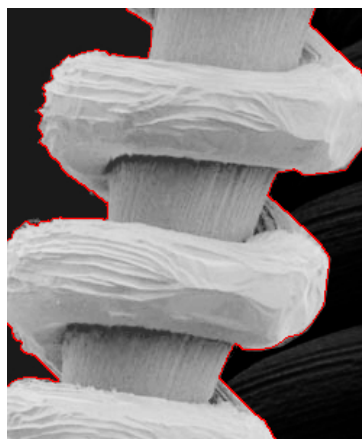


Figure 122: Example fiber image segmentation result (SEM)

On these image we can clearly see that by using the region merging as a post-processing step, we are able to remove the small irrelevant segments.

Gabor filtering

Explanation of the technique:

Gabor filtering is one of the most used techniques in low-level image processing. The Gabor filtering technique shows many similarities with the structure of the light sensors in the visual cortex. The input image is filtered using a band-pass Gabor filter having an impulse response:

$$\begin{aligned} h(x, y) &= g(x, y)e^{-j2\pi(Ux+Vy)} \\ &= \frac{1}{2\pi\sigma_g^2} e^{-\frac{(x^2+y^2)}{2\sigma_g^2}} e^{-j2\pi(Ux+Vy)} \end{aligned}$$

And with 2-D Fourier transform:

$$\begin{aligned} H(u, v) &= G(u-U, v-V) \\ &= e^{-2\pi^2\sigma_g^2((u-U)^2+(v-V)^2)} \end{aligned}$$

In other words, we perform band-pass filtering with center frequencies (U,V) and the parameter σ_g determines the bandwidth.

Experimental results of the technique:

Every set of different parameters (U,V, σ_g) highlights structures in the image with a certain orientation and horizontal and vertical periodicity. So we can use this method to highlight structural irregularities in textile images (possibly caused by watermarking).

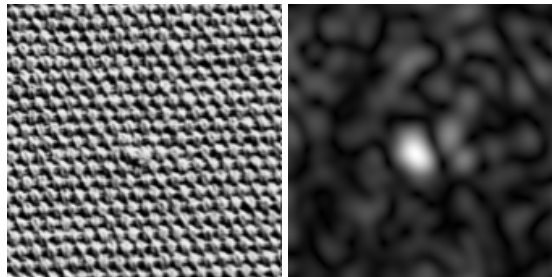


Figure 123: Exemplary Gabor filtering result of a blob

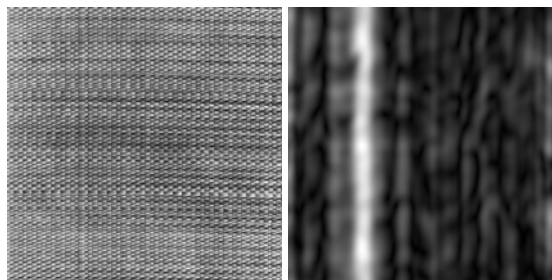


Figure 124: Exemplary Gabor filtering result of a line

The bright white parts indicate the irregularities.

Wavelet based texture gradient

Explanation of the technique:

The last technique we will discuss is the wavelet based texture gradient. It calculates a gradient that is specifically adapted to highlight the borders between different texture regions. That gradient can then be used as an input gradient for the watershed image segmentation algorithm. If we would use the traditional intensity based gradient to segment the textures with the watershed technique, we would get severe over segmentation or in other words totally unusable results.

The technique is originally developed by Hill. First, a non-decimated complex wavelet decomposition is performed on the input image to quantify the texture contained in the image. The method produced 18 complex coefficient images. Each coefficient image contains information about the location of a texture with a certain orientation and scale. The wavelet decomposition produces 3 scales and within each scale 6 different orientations are highlighted. These orientations are shown in Figure 125 for the second and third scale.

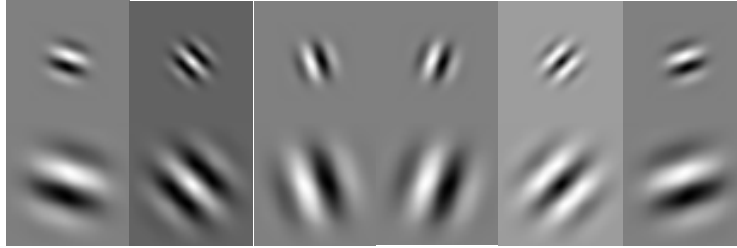


Figure 125: Impulse answers for the second and third scale

If we compare it to Gabor filtering, the technique can be seen as a more advanced and more structured way to cover the frequency domain. The low-pass and high-pass filters in fact very closely resemble Gabor filters. The tiling of the frequency domain is shown in figure 126.

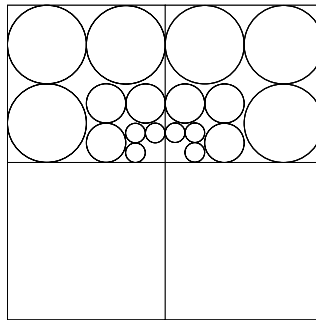


Figure 126: Tiling of the frequency domain

After obtaining the 18 complex coefficient images, the following steps are executed on each complex coefficient image to obtain a gradient image:

- Norm of the complex coefficients
- Median filtering to remove small isolated peaks
- Gaussian derivative to produce a gradient image

The final step is the normalized summation of each gradient image. We now have the combined texture gradient. After applying the watershed algorithm with a certain drowning threshold on the texture gradient, we get the texture segmentation.

Experimental results of the technique:

The image was constructed out of a database of individual textures. On real images of textile it would be much more difficult to get a good segmentation result, but the technique could be a good starting point for a complete framework that includes more a priori information or higher level knowledge about the specific application/image type.

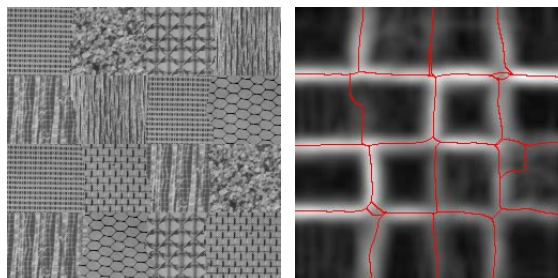


Figure 127: Left: Original image, Right: The texture gradient together with the segmentation

2.2.12. Products authentication protocol

The last step consisted in the design of an authentication protocol. The optical reading device and the MAP are a part of this protocol which is defined laws and rules in the use of the optical reading device and of the MAP. The first approach was a scheme using a private key, but after study, it appears that a public keys infrastructure with a digital signature scheme is more suitable.

The setup of the infrastructures for the private keys interchange (private and secure channels) is too heavy. To give the MAP in accordance with the protocol, the MAP is composed by a binary string of 1024 bits at least which corresponds to the TRIF (TRacing Information Frame) and to the MDS (Manufacturer Digital Signature). The TRIF doesn't contain any confidential information. The TRIF's length is adjustable but the MDS's length is fixed and depends on the TRIF and on the manufacturer. The MDS signature is calculated for every new MAP. This MAP is added on each series of pieces produced with the same mould during a time defined by the manufacturer itself.

The TRIF contains:

- ID: Product manufacturing ID
- DATE1: Manufacturing date,
- DATE2: MAP validity date,
- ROUTING: Routing coded information.

The TRIF is then digitally signed with a strong cryptographic signature algorithm such as the standard RSA or DSS (Digital Signature Standard).

The IAO (International Authenticating Organization) is not currently defined but it will manage the public keys and will certify the reader (ORD).

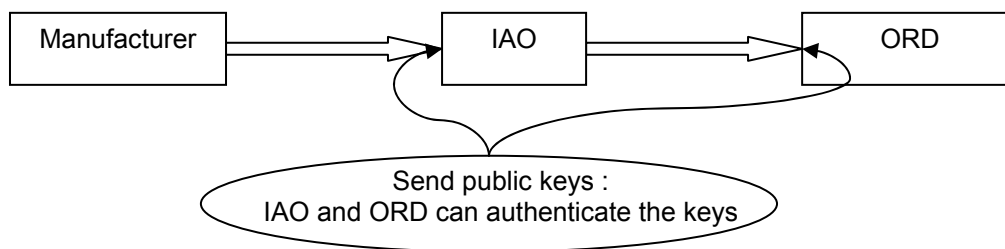


Figure 128: Schematic of the protocol.

The coupling between the traceability information (TRIF) and the signature (MDS) doesn't avoid the counterfeiting of plastics pieces because a piece with a MAP will be duplicated one day. But, the insertion of the MDS prevent from designing of a new MAP by the counterfeiter. If he modifies the TRIF or/and the MDS, the check of the signature will fail. If he designed his own TRIF to mislead the authenticator, he will have to create a MDS. He doesn't know the private key of the manufacturer thus his MDS will never be correct. Consequently, the pirate can't copy the whole MAP. The duplication of the piece, and of the MAP, need time and effort, and the validity date (DATE2) of the MAP will be reached when the counterfeiter will succeed to produce a piece with a copied MAP.

2.3. Standardization activities

Centexbel realised a complete survey of existing and "to be published" standards (Deliverable 4.1). This study was focused on the fields of:

1. Tracking standards dealing with the common ways used to identify/recognise objects by means of a label, RFID tag, etc.

Commonly objects are identified/marked by using:

- A written or printed label with human-readable characters.
- A label imprinted with a barcode.
- A radiofrequency identifier (RFID).

More likely human beings are identified/marked by using:

- A magnetic card.
- A smart card.
- An optical card.
- Biometrics.

Other possibilities include (not adequate for our purpose):

- A contact memory.
- A label printed with magnetic ink.
- Real time locating systems (RTLS).
- Electronic article surveillance (EAS).
- Machine vision.

2. Numbering standards dealing with the way to give a specific number to world objects in such a way they are uniquely identified and possibly characterised.

Several different schemes were developed during the years for books, medicines, postal goods, auto-identification, etc.

3. Encoding/encryption standards allowing for restricting access of information to mandated persons only.

Private and public encryption schemes are available.

Lots of standards originate from ISO/IEC. Most of the time other standards were built by other organisations but were included in ISO afterwards. Some other standard authorities are:

- AIM, ANSI, ASTM, CEN, EAN, IEEE, UCC, VICS at the general level.
- ETSI, EIA, TCIF/ATIS, INCITS for electronics and telecommunication.
- NISO for library matters.
- Universal Postal Union.
- AIAG for automotive industry.
- HIBC for health industry.

During the first year, Centexbel selected the numbering schema for certified goods. After some discussion with Multitel, it was agreed to align our information format on standards developed by the EAN/UCC organisation. We chose the UCC-128 Application Identifier Standard in such a way we ease the interoperability with EDI and EANCOM (for global trade electronic data interchange) envisioned by this standard. We also determined the size for the information pattern keeping in mind the compromise between Redundancy and Anti-forgery, keeping in mind that redundancy helps the reading and the recognition of altered patterns (due to scratches, etc...) **BUT** redundancy also allows for recognition of more or less imperfect counterfeited patterns. The numbering schema has however evolved during the whole project in parallel with the MAP structure.

Moreover, the "Certification and distribution" aspects were discussed between Centexbel and Multitel leading to:

- A further analysis of the Protocol Proposal for Authentication using Micrometric Authentication Pattern
- The choice of creation of a private "Demo Distribution Web Site" over the use of VeriSign via PinkRoccade;
- The move from the use of private keys to public keys for data encryption

Standardization activities related to "Watermarking 3D graphical objects represented as a MeshGrid model"

ISO/IEC 14496-16:2003, Information technology – coding of audio-visual objects – Part 16: Animation Framework eXtension (AFX).

A. Salomie, A. Munteanu, R. Deklerck and P. Schelkens "MPEG2003/m10377: Update of flags from the MESHGRID decoder specific info," *presented at ISO/IEC JTC1/SC29/WG11 MPEG-4, Waikoloa, USA, 2003.*

A. Salomie, A. Munteanu, R. Deklerck and P. Schelkens "MPEG2-4/m11046: Proposal for the XMT-A specifications for MESHGRID," *presented at ISO/IEC JTC1/SC29/WG11 MPEG-4, Redmond, USA, 2004.*

A. Salomie, R. Deklerck, D. Cernea, A. Markova, A. Munteanu and P. Schelkens "MPEG 2005/m12377: Updates to MeshGrid," *presented at ISO/IEC JTC1/SC29/WG11, Poznan, Poland, 2005.*

D. Cernea, A. Markova, A. Salomie, A. Alecu, P. Schelkens, A. Munteanu and R. Deklerck "MPEG 2005/m12612: Updates to the AFXEncoder related to MeshGrid," *presented at ISO/IEC JTC1/SC29/WG11, Nice, France, 2005.*

2.4. References

2.4.1. References related to "Watermarking 3D graphical objects represented as a MeshGrid model"

- [1] ISO/IEC 14496-16:2003, Information technology – coding of audio-visual objects – Part 16: Animation Framework eXtension (AFX).
- [2] I.A. Salomie, A. Munteanu, A. Gavrilesco, G. Lafruit, P. Schelkens, R. Deklerck, J. Cornelis, "MeshGrid – a compact, multiscalable and animation-friendly surface representation", *IEEE CSVT, special issue on MPEG-4 SNHC, July 2004*, pp. 950- 966.
- [3] I.A. Salomie, "Extraction, hierarchical representation and flexible compression of surface meshes derived from 3D data", *Vrije Universiteit Brussel, Brussels, PhD thesis, January 2005.*
- [4] I. A. Salomie, A. Munteanu, A. Gavrilesco, G. Lafruit, P. Schelkens, R. Deklerck, J. Cornelis, "MESHGRID – A compact, multi-scalable and animation-friendly surface representation," *Proc. IEEE International Conference on Image Processing (ICIP 2002), Rochester, New York, USA, vol. 3, pp 13-16, September 2002.*
- [5] I. A. Salomie, A. Gavrilesco, R. Deklerck, I. Ravysse, J. Cornelis, M. Preda "Efficient animation of MESHGRID models using a Skin & Bone system," *Proc. IEEE Signal Processing Symposium (SPS-2002), Leuven, Belgium, pp. 21-24, March 2002.*
- [6] M. Preda, I.A. Salomie, F. Preteux, G. Lafruit, *Virtual character definition and animation within the MPEG-4 standard*, in: M. Strintzis, N. Sarris (Ed.), *3-D Modeling and Animation: Synthesis and Analysis Techniques for the Human Body*, chapter 2, Idea Group Inc., Hershey, PA, USA, August 2003.
- [7] A. Khodakovsky, P. Schröder, W. Sweldens, "Progressive geometry compression," *SIGGRAPH 2000*, pp. 271-278, 2000.
- [8] O. Benedens, "Geometry-Based Watermarking of 3D Models", *IEEE*, January/February 1999.
- [9] R. Ohbuchi, H. Masuda, and N. Aono, "Watermarking Three-Dimensional Polygonal Models", *ACM Multimedia 97*, 1997, ACM Press, New York, pp. 261-272.
- [10] Y. Boon-Lock and M. Minerva, "Watermarking 3D Objects for Verification", *IEEE Computer Graphics, Special Issue on Image Security*, pp. 36–45, January/February 1999.
- [11] O. Benedens and C. Busch, "Towards Blind Detection of Robust Watermarks in Polygonal Models", *EUROGRAPHICS 2000*.
- [12] E. Koch, J. Rindfrey, J. Zhao, "Copyright protection for multimedia data", *Proc. of the Int. Conf. on Digital Media and Electronic Publishing*, 1994.
- [13] I. J. Cox, J. Kilian, T. Leighton, T. Shamon, "Secure Spread-Spectrum Watermarking for Multimedia" *IEEE Transactions on Image Processing*. Vol. 6, No. 12, 1673-1687, December 1997.
- [14] R. Ohbuchi, S. Takahashi, T. Miyazawa, A. Mukaiyama, "Watermarking 3D Polygonal Meshes in the Mesh Spectral Domain", *IEEE Journal on Selected Areas in Communications*. 16(14):551–560, May 1998.
- [15] L. Yongliang, W. Gao, M. Cui, Y. Song, "General Blind Watermark Schemes", *IEEE*, 2002.
- [16] M. S. Yasein, P. Agathoklis, "A Wavelet-based Blind and Readable Image Watermarking Algorithm", *IEEE*, 2002.
- [17] V. Solachidis, I. Pitas, "Watermarking Polygonal Lines Using Fourier Descriptors", *IEEE Computer Society*, May/June 2004.
- [18] *Proc. IEEE*, special issue on identification and protection of multimedia information, vol. 87, no. 7, 1999.
- [19] *IEEE J. Selected Areas Comm.*, special issue on copyright and privacy protection, vol. 16, no. 4, May 1998.
- [20] F. Hartung, J.K. Su, and B. Girod, "Spread Spectrum Watermarking: Malicious Attacks and Counter-Attacks," *Proc. SPIE: Security and Watermarking of Multimedia Contents*, vol. 3657, SPIE, 1999, pp. 147-158.
- [21] S. Craver et al., "Resolving Rightful Ownerships with Invisible Watermarking Techniques: Limitations, Attacks, and Implications," *IEEE J. Selected Areas Comm.*, vol. 16, no. 4, May 1998, pp. 573-586.
- [22] I.J. Cox and J.P. Linnartz, "Some General Methods for Tampering with Watermarks," *IEEE J. Selected Areas Comm.*, vol. 16, no. 4, May 1998, pp. 587-593.
- [23] I. Hong, I. Kim, S. S. Han, "A Blind Watermarking Technique Using Wavelet Transform", *ISIE 2001*.

- [24] Víctor V. Hernández Guzmán; Mariko Nakano Miyatake; Héctor M. Pérez Meana, “Analysis of a Wavelet-based Watermarking Algorithm“, *IEEE*, 2004.
- [25] Mauro Barni, Franco Bartolini, Alessandro Piva, “Improved Wavelet-Based Watermarking Through Pixel-Wise Masking” *IEEE Transactions on Image Processing*, Vol. 10, No. 5, May 2001.
- [26] G. Taubin and J. Rossignac, *Geometric compression through topological surgery*, *ACM Transactions on Graphics*, vol. 17, no. 2, pp. 84-115, 1998.
- [27] G. Taubin, A. Guézic, W. Horn, and F. Lazarus, *Progressive forest split compression*, *Proc. SIGGRAPH’98*, pp. 123-132, 1998.
- [28] A. Khodakovsky, P. Schröder, W. Sweldens, *Progressive geometry compression*, *Proc. SIGGRAPH 2000*, pp. 271-278, 2000.
- [29] A. Alecu, A. Munteanu, P. Schelkens, J. Cornelis, and S. Dewitte, *Wavelet-based fixed and embedded L-infinite-constrained image coding*, *SPIE Journal of Electronic Imaging*, vol. 12, no. 3, pp. 522-538, July 2003.
- [30] A. Alecu, *Wavelet-based scalable L-infinity-oriented coding*, Vrije Universiteit Brussel, Brussels, PhD thesis, 2004.
- [31] A. Munteanu, J. Cornelis, G. Van der Auwera, P. Cristea, A wavelet-based lossless compression scheme with progressive transmission capability, *International Journal of Imaging Systems and Technology* vol. 10, no. 1, pp. 76-85, Jan. 1999.
- [32] D.S. Taubman, M.W. Marcellin, *JPEG2000: Image Compression Fundamentals, Standards and Practice*, Kluwer Academic Publisher, 2002.
- [33] D. C. Cernea, I. A. Salomie, A. Alecu, P. Schelkens, A. Munteanu, “Wavelet-based scalable L-infinite-oriented coding of MPEG-4 MeshGrid surface models”, *Proceedings of SPIE (OpticsEast)*, 23–26 October 2005, Boston, Massachusetts, USA, Vol. #6001, contrib. 21.
- [34] A. Salomie, A. Munteanu, R. Deklerck, P. Schelkens, MPEG contribution: document m10377 – “Update of flags from the MeshGrid decoder specific info”, MPEG meeting Hawaii (8-12 December), 2003.

2.4.2. References related to “Texture and morphology analysis”

- [1] J. Puzicha, T. Hofmann, and J. M. Buhmann, “Histogram clustering for unsupervised segmentation and image retrieval”, *Pattern Recognition Letters*, vol. 20, no. 9, pp 899–909, 1999.
- [2] T. Kanungo, D.M. Mount, N.S. Netanyahu, C. Piatko, R. Silverman, and A.Y. Wu, “An efficient k-means clustering algorithm: Analysis and implementation”, *IEEE Trans. on Pattern Analysis and Machine Intelligence*, vol. 24, no. 7, pp. 881–892, 2002.
- [3] G. Karypis, E.H. Han, and V. Kumar, “Chameleon: A hierarchical clustering algorithm using dynamic modeling”, *IEEE Computer: Special Issue on Data Analysis and Mining*, vol. 32, no. 8, pp. 68–75, 1999.
- [4] L. Hermes, T. Zoller, and J.M. Buhmann, “Parametric distributional clustering for image segmentation”, *European Conference on Computer Vision*, 2002.
- [5] P.A. Bromiley, N.A. Thacker, and P. Courtney, “Colour image segmentation by nonparametric density estimation in feature space”, *Proceedings of The British Machine Vision Conference*, 2001.
- [6] C. Xu and J.L. Prince, “Snakes, shapes, and gradient vector flow”, *IEEE Trans. on Image Processing*, vol. 7, no. 3, pp. 359–369, 1998.
- [7] J.F. Canny, “A computational approach to edge detection”, *IEEE Trans. on Pattern Analysis and Machine Intelligence*, vol. 8, no. 6, pp. 679–698, 1986.
- [8] R. Beveridge, “Segmenting images using localized histograms and region merging”, *Computer Vision, Graphics, Image Processing*, vol. 2, pp. 311–347, 1989.
- [9] S. Chen, W. Lin, and C. Chen, “Split-and-merge image segmentation based on localized feature analysis and statistical tests”, *Computer Vision, Graphics, Image Processing: Graph, Models Image processing*, vol. 53, pp. 457–475, 1991.
- [10] J. De Bock, P. De Smet, and W. Philips, “A Fast Sequential Rainfalling Watershed Segmentation Algorithm”, *Lecture Notes in Computer Science*, vol. 3708, pp. 476–482, 2005.
- [11] R. L. Pires, P. De Smet, and W. Philips, “Watershed segmentation and region merging”, *IS&T/SPIE's 16th Annual Symposium Electronic Imaging 2004, Visual Communications and Image Processing*, vol. 5308, 2004.
- [12] J. Shi and J. Malik, “Normalized cuts and image segmentation”, *IEEE Trans. on Pattern Analysis and Machine Intelligence*, vol. 22, no. 8, pp. 888–905, 2000.
- [13] C. Samson, L. Blanc-Féraud, G. Aubert, and J. Zerubia, “A Variational Model for Image Classification and Restoration”, *IEEE Trans. on Pattern Analysis and Machine Intelligence*, vol. 22, no. 5, pp. 460-472, 2000.
- [14] Faguo Yang and Tianzi Jiang, “Pixon-based image segmentation with Markov random fields”, *IEEE Trans. on Image Processing*, vol. 12, no. 12, pp. 1552–1559, 2003.
- [15] T.P. Weldon, W.E. Higgins, and D.F. Dunn, “Gabor filter design for multiple texture segmentation”, *Optical Engineering*, vol. 35, no. 10, pp. 2852–2863, 1996.
- [16] P. Hill, C. Canagarajah, and D. Bull, “Image segmentation using a texture gradient-based watershed transform”, *IEEE Trans. on Image Processing*, vol. 12, no. 12, pp. 1618–1633, 2003.

- [17] R. Paget and I.D. Longstaff, "Texture synthesis via a noncausal nonparametric multiscale Markov random field", IEEE Trans. on Image Processing, vol. 7, no. 6, pp. 925–931, 1998.
- [18] R.M. Haralick, K. Shanmugam, and I. Dinstein, "Textural Features for Image Classification", IEEE Trans. on Systems, Man and Cybernetics, vol. 3, no. 6, pp. 610–621, 1973.
- [19] M.M. Galloway, "Texture analysis using gray level run lengths", Computer Graphics and Image Processing, vol. 4, pp. 172–179, 1975.
- [35]

2.5. Appendices

2.5.1. Nickel electroforming, Processes and applications

Origins and Progress

The specialized use of the nickel plating process for electroforming results in the manufacture of tools and products those are unique and often impossible to make economically by traditional methods of fabrication. These tools are indispensable for operations in the textile, communication, aerospace and other industries.

Its origins are well-documented. Professor Jacobi discovered electroforming during his investigations on galvanic cells. Jacobi used an engraved copper printing plate as the cathode in a copper sulfate solution and electrodeposited copper upon it. Although he had difficulty separating the electrodeposit from the engraved printing plate, where it could be separated, the deposit had accurately reproduced the details engraved on the original plate.

In 1842, R. Boettger successfully electroformed articles of nickel using nickel ammonium sulfate solutions. During the latter half of the 19th century electroforming with iron was investigated.

Modern applications of electroforming are diverse and today nickel is used in a great variety of different electroforming applications. The reasons for its popularity include the fact that electrodeposited nickel can be strong, tough and resistant to corrosion, erosion and wear. Its mechanical properties can be varied at will between wide limits by changing plating conditions, by alloying with other elements, and by incorporating particles and fibers within the electrodeposited nickel matrix.

What is electroforming?

Electroforming is the fabrication of simple and complicated components by means of electroplating. The basic fabrication steps are as follows:

- A suitable mandrel is fabricated and prepared for electroplating;
- The mandrel is placed in the appropriate electroplating solution and metal is deposited upon the mandrel by electrolysis;
- When the required thickness of metal has been applied, the metal-covered mandrel is removed from the solution;
- The mandrel is separated from the electrodeposited metal.

The electroform is a separate, free-standing entity composed entirely of electrodeposited metal.

When to specify electroforming?

The question of when to specify electroforming as the method for producing a part is important. The answer will depend on the extent to which the designer or engineer can take advantage of the capabilities of the process.

The process can reproduce fine surface detail with great accuracy. An excellent example of this is in the production of electroformed nickel stampers (molds) for pressing compact audio and video discs. The accuracy of reproduction is within a fraction of a micrometer and this degree of accuracy makes possible the high quality stereophonic recordings available today.

An extension of this capability is in the duplication of complex surface finishes. Bright, roughened surfaces and combinations of these can be reproduced without the need for machining or polishing individual components after fabrication. Wood-grains, leather patterns and other textures can be incorporated into molds and dies for plastics, zinc, and other materials - natural textures impossible to duplicate as faithfully as by electroforming.

The combination of modern photolithographic methods of generating patterns with the electroforming process makes it possible to reproduce flat parts with extreme precision and fineness of detail, including giving edges and walls of holes predetermined angles, and is being extended to the forming of movable microdevices for medical, optical and mechanical applications.

Parts can be reproduced in quantity with a very high order of dimensional accuracy. The accuracy attainable will depend on the nature of the mandrel material and the accuracy with which it can be machined - usually within about 0.004 micrometers. Once the mandrel is prepared, all parts produced from it will be dimensionally accurate.

The mechanical and physical properties of the electroform can be closely controlled by selecting the composition of the electroplating solution and the conditions of deposition. Composites of various metals can be created; for example, radar wave guides of copper and nickel with inner linings of silver or gold have been fabricated by electroforming.

There is virtually no limit to the size of the object that can be electroformed. Nickel foil 4 micrometers thick is produced on a continuous basis, as well as textile printing screens up to six meters long.

Shapes can be made and reproduced that are not possible by any other method of fabrication; for example, seamless radar wave guides with two right-angle bends and with the interior made to close dimensional tolerances and with high surface finish.

Electroforming is applicable to the making of single pieces or large production runs. In its latter case, it is possible to start with one master and build up in several generations a number of successively negative and positive electroforms. As the number of positives produced increases, these are used to make more negatives, thus increasing the production rate until the desired capacity is reached, after which nothing but negatives are produced.

In the specific case of molds and dies for making plastics, zinc, and glass parts, electroforming can provide tooling with resistance to corrosion, erosion, and abrasion; with good heat conductivity and precise parting lines to minimize and eliminate flashing; and with high wear-resistance over long production runs.

The engineer should, also, be familiar with the limitations of the electroforming process. The cost of an electroformed article may be relatively high if the same article can be mass-produced by a completely automated process. In the case of shapes, surface finishes, and fineness of detail that cannot be reproduced by any other means, cost becomes a secondary consideration. In the case of tooling, electroforming can be more versatile than and cost-competitive with pantographic machining, hobbing, chemical and electrochemical machining, and other die-making techniques. The time to produce an individual piece by electroforming may be relatively long if wall thickness is great, but high-speed plating processes and the use of backing materials may overcome this. There are limitations in design; for example, sharp angles, corners, and very deep, narrow recesses may cause problems.

It is difficult to achieve great or sudden changes in wall thickness by electroforming. Mandrels must be handled with care since defects caused by accidental damage will be reproduced in the electroform.

The engineer should, therefore, specify electroforming whenever:

- The difficulty and hence, the cost of producing the object by mechanical means is unusually high;
- Unusual mechanical and physical properties are required in the finished piece;
- Extremely close dimensional tolerances must be held on internal dimensions and on surfaces of irregular contour;
- Very fine reproduction of detail and complex combinations of surface finish are required; and
- The part cannot be made by other available methods.

Mandrel types and materials

Mandrels may be classified as conductors or nonconductors of electricity, and each of these may be permanent, semi-permanent, or expendable (Table I). Whether or not a mandrel is a conductor will determine the procedures required to prepare it for electroforming.

Conductive mandrels are usually pure metals or alloys of metals and are prepared by the usual procedures, but may require application of a thin parting film to facilitate separation of the electroform from the mandrel (unless the mandrel is removed by melting or chemical dissolution).

Nonconductors must be made conductive by spraying the surface with a thin metallic film, usually silver. The thin film of silver, also, serves to facilitate separation of the electroform from the mandrel.

Whether or not a permanent or expendable mandrel should be used is largely dependent on the particular article that is to be electroformed. If no re-entrant shapes or angles are involved, it is possible to use permanent, rigid mandrels that can be separated from the finished electroform mechanically and re-used. If re-entrant angles and shapes are involved, it is necessary to use mandrel materials that can be removed by melting or by chemical dissolution, or materials that are collapsible, such as polyvinyl chloride and other plastics.

The various types of mandrel materials each have their own advantages and disadvantages.

Permanent Conductive Mandrels

Austenitic stainless steel is an excellent material to use as a permanent, conductive mandrel. Although machining may be relatively difficult, it can be machined to close tolerance and given a high finish. Resistance to damage in use is good and being conductive, there is no need to metallize the surface before beginning the electroforming process. Austenitic grades of stainless steel readily form stable, passive films that prevent adhesion between electroform and mandrel.

Copper and brass are, also, used as permanent, conductive mandrels and are less costly than stainless steel. They are relatively easy to machine and are ideal when intricately engraved or textured surfaces are required. Separating the electroform from a copper or brass mandrel is easy provided the proper parting film is used (see below). Alternatively, copper and brass mandrels can be electroplated with thin deposits of nickel and/or chromium to facilitate parting and to prevent attack of the mandrel by the processing solutions.

Conventional steel can be used as a mandrel material; it is inexpensive and easily machined. It is usually necessary to nickel plate the entire mandrel and use a simple chemical treatment to ensure release from the mandrel (See Section 5).

Invar or Kovar are alloys that have low coefficients of thermal expansion and are relatively expensive. They are used in critical cases where dimensional accuracy is the chief concern. The electroform and mandrel are heated, and the greater thermal expansion of the electroform permits separation of the mandrel. They are resistant to damage in handling.

Pure nickel, although difficult to machine, may be used as a permanent mandrel. It requires simple treatment to ensure release from the mandrel.

Expendable Conductive Mandrels

Aluminum and its alloys may be used as expendable mandrel materials. They are easy to machine and can be given a high surface finish. They are relatively expensive, easily damaged and may not require metallization prior to electroforming. When used as an expendable mandrel, aluminum and its alloys can be dissolved away from a nickel electroform in a 10 per cent solution of sodium or potassium hydroxide solution at room temperature.

Zinc-based alloys have similar characteristics and are used as expendable mandrels. The mandrel can be dissolved in a cold 10 per cent hydrochloric acid solution.

Superplastic zinc alloys (zinc-aluminum-magnesium alloys) can be blow-molded into complex shapes at relatively low temperatures, 250°C. Bismuth can embrittle copper and nickel electroforms if it is not completely removed from the inside of the electroform, in which case the use of bismuth-free tin-zinc alloys are required.

Nonconductive Mandrel Materials

Waxes are useful because some can be readily cast and easily melted out of the finished electroform, but they have many disadvantages. They may be brittle, may have a poor surface finish, and are easily damaged. They are inexpensive, require metallization, and cannot be used to maintain high tolerances. Cheap grades of wax melt or soften when exposed to electroplating solutions

operated at normal temperatures. There are only a few grades of wax, such as beeswax, that can be successfully silver-sprayed. Graphite-loaded wax which is conductive has been used successfully as an expendable mandrel.

Plastics materials can be used to fabricate permanent or semi-permanent mandrels, but being nonconductive, require the use of silver-spraying or other metallization techniques. In general, plastics are relatively cheaper and have inferior mechanical properties than metal mandrels, and cannot be made to close dimensional tolerances and with very high surface finish. Rigid plastic mandrels are often made from epoxy resins in the case of electroforms without re-entrant angles. For electroforms with re-entrant angles or shapes, collapsible plastics materials, such as polyvinyl chloride (PVC), are used. Special care is required in using these materials if an acceptable mandrel is to result.

Glass is very difficult to machine, is easily damaged, is relatively expensive, and requires metallization, but surface finish can be excellent and close tolerances can be maintained. It is, therefore, sometimes used as a mandrel material.

Wood, leather and fabrics can be used as mandrel materials when it is desired to reproduce their surface textures and patterns. These materials are porous, must be sealed, and then made conductive. It is often easier to duplicate the desired surface finish by casting with polyvinyl chloride and then electroforming onto the plastic replica of the surface.

Many solid materials can be used to fabricate mandrels for electroforming, but the following generalizations may help in selecting a suitable material:

- Permanent mandrels are preferred for accuracy and for large production runs;
- Expendable mandrels must be used whenever the part is so designed that a permanent mandrel cannot be withdrawn. Expendable mandrels of low-melting point alloys may be used for low-cost items not requiring close tolerances. Collapsible plastic mandrels have been used to fabricate parts with re-entrant shapes or angles.
- It is important that the mandrel retain its dimensional stability in warm plating baths. Wax and most plastics expand when exposed to electroplating solutions operated at elevated temperatures. In such cases, it may be necessary to use acid copper, nickel sulfamate and other electroplating solutions that function at room temperature.

Nickel electroforming processes

The nickel electroplating solutions commonly used for electroforming are the Watts, and conventional and concentrated nickel sulfamate solutions with and without addition agents.

Nickel fluoborate solutions are used, but their popularity appears to be declining. From a commercial perspective, the most important ones are those based on nickel sulfamate.

The advantages of nickel electroforming from sulfamate solutions are the low internal stress of the deposits and the high rates of deposition that are possible, especially from the concentrated solution (Ni-Speed).

Watts Solutions

The Watts bath contains nickel sulfate, nickel chloride and boric acid, and yields nickel deposits that are matte in appearance and that are stressed in tension. The solution is relatively inexpensive and is successfully used for electroforming. Nickel sulfate is the main source of nickel ions in the Watts solution. Nickel chloride increases solution conductivity and has a beneficial effect on the uniformity of metal distribution at the cathode. Boric acid acts as a buffer to control pH at the cathode-solution interface. Anti-pitting agents (wetting agents) are essential for avoiding pitting due to the clinging of air and hydrogen bubbles.

With considerable care, the internal stress of the electroformed nickel can be controlled by means of organic addition agents. Typical stress reducers are saccharin, paratoluene sulfonamide, meta-benzene disulfonate, and 1-3-6 sodium naphthalene trisulfonate. All of these organic stress-reducing agents introduce sulfur into nickel deposits and this limits the temperature at which the electroform can be used in service. Nickel electrodeposits with small amounts of sulfur become embrittled when exposed to temperatures above 200°C.

The exact temperature of embrittlement depends on the sulfur content, the time at the elevated temperature and other factors. Control of internal stress by means of organic addition agents requires an optimum level of the additive, regular replenishment as it is consumed, and frequent (or

continuous) carbon treatment to control the concentration of decomposition products which form as a result of reduction of the additive at the cathode.

Conventional Nickel Sulfamate Solutions

A formulation for conventional nickel sulfamate solutions is included in Table II. In essence, these are analogous to Watts solutions in which the nickel sulfate is replaced with nickel sulfamate. The internal stress is lower than in the Watts solution, as indicated by the information at the bottom of the table. The zero stress level may be obtained by maintaining the solution in a high state of purity and by eliminating the nickel chloride. To assure efficient dissolution of nickel anode materials in the absence of chlorides, it is essential to use sulfur-activated nickel anode materials, such as S-Rounds electrolytic nickel or S-Nickel pellets. Even with extreme care, a zero stress level may be difficult to maintain without using small amounts of the organic addition agents referred to above.

The additives function in nickel sulfamate, as well as in Watts, solutions.

A stable tensile stress can be maintained in conventional nickel sulfamate solutions by including nickel chloride in the formulation, by using an adequate anode area (1.5 to 2 times the area of the cathode), and by using a fully-active nickel anode material to maintain the potential on the anode basket as low as possible, thus avoiding oxidation of the sulfamate anion (described below). Under these conditions, the stress level normally is between 35 and 55 MPa (5000 to 8000 psi) tensile for a well-worked solution.

Anodic Oxidation of Sulfamate Anions

A phenomenon, which apparently only occurs in sulfamate solutions, is anodic oxidation of the anion to form species, which diffuse to the cathode where they are reduced. In some cases, this results in incorporation of sulfur, which acts to lower internal stress and brighten the deposit. This occurs, for example, at insoluble primary or auxiliary anodes, or at nickel anodes that are operating at high potentials.

At an insoluble platinum anode, a stress reducer forms which was identified as an azodisulfonate; it reacts at the cathode and introduces sulfur into the nickel deposit. The use of a small auxiliary platinum anode along with primary anodes to control stress by passing one to two per cent of the total current through the platinum is feasible and has been evaluated on a laboratory scale; although stress was controlled at a low value (compressive), the work confirmed that sulfur co-deposits and affects the ductility and other mechanical properties of the nickel, and its tendency to become embrittled when heated.

The long-time effects of employing an insoluble auxiliary anode in this way have not been determined. More than one sulfamate oxidation product may form. The one that forms depends on the anode potential. At an insoluble platinum anode, the electrode potential is high (1.2 volts vs. SCE), whereas in the concentrated solution (Ni-Speed) the electrode potential on the anode in the conditioning tank is controlled at a lower level, about 0.2 volts vs. SCE. The existence of several oxidation species in sulfamate solutions was confirmed by Chinese investigators in 1988. The Ni-Speed process discussed in the next section permits zerostress plating at high rates while avoiding the co-deposition of sulfur.

Concentrated Nickel Sulfamate (Ni-Speed)

The concentrated nickel sulfamate process, Ni-Speed, was developed by Inco Europe Limited. It permits the deposition of nickel at high rates and at low stress levels in the deposit. It is particularly useful for electroforming where zero-stress conditions are required to produce perfectly flat electroforms and where thick deposits may be built up rapidly. Because low to zero-stress conditions can be achieved without organic addition agents, there is no incorporation of sulfur and the deposits do not become embrittled when heated above 200°C.

Nickel-Cobalt Alloy Plating

Nickel-cobalt alloys can be deposited from concentrated nickel sulfamate solutions with controlled internal stresses. The cobalt in solution can be maintained by the addition of cobalt sulfamate or by using electrolytic cobalt anodes connected to a separate power supply alongside the nickel anodes. The code position of cobalt increases the hardness and strength, and enhances the high temperature properties of the deposits. The cobalt content of the deposit rises with increasing amounts of cobalt in solution and declines as the current density increases. As the cobalt content of the solution is increased, the hardness of the deposit increases to a maximum value. The peak occurs at 35 per cent cobalt in the deposit which corresponds to about 6g/l cobalt in solution. The internal stress of the deposit increases with current density and also with cobalt content of the solution.

Nickel-cobalt alloys can be deposited from conventional nickel sulfamate solutions and from nickel sulfate-based solutions, but the deposition of the alloys from the concentrated solution provides a means to control the internal stress without the use of organic addition agents.

3. Achieved goals and industrial considerations

3.1. The Users Committee

The Users Committee was composed of persons from the industry, interested in the project and particularly in the forthcoming research results.

As potential end-users of the technology under development, they brought regular feedback about the research under development.

The TRACING project philosophy: develop technology for the industry using requirements coming from the industry.

Name	Company	Contact Info
M. Tchen	SIGNATISS S.A.	Mr. Tchen, Managing Director, Rue Théodore Klüber 7, 7711 DOTTIGNIES, tél +32 (0)56 48 35 55, fax +32 (0)56 48 35 65
M. Cochaux	FEBELTEX	Mr. Cochaux, Secrétaire général Wallonie Bruxelles, Rue Montoyer 24 Bte 1, 1000 BRUXELLES, tél +32 (0)2 287 08 11, fax +32 (0)2 287 08 61, ac@febeltex.be
Philippe Willems	BOPACK Systems	Philippe Willems , Bopack Systems , Koralenhoeve 10 , 2160 Wommelgem, p.willems@bopack.com
Jan Mertens	BOPACK Systems	Jan Mertens , Bopack Systems , Koralenhoeve 10 , 2160 Wommelgem, j.mertens@bopack.com
Bart de Laender	CHEP	Bart De Laender , Product Engineer , Bart.DeLaender@chep.com , Tel. +32 3 8205 530 , Mob., +32 495 585 746, Guarden Square , Laarstraat 16 - 2610 Antwerp
Jan Borlez	KMO-IT	Jan Borlez, KMO-IT Centrum vzw , Kapeldreef 60 - B-3001 Heverlee, Tel. : + 32 (0)16-29.83.20 , Fax : + 32 (0)16-29.84.21 , GSM : +32 (0) 478-27.28.77, Jan.Borlez@kmo-it.be
François Koeune	UCL/Crypto Group	François Koeune, Place du Levant, 3, B-1348 Louvain la Neuve, +32.10.47.8141, +32.10.47.2598, http://www.dice.ucl.ac.be/~fkoeune/koeune.html , Koeune@dice.ucl.ac.be
Joël Hancq	TCTS Lab, Faculté Polytechnique de Mons	Joël Hancq, TCTS Lab - FPMs, Parc Initialis, Avenue Copernic 1, B-7000 Mons, hancq@multitel.be
Pierre van den Bulck	BARCO Vision	Pierre van den Bulck, Barco Vision, President Kennedypark 35, B-8500 Kortrijk, Pierre.vandenBulck@barco.com , Tel +32 56262632, Fax +32 56262690
Olivier Craenen	BANKSYS	olivier.craenen@banksys.com
Christine Tholomé	GlaxoSmithkline Biologicals	Christine Tholomé, Equipment Development Mechanical Engineer, GSK Biologicals, Parc de la Noire Epine, Rue Fleming 20, 1300 Wavre, christine.tholome@gsk.com
Axel Kupisiewicz	LASEA	LASEA SA, Liège Science Park, Rue des Chasseurs Ardennais, 4, 4031 ANGLEUR, Tel.: +32.4.365.02.43, Fx.: +32.4.384.37.55, akupisiewicz@lasea.be

3.2. Publications

During the project, the ETRO laboratory from VUB published a series of scientific papers around the MESHGRID representation:

M. Preda, I.A. Salomie, F. Preteux, G. Lafruit, Virtual character definition and animation within the MPEG-4 standard, in: M. Strintzis, N. Sarris (Ed.), 3-D Modeling and Animation: Synthesis and Analysis Techniques for the Human Body, chapter 2, Idea Group Inc., Hershey, PA, USA, August 2003.

A. Salomie, A. Munteanu, A. Gavrilescu, G. Lafruit, P. Schelkens, R. Deklerck, J. Cornelis, "MeshGrid – a compact, multiscalable and animation-friendly surface representation", IEEE CSVT, special issue on MPEG-4 SNHC, July 2004, pp. 950- 966.

A. Salomie, A. Munteanu, R. Deklerck, P. Schelkens and J. Cornelis "From TRISCAN surface extraction to MESHGRID surface representation from MPEG-4," *presented at Proceedings of 7th IASTED International Conference on Computer Graphics and Imaging (CGIM), Kauai, USA, 2004.*

A. Salomie, "Extraction, hierarchical representation and flexible compression of surface meshes derived from 3D data", Vrije Universiteit Brussel, Brussels, PhD thesis, January 2005.

A. Salomie, R. Deklerck, D. Cernea, A. Markova, A. Munteanu, P. Schelkens and J. Cornelis "Special Effects: Efficient and Scalable Encoding of the 3D Metamorphosis Animation with MeshGrid ," *presented at PCM 2005: 6th Pacific Rim Conference on Multimedia, vol. 3767, pp. 84 - 95 , Jeju Island, Korea, 2005.*

D. C. Cernea, I. A. Salomie, A. Alecu, P. Schelkens, A. Munteanu, "Wavelet-based scalable L-infinite-oriented coding of MPEG-4 MeshGrid surface models", *Proceedings of SPIE (OpticsEast), 23–26 October 2005, Boston, Massachusetts, USA, Vol. #6001, contrib. 21.*

A. Markova, R. Deklerck, D. Cernea, I. A. Salomie, A. Munteanu, and P. Schelkens, "Addressing View-Dependent Decoding with MeshGrid", accepted for presentation at *SPS-DARTS 2006: The second annual IEEE BENELUX/DSP Valley Signal Processing Symposium, Antwerp, Belgium, March 2006.*

MPEG-standardisation documents:

ISO/IEC 14496-16:2003, Information technology – coding of audio-visual objects – Part 16: Animation Framework eXtension (AFX).

A. Salomie, A. Munteanu, R. Deklerck and P. Schelkens "MPEG2003/m10377: Update of flags from the MESHGRID decoder specific info," *presented at ISO/IEC JTC1/SC29/WG11 MPEG-4, Waikoloa, USA, 2003.*

A. Salomie, A. Munteanu, R. Deklerck and P. Schelkens "MPEG2-4/m11046: Proposal for the XMT-A specifications for MESHGRID," *presented at ISO/IEC JTC1/SC29/WG11 MPEG-4, Redmond, USA, 2004.*

A. Salomie, R. Deklerck, D. Cernea, A. Markova, A. Munteanu and P. Schelkens "MPEG 2005/m12377: Updates to MeshGrid," *presented at ISO/IEC JTC1/SC29/WG11, Poznan, Poland, 2005.*

D. Cernea, A. Markova, A. Salomie, A. Alecu, P. Schelkens, A. Munteanu and R. Deklerck "MPEG 2005/m12612: Updates to the AFXEncoder related to MeshGrid," *presented at ISO/IEC JTC1/SC29/WG11, Nice, France, 2005.*

3.3. Patents activities

The consortium estimated that the research results obtained, and specially the innovating ideas around the new MAP design, and the whole process based on:

- the physical marking (insertion of the information on the flat surfaces) ;
- the optical reading process ;
- the micro replication technique,
- and the whole authentication process for anticounterfeiting purposes,

where patentable. For that reason the TRACING project consortium started during the period September-december 2005 a patent preparation process.

The consortium established a Collaboration Agreement which was signed by all parties where it is stipulated the IPR management and the way the consortium will protect and exploit commercially the research result.

During the last year of the project (year 2005), the consortium obtained from Marc Verwilghen, the Minister for the Science Policy, an agreement for transferring the IPR from the Belgian Federal Government to the whole consortium which now has the rights to exploit the results of the research.

For the moment (February 2006), the patent preparation is still in progress.

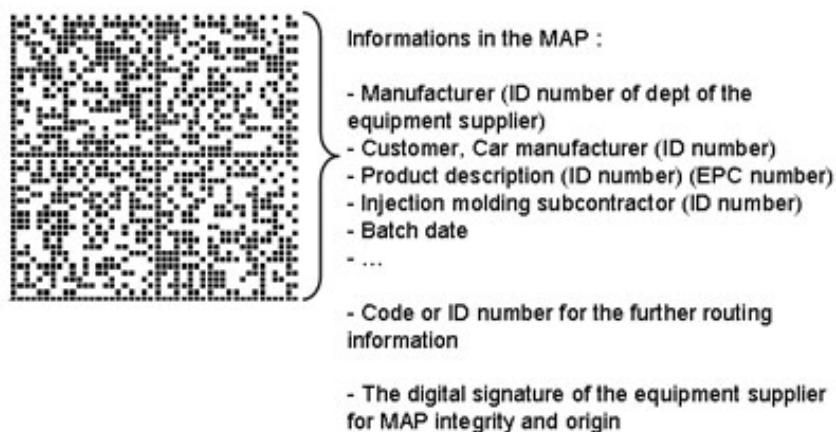
3.4. Industrial exploitation possibilities

A scenario was elaborated to simulate the way of using the micro-structuration for the counterfeiting protection of a plastic component. This scenario is a typical example of what could be used to manage the production and the distribution of spare parts in the automotive industry.

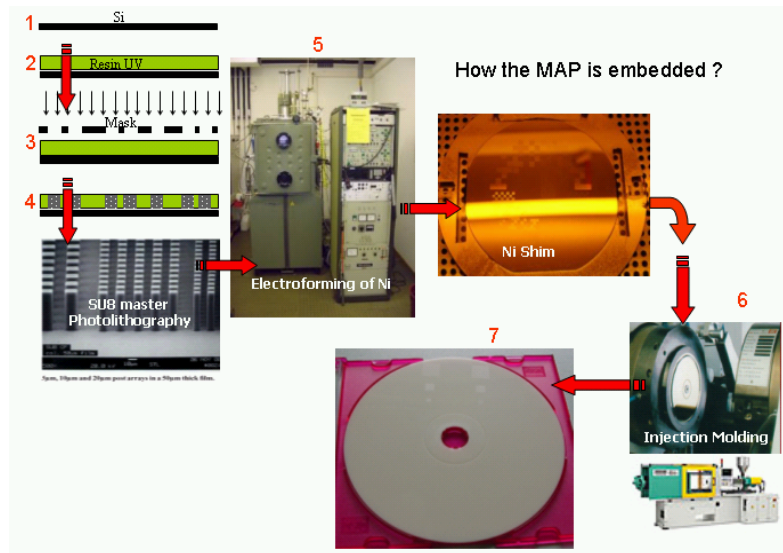
Basically, a car producer subcontracts the manufacturing (and more and more even the development) of a car component to manufacturers of automotive parts or equipment suppliers (Valeo, Bosch, Champion, Delphi, Continental Teves, Plastic Omnium,...etc).

Most of time, the product (a headlamp e.g.) is a part of a “platforms” which is a base-concept applied to several models and even to several car manufacturers or trademarks (VW “Sharan” and Ford “Galaxy” e.g. have some common components). Because of this concept, the sizes of the series for such products are really high and can exceed several millions per year. For this type of production, the investments are consequent and the equipment suppliers require an order commitment for a minimum amount and an exclusive contract for the market of the second mounted parts.

After the agreement between the car manufacturer and the equipment supplier, the components are most of time subcontracted to specialized manufacturers (injection moulding workshop for a plastic component, die-casting foundry for metal parts, ...). For example, VALEO develops a new headlamp for the platform X used by VW, Ford and Seat. A typical plastic component like the style-shape is subcontracted to an injection moulders. One of the specifications on that product is the information which has to be embedded on it. The equipment supplier has to define the MAP and the information encrypted inside.



This information is defined in accordance with the car manufacturer. The manufacturing of the MAP is then subcontracted by the equipment supplier: the photoresist master and the Ni Shim are carried out by accredited laboratories.



Several copies of the Ni Shim can be made and supplied to the equipment supplier who controls the quality and the integrity of the information before providing the injection moulding workshop with them by a safe way.

The components are at that time produced with the embedded information. The control of the integrity of the information is performed by the injection moulder and the other specifications as well (dimensions, tolerances, ...)

The equipment supplier gets the components from the injection moulder and carries out the final assembly. At this step, a final control is performed to verify the presence of the MAP with the embedded information and also the integrity and the validity of the information.

This control allows verifying that the subcontractor respects the Good Manufacturing Procedures (GMP) and the process specifications and that a further control would be possible after delivery to the dealers.

At that time, there are two possible ways for the components:

- The equipment supplier feeds the supply chain of the car manufacturer. In that case the components are used for the first assembling line. The risks of counterfeiting are non-existent because there is absolutely no intermediary between the component manufacturer and the final dealer and customer.
- The equipment supplier supplies the marked for the second mounted parts. This second way is the most “counterfeiting-critical”.

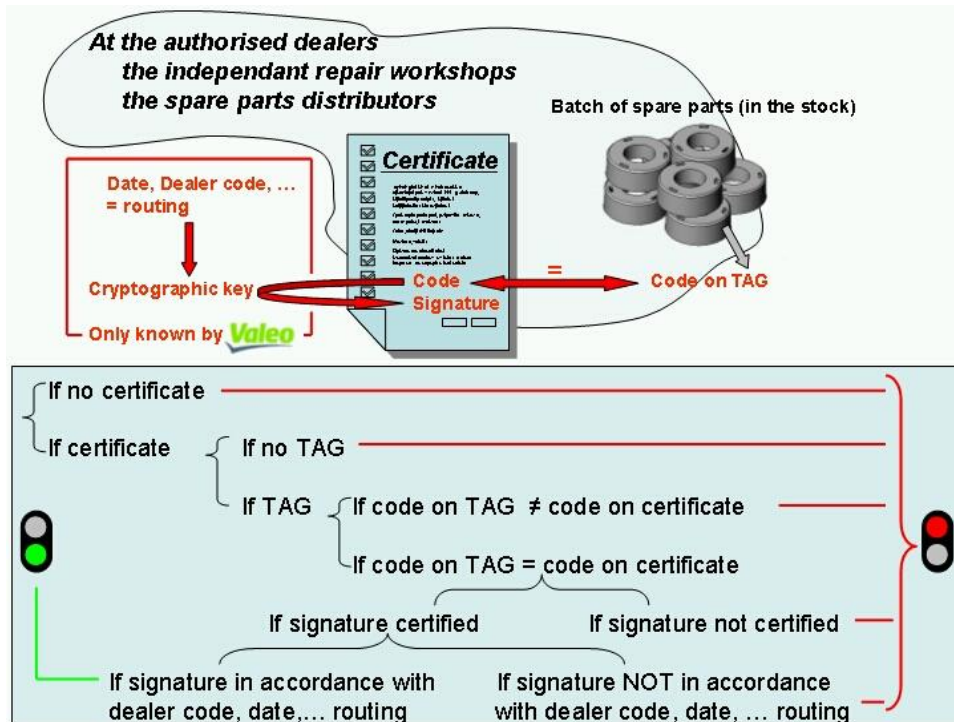
For the second mounted parts, most of equipment suppliers have a subsidiary company dedicated for the distribution of the spare parts (VALEO SERVICE for VALEO e.g.). Via this subsidiary company, the parts are supplied to the authorized dealers, the independent repair workshops and the spare parts distributors. An important remark is that the second mounted parts market is, in the same time, the most paying market but also the most counterfeiting prone because of the number of intermediaries in the supply chain. The risks of counterfeiting are high because of the growth of well-organized parallel networks with high-technology capabilities like reverse engineering, laser scanning and rapid manufacturing, high performance workshops and distributions facilities.

For this type of risk, the MAP is either not present or copied from another one. In both cases the embedded information (if any) is not complying with external information like the routing for example.

An other type of risks is coming from the refurbishment networks of second-hand parts. In this case the embedded information is either inexistent or damaged or worn or simply not complying with the information of the routing.

To be efficient, the anti-counterfeiting protection requires a MAP control at random at the dealer places by a sworn agent . This control could be a “light” control. For example a repair is asked to a dealer and the spare parts are controlled by the sworn agent. This control is just to see if a MAP is

embedded in the spare parts but is not enough for a full protection or guarantee. The control could be also deeper. The batch of spare parts are controlled and compared with a certification document. This full control is illustrated on the next figure.



The batch of the spare parts are supplied by the subsidiary distribution company (VALEO SERVICE e.g.) with a certificate. This certificate contains two critical information (and many more): a code which is correlated in an univocal way to the information embedded on the parts and a signature which can only be generated with three information: the code, the route information and a cryptographic key which is only known by the supplier (VALEO SERVICE e.g.).